# Study on one-pot oxidation of benzene to phenol by tungstate-based polyoxometalates photocatalysts

汪，子孺

# Doctoral Thesis

## Study on one-pot oxidation of benzene to phenol by tungstate-based polyoxometalates photocatalysts

タングステン系ヘテロポリ酸光触媒によるベンゼンからフェノールへの一段合成反応に関する研究

By

WANG ZIRU

Molecular and Material Science

Interdisciplinary Graduate School of Engineering Science

Kyushu University

March 2022

**Study on one-pot oxidation of benzene to phenol by tungstate-based polyoxometalates photocatalysts**

By

WANG ZIRU

Molecular and Material Science

Interdisciplinary Graduate School of Engineering Science

Kyushu University

March 2022

# Study on one-pot oxidation of benzene to phenol by tungstate-based polyoxometalates photocatalysts

## Table of content

# Chapter 1:

General introduction

# Chapter 1: General introduction

## 1.1 Synthesis of phenol from benzene

Organic synthetic chemistry plays an important role in the manufacture chemicals including pharmaceuticals, pesticides, and food additives which are an integral part of people's daily life [1, 2]. Among these chemicals, phenol (hydroxybenzene) is an important example since it is a precursor of the industrial production of many materials and useful compounds [3-6]. For example, phenol is used to make bisphenol A, which is important to produce polycarbonates. Another example is that phenolic resin is product from the reaction between phenol and substituted phenol with formaldehyde. Phenol is also can be reduced to cyclohexanol which is important for the polyamides production. Nowadays, annual production of phenol is 8.9 million tonnes worldwide and almost of them (~95%) is industrially produced from benzene by the three-step cumene process. This process is energy consuming due to the requirement of high temperature and high pressure. Moreover, the highly explosive cumene hydroperoxide is produced as an intermediate, while equal amount of acetone as byproduct was produced in the cumene process (Fig. 1).
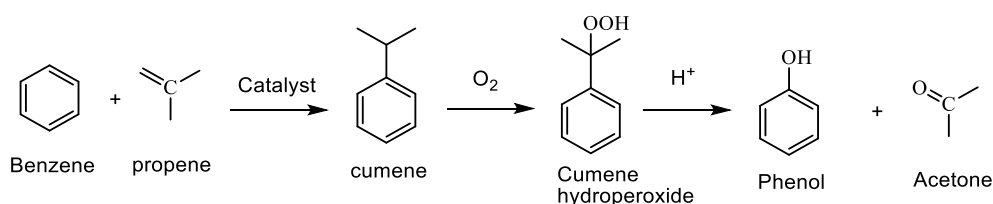


**Fig. 1** Reaction steps for phenol synthesis via the cumene process

In the first step, benzene and propene were react in the presence of acid catalysts. The excess benzene is necessary to prevent the polyalkylations and the side-reactions of the oligomerization of propene. Zeolite was also utilized as a more environmental catalyst in this reaction process. However, the formation of isomers other than cumene decreased the selectivity.

In the second step, the cumene converted to cumene hydroperoxide in the presence of little amount of radical initiator (such as benzoyl peroxide) at air atmosphere. Then, the reaction was catalyzed by cumene hydroperoxide at 77-117 °C and 1-7 atm pressure.

Finally, the phenol and acetone were produced after adding sulfuric acid to react with cumene hydroperoxide at 40-100 °C. Then, the products can be separated from distillation columns. The

overall phenol yield is about 5% by this cumene process. Due to the disadvantage of cumene process, it is highly desirable to develop alternative synthesis process which is more efficient and environmentally benign.

In this context, great interest has been devoted to the one-pot oxidation of benzene to phenol by various oxidant reagents (Fig. 2). However, this goal is not easy based on the experimental results published up to now, even the high benzene conversion is possible. Table 1 shows the thermodynamic data of the benzene, phenol and oxidants, which indicates that the benzene oxidation reaction is irreversible, and 100% conversion is possible.
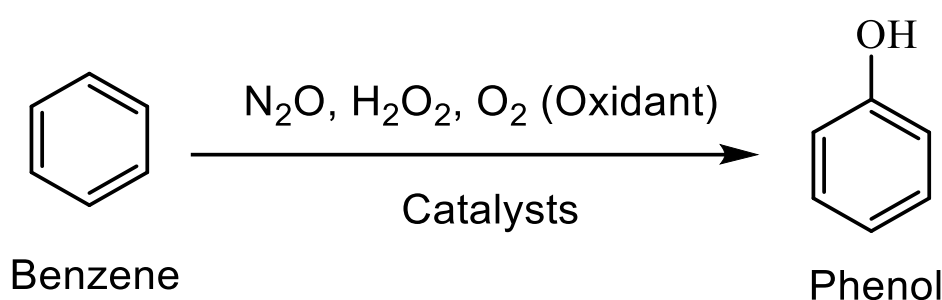


**Fig. 2** One-pot oxidation of benzene to phenol

**Table 1** Standard heat of reaction and standard Gibbs free energy for benzene, phenol and oxidants

|  | Component | $\Delta H°$ at 298 K (KJ/mol) | $\Delta G°$ at 298 K (KJ/mol) |
|---|---|---|---|
| Reagent | Benzene (l) | 48.99464 | 124.34848 |
|  | Benzene (g) | 82.92688 | 129.66216 |
| Oxidant | $H_2O_2$ (l) | -136.10552 | -105.47864 |
|  | $N_2O$ (g) | 82.04824 | 104.1816 |
|  | $O_2$ (g) |  |  |
| Product | Phenol (s) | -165.01696 | -50.4172 |
|  | Phenol (g) | -96.35752 | -32.88624 |
|  | $H_2O$ | -285.82996 | -237.178408 |

High phenol selectivity can be achieved by using strong oxidants such as $N_2O$ and $H_2O_2$, but the source of these oxidant is limited [7-11]. Dioxygen ($O_2$) is a more promising oxidant because it is easily available. For this reason, various homogenous and heterogenous catalysts have been utilized

for benzene oxidation to phenol by using $O_2$ as oxidant. However, the reported catalytic systems usually use high temperature or high pressure since the low activity of benzene oxidation with $O_2$. For example, Wang et al., reported that benzene can be hydroxylated to phenol using a vanadium-zirconium catalyst under 80℃ at 3.0 MPa $O_2$ atmosphere [12]. Furthermore, overoxidation of phenol can be easily occurred under this harsh reaction condition. Thus, some reductants such as $H_2$ and CO were further utilized to active $O_2$ under relative mild conditions. The addition of additional reductants has increased the cost of the production of phenol.

In recent years, photocatalysts has been reported as a green alternative for benzene oxidation reaction, since active species can be generated from both heterogenous and homogenous photocatalysts after light irradiation under low temperature and pressure.

## 1.2 Photocatalysis for benzene oxidation to phenol

The most studied heterogenous photocatalysts are semiconductor-based materials. They showed high activity under light irradiation, due to the generation of high activity species such as holes and hydroxyl radical (Fig. 3) [13]. Typically, the light-induced electron generated from conduction band (CB) is active for various reduction reactions such as $H_2$ production and $CO_2$ reduction. On the other hand, the oxidation reactions will be occurred at the valence band (VB) because the generation of holes. These oxidation reactions are widely utilized to the degradation of pollutants in both liquid and gas phase.
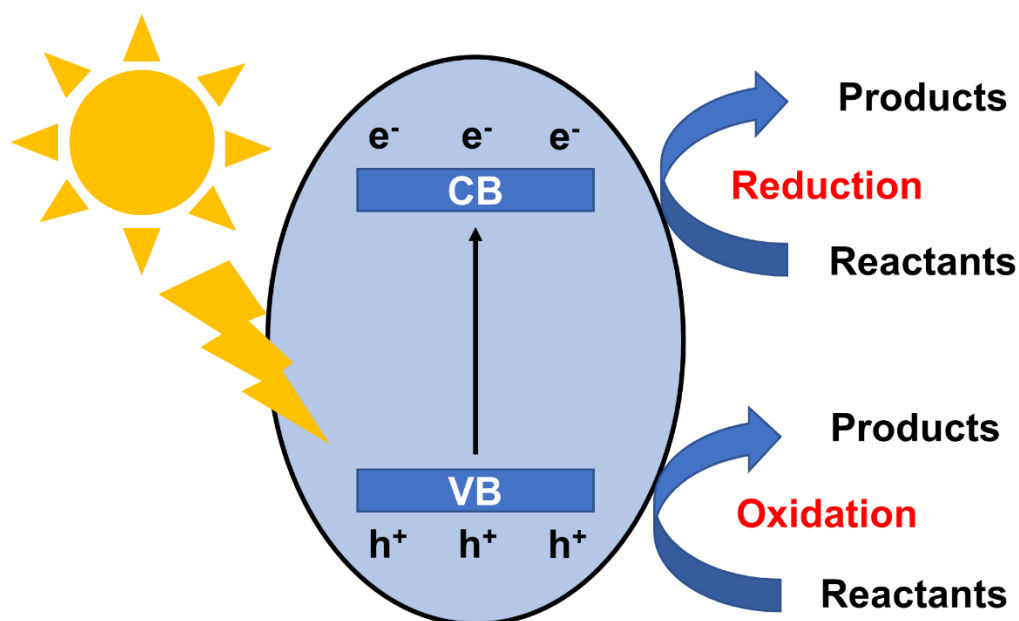
**Fig. 3.** The scheme of photocatalytic process of semiconductor

Among them, the most studied and reported semiconductor-based photocatalysts are $TiO_2$-based materials [14-16]. In these semiconductor systems, light activated hole also can react with water to generate hydroxyl radical ($^\cdot OH$) that directly oxidize benzene to phenol. The route is believed to be dominated in the phenol formation reaction. On the other hand, the light-induced holes can react directly with benzene under mild condition, leading to the generation of benzene cation radical for phenol formation. However, the holes and hydroxyl radical showed high activity and unselective oxidation behavior, which lead to the overoxidation of phenol to unwanted byproducts and $CO_2$ in most cases. Thus, they have been commonly utilized in degradation of pollutants as described above. Only few reports for the benzene oxidation to phenol using semiconductor-based photocatalysts, and most of them using noble metal as cocatalysts or additional oxidant.

Several methods have been utilized to improve the phenol formation in photocatalytic systems. One method is to consider the polarity difference between benzene molecular and phenol molecular. For example, Zhang et al., reported that surface modification of photocatalysts can change the absorption/desorption behavior and enhance the phenol selectivity [17]. In their work, the phenol selectivity was increased on titania incorporated in hydrophobically modified mesocellular siliceous foam ($TiO_2$@MCF). This work is inspired by the different structure and property between benzene molecular and phenol molecular. The interior of the hydrophobically modified MCF provides a hydrophobic environment where the reactant benzene molecules are preferentially attracted into mesopores. After reaction, the hydrophilic product phenol molecules are rapidly released out of the pores before overoxidation within the MCF cages. As a result, the phenol yield and selectivity were increased, although the selectivity is still low (34.7%). This maybe because this method can only prevent the direct reaction between phenol and photo-induced holes. The excess active species such as $^\cdot OH$ generated from water oxidation with holes also can oxidize phenol, resulting the formation of byproducts and low phenol selectivity. Another explanation is that the direct oxidation of benzene with photo-induced holes usually lead the direct oxidation of benzene to $CO_2$, which dramatically decrease the phenol selectivity [18, 19]. As a result, even the phenol product can be efficiently released, the phenol selectivity still low.

5

To achieve high phenol selectivity, choose suitable photocatalyst other than TiO₂ and modify their band structure to fit the benzene oxidation potential is possible. Li et al., reported that a layered double hydroxide (LDH) with suitable band structure showed excellent photocatalytic benzene oxidation to phenol (4.6% phenol yield, 81.1% selectivity) [20]. As shown in Fig.4, the value band (VB) of as-prepared $Zn_2Ti$-LDH (2.52 V) is very close to the oxidation potential of benzene (2.48 V) after modification of the surface oxygen vacancy, which is much different with the other three kinds of photocatalysts including P25, anatase TiO₂ and ZnO. As typical photocatalysts, these three photocatalysts gave phenol selectivity of ~71.8%, 21.7%, and 25.9%, respectively. $Zn_2Ti$-LDH showed higher phenol selectivity of 81.1%. However, a low benzene conversion of 5.7% after 3 h was observed. Recently, similar benzene conversion (7.3%) also reported by using a $Bi_2WO_6$/CdWO₄ hierarchical heterostructure [21].
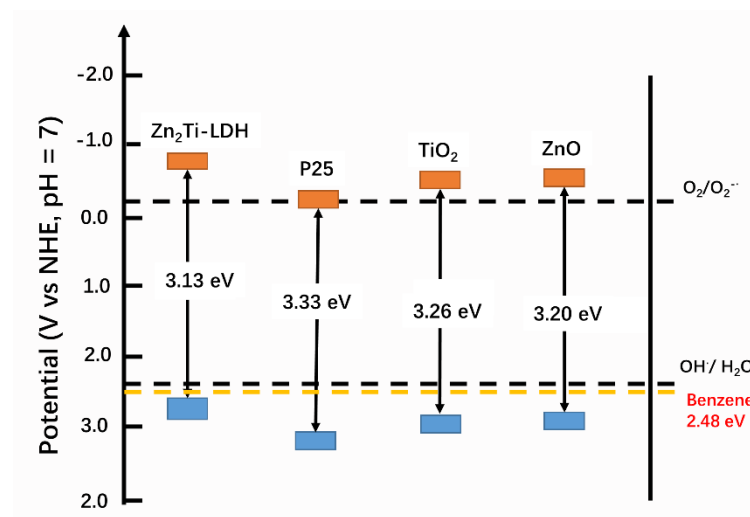


**Fig.4.** Band structure of different photocatalysts

Another method is to utilize new type of photocatalysts other than semiconductor for benzene oxidation. For example, some organic homogenous photocatalysts have been utilized for the benzene oxidation reaction in organic solvents reported by Fukuzumi's group. Typically, photoinduced electron transformation can be occurred from benzene to photo-activated quinolinium ions, resulting the formation of phenol after a successive reaction step. This organic homogenous photocatalyst showed promising phenol formation (30%) and selectivity (98%). The higher activity may be because that the interaction of benzene with photocatalysts in homogenous reaction systems can be promoted. In addition, the high phenol selectivity may be due to the different reaction

mechanism of this organic photocatalytic system with semiconductor photocatalysts. Very recently, another organic homogenous photocatalysts also showed high phenol yield reported by the same group [22]. Although the promising activity have been achieved by organic photocatalysts, the non-reusability hinders their application. In this context, it is important but challenge to develop inorganic photocatalysts that can be oxidize benzene to phenol with high phenol formation and reusability.

**1.3 Structure and properties of polyoxometalates**

Polyoxometalates (POMs) are a serial of inorganic materials composed of cations and diverse polyanion clusters [23]. The research of POMs is an ancient topic, which is still actively researched in various field such as materials chemistry, catalytic chemistry, coordination chemistry, and medicine. The basic construction units are the oxometal polyhedral of $MO_x$, where the M represents some early transition metals such as W, Mo and V. The polyanions of POMs are generally centered by some heteroatoms such as Si, P, S, Ge and so on. Abundant oxygen atoms on the surface of the polyanions can donate electrons, which make POMs as soft bases. In addition, the metal ions on the skeleton of polyanions involve unoccupied orbitals which can obtain electrons from electron donors. Thus, POMs can also act as Lewis acids. In addition, the ability to obtain and release electrons indicates the redox nature of POMs.

Generally, the properties of POMs can be adjusted by variation of the heteroatoms and the general structure of the POMs, including Keggin, Dawson, Anderson, Lindqvist, Waugh, Silverton [23]. As the most studied POMs, POMs with Keggin structure have proved to be thermal stable and high activity in various catalytic reactions. With this advantage, some of them has been large scare manufactualed and applicated in several important industrial reactions such as oxidation of methacrolein and olefins (propene and butenes), polymerization of tetrahydrofuran [24]. As shown in Fig. 5, the Keggin structure have a central tetrahedron ($XO_4$, X = P, Si...) surrounded by four vertex-sharing trimers ($M_3O_{13}$, M = Mo, W…). Each trimer has three octahedras ($MO_6$) which linked in a triangular arrangement by sharing edges. In addition, lacunary Keggin-type POMs will be formed by removing the octahedras, which affect the properties and activity.
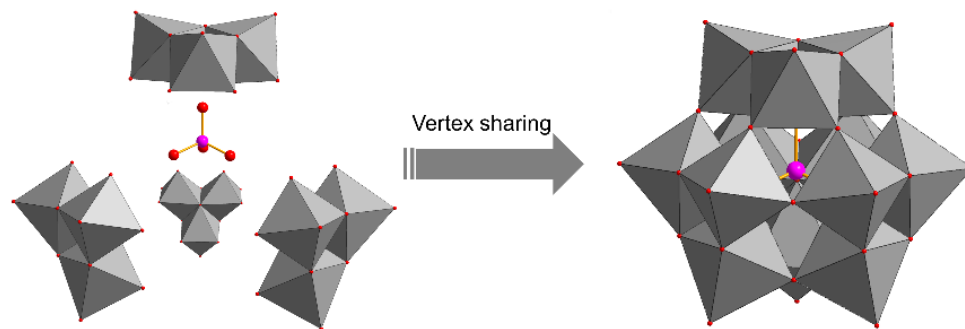
**Fig. 5.** The structure of POMs with Keggin structure.

Some other parameters may also affect the properties of POMs in catalysis, such as solvents and cations. These parameters mainly function by interaction with POM anions. The electronic properties of POMs can be changed by these interactions. In addition, the cations in POMs also impact the electronic and crystallographic properties and solubilities. For example, the parent acids of POMs only contain protons as their cations are called heteropolyacids (HPAs). The HPAs even showed higher Brønsted acidity than classical mineral acid in some cases. The most common cations are inorganic cations, including $H^+$, $Na^+$, $K^+$, $Cs^+$, $NH^{4+}$, $Ag^+$, etc. On the other hand, organic cations with designable structure can be involved in the POMs structure, and their functions can be multiple. Quaternary ammonium ions are the most common organic cations in POMs.

**1.4 Polyoxometalates for acid catalytic reactions**

POMs can serve as acid catalysts because the presence of acidic sites, acidic protons, and metals with Lewis acidity [24]. As a result, they were widely studied for acid catalysis. The dehydration of alcohols to alkenes can be catalyzed by POMs as strong Brønsted acid. Marcì et al., reported the dehydration of 2-propanol by supported $H_3PW_{12}O_{40}$. They demonsrated that the proton on the $H_3PW_{12}O_{40}$ surface is coordinated by two water molecules forming the $H_5O_2^+$, and these species form bridges between the Keggin ions units [25]. Ivanov et al. reported the propene hydration reaction catalyzed by POMs also played by $H_5O_2^+$ [26]. As for some other acid-catalytic reactions, POMs showed higher activity than the mineral acid such as sulfuric acid. This fact is explained by the calculated deprotonation enthalpies (DPE) based on the result of density functional theory (DFT), which reported by Iglesia's group in 2007 [27]. In addition, the acidity can be further adjusted by change the X atom (X = P, Si, Al, Co). The acidity tendency is $H_3PW_{12}O_{40} > H_4SiW_{12}O_{40} >$

8

$H_5AlW_{12}O_{40} > H_6CoW_{12}O_{40}$.
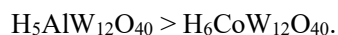
## 1.5 Polyoxometalates for catalytic oxidation

Catalytic oxidation reaction is important chemical process because it not only can produce various organic chemicals, but also act as a method for pollutant decomposition. As for the catalytic oxidation reactions, metal catalysts are actively studied due to their high activity. Compared with organometallic catalysts, POMs are promising catalysts due to their high stability under oxidative systems. In the $H_2O_2^-$ and $O_2^-$ based systems, POMs have been proved be efficient catalysts which can not only oxygenate the C sites in alkenes, aromatic rings, and even inert aliphatic alkanes, but also oxygenate the S sites and N sites in organic compounds [24].

Typically, V-based POMs have been proved to be strong oxidative catalysts which are active for oxidation of various organic compounds including benzene molecular. For example, Neumann's group reported the phosphovanadomolybdate ($H_5PV_2Mo_{10}O_{40}$) can active dioxygen for oxidation reactions [28]. They are active for electron transfer oxidations of substrates and subsequently reoxidized by $O_2$. Particularly, an electron transfer-oxygen transfer was involved in $H_5PV_2Mo_{10}O_{40}$ and its analogues can mediated reactions, in which oxygen atoms are transferred from the POMs to the substrate. This unique property has enabled correspondingly unique transformations involving C−C, C−H bond activation. Then, the reoxidation of POMs with $O_2$ by an inner-sphere reaction. This process is distinguished with that one-electron reduced W-based POMs, which has been shown through intensive research to be an outer-sphere reaction. Based on this reaction pathway, they also reported that C−H bond in benzene molecular can be activated to generated phenol in >50% aqueous $H_2SO_4$ as solvent [29].

## 1.6 Polyoxometalates for photocatalytic reactions

The POMs can be act as photocatalysts has been known in literature for decades. The application of POMs as photocatalysts has been well studied for both pollutant degradation and organic conversion reactions in the last decades. Typically, intramolecular charge will transfer from the $O^{2-}$-based highest occupied molecular orbital (HOMO) to the $W^{6+}$-based lowest unoccupied molecular orbital (LUMO) under light irradiation. This process will be leading to the formation of photoexcited states, which showed higher activity than the ground sates of POMs in both oxidation reactions and reduction reactions. Thus, POMs can be utilized for various photocatalytic reactions,

including the oxidation of alcohol, arenes, alkenes and reduction of $CO_2$. Furthermore, some HPAs were also found to be active for the photo-assisted propene hydration reaction [25].

In a typical photocatalytic cycle, the Keggin-type phosphotungstic acid ($H_3PW_{12}O_{40}$) transferred first into a reduced POM (heteropoly blue) under light irradiation in the presence of substrate. This heteropoly blue is readily reoxidized to original state with $O_2$ in air to complete the reaction cycle. In addition, POMs are stable in the photoirradiation which can maintain their structure for various reactions. This advantage ensures POMs can be promising photocatalysts compared with other homogenous photocatalysts such as organometallic coordination complexes and organic dyes. Current systems using $H_3PW_{12}O_{40}$ mainly carried out for various pollutant degradation which showed promising application potential [30, 31].

Dacatungstate ($W_{10}O_{32}^{4-}$) is another well-studied POMs due to its high photocatalytic activity and broader light absorption range than $H_3PW_{12}O_{40}$. Their anion structure as shown in Fig. 6. As described above, the solubility of decatungstate can be adjusted by change the organic cation or inorganic cation. For example, decatungstate with tetra-n-butylammonium (TBA) as cation showed high solubility in organic solvents. Thus, it is extensively studied in the organic synthesis reactions including the formation of C−C, C−N, C−Si, and C−F, and so on. In these reactions, a hydrogen atom transfer process occurred after the reaction between photoactivated catalyst and substrate, leading to the formation of products. For example, the (TBA) salt of $W_{10}O_{32}^{4-}$ selective oxygenation of cyclohexane in an acetonitrile solution. On the other hand, decatungstate with $Na^+$ as cation was utilized as effective photocatalyst for pollutant degradation because its high solubility in aqueous solution. For example, Pasti et al., reported that sodium decatungstate can efficiently decompose the drug in aqueous solution. Although the decomposition of substrate by sodium decatungstate is as high as that of $TiO_2$, the minimerization is much lower. This disadvantage hampered the application of sodium decatungstate for complete pollutant degradation.
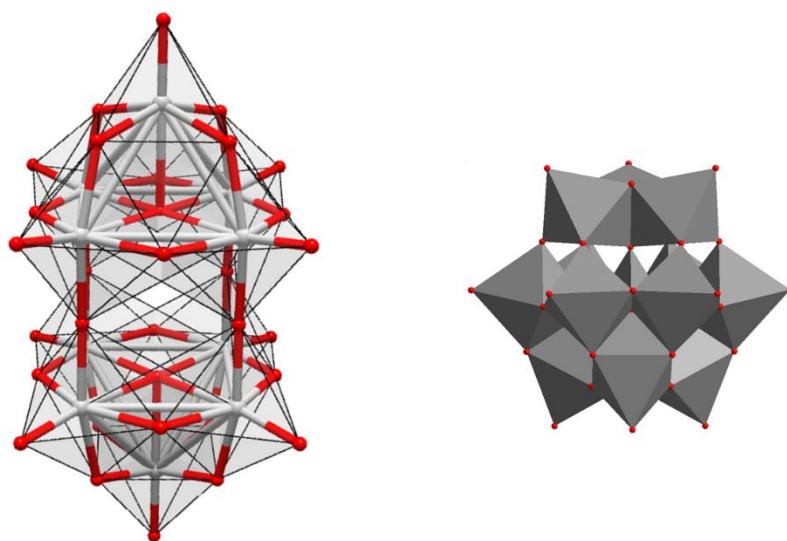
**Fig. 6** Anion structure of $H_3PW_{12}O_{40}$ and decatungstate

The advantage of homogenous systems including high redox activity, high structural stability, and easy reoxidation of reduced species. On the other hand, researchers paid attention into the heterogenized POMs for the purpose of recovery and application. POMs were usually supported onto various support materials such as $TiO_2$, $SiO_2$, $ZrO_2$, etc. In addition to solidification of POMs, the porous support materials will increase the surface area of POMs which can promote the reaction by increase the interaction between catalysts and substrate. However, the leaching of the POMs especially in the polar solution is a challenge for the supported POMs as photocatalysts.

**1.7 Configuration of the present thesis**

The organic transformations under low temperature and pressure are important for its inherent advantage and practical applicability. In this context, this dissertation focuses on the development of efficient photocatalytic systems for the one-pot oxidation of benzene to phenol under ambient conditions using $O_2$ as oxidant. Several typical polyoxometalates as inorganic homogenous photocatalysts were investigated for this purpose, while the experiments were kindly designed. More specifically, attentions were paid on the operation conditions for obtaining high phenol yield and selectivity. The applicability of supported polyoxometalates as heterogenous photocatalysts was also investigated. In addition, several typical semiconductor-based photocatalysts as potential alternative heterogenous tungstate-based photocatalysts for selective benzene oxidation to phenol

has been investigated. The present thesis consists of general introduction and following four chapter.

In the chapter 2, it was showed that a heteropolyacid $H_3PW_{12}O_{40}$ functions as a photocatalyst for benzene oxidation reaction in an aqueous acetonitrile solution using $O_2$ in high phenol yield (23 – 41%) and selectivity (80 – 90%). The addition of acetonitrile to the reaction solution significantly inhibited the complexation between phenol and $H_3PW_{12}O_{40}$, preventing phenol overoxidation. This photocatalyst can be used repeatedly with only a slight decrease in the rate of phenol formation. The reaction mechanism was investigated in detail.

In the chapter 3, decatungstate as another typical polyoxometalate other than heteropoly acid was investigated. Perticurlily, the photocatalytic hydroxylation of benzene to phenol with $O_2$ by using sodium decatungstate ($W_{10}O_{32}^{4-}$) in air atmosphere (1 atm) and at low temperature (10 °C). $W_{10}O_{32}^{4-}$ was active for the benzene hydroxylation process in pure water, which achieved a ca. 16– 23% phenol yield with a ca. 61–70% selectivity within 60 min. The phenol yield and the selectivity were improved through the addition of acetic acid to the reaction solution. This enhancement was due to the improved benzene solubility and suppressed benzene vaporization and phenol overoxidation.

In the chapter 4, heteropoly acid $H_3PW_{12}O_{40}$ was loaded onto mesoporous silica SBA-15 by direct sol-gel and wet impregnation methods. The samples prepared by the direct sol-gel method show a high dispersion for $H_3PW_{12}O_{40}$ on SBA-15 and strong interaction between $H_3PW_{12}O_{40}$ and the silica matrix. The samples prepared by the direct sol-gel method exhibit lower activity for photocatalytic benzene oxidation to phenol in an aqueous solution. The leached species as homogenous photocatalyst found to be dominant in the photocatalytic reaction.

In the chapter 5, Heterogenous photocatalytic oxidation of benzene to phenol has been compared by several typical photocatalysts including $TiO_2$, $C_3N_4$, $WO_3$, $ZnWO_4$, $Bi_2WO_6$. We choose these photocatalysts because they represent different type of semiconductor-based photocatalysts. Most suitable photocatalyst for phenol formation has been obtained and detailed reaction mechanism has been discussed, which is useful to design novel photocatalyst for selective oxidation.

In the chapter 6, a conclusion was drawn for the thesis.

**Reference**

[1] L. Chen, J. Tang, L.-N. Song, P. Chen, J. He, C.-T. Au, S.-F. Yin, Heterogeneous photocatalysis for

selective oxidation of alcohols and hydrocarbons, Applied Catalysis B: Environmental, 242 (2019) 379-388.

[2] J.-Y. Li, Y.-H. Li, M.-Y. Qi, Q. Lin, Z.-R. Tang, Y.-J. Xu, Selective Organic Transformations over Cadmium Sulfide-Based Photocatalysts, ACS Catalysis, 10 (2020) 6262-6280.

[3] Z. Long, Y. Zhang, G. Chen, J. Shang, Y. Zhou, J. Wang, L. Sun, Nitrogen-Doped Biomass Carbons Meet with Polyoxometalates: Synergistic Catalytic Reductant-Free Aerobic Hydroxylation of Benzene to Phenol, ACS Sustainable Chemistry & Engineering, 7 (2019) 4230-4238.

[4] T. Jiang, W. Wang, B. Han, Catalytic hydroxylation of benzene to phenol with hydrogen peroxide using catalysts based on molecular sieves, New Journal of Chemistry, 37 (2013).

[5] P. Devaraji, N.K. Sathu, C.S. Gopinath, Ambient Oxidation of Benzene to Phenol by Photocatalysis on Au/Ti0.98V0.02O2: Role of Holes, ACS Catalysis, 4 (2014) 2844-2853.

[6] S. Fukuzumi, K. Ohkubo, One-Step Selective Hydroxylation of Benzene to Phenol, Asian Journal of Organic Chemistry, 4 (2015) 836-845.

[7] J.-H. Yang, G. Sun, Y. Gao, H. Zhao, P. Tang, J. Tan, A.-H. Lu, D. Ma, Direct catalytic oxidation of benzene to phenol over metal-free graphene-based catalyst, Energy & Environmental Science, 6 (2013).

[8] G. Wen, S. Wu, B. Li, C. Dai, D.S. Su, Active sites and mechanisms for direct oxidation of benzene to phenol over carbon catalysts, Angew Chem Int Ed Engl, 54 (2015) 4105-4109.

[9] X. Ye, Y. Cui, X. Qiu, X. Wang, Selective oxidation of benzene to phenol by Fe-CN/TS-1 catalysts under visible light irradiation, Applied Catalysis B: Environmental, 152-153 (2014) 383-389.

[10] T. Zhang, D. Zhang, X. Han, T. Dong, X. Guo, C. Song, R. Si, W. Liu, Y. Liu, Z. Zhao, Preassembly Strategy To Fabricate Porous Hollow Carbonitride Spheres Inlaid with Single Cu-N3 Sites for Selective Oxidation of Benzene to Phenol, J Am Chem Soc, 140 (2018) 16936-16940.

[11] Y. Morimoto, S. Bunno, N. Fujieda, H. Sugimoto, S. Itoh, Direct hydroxylation of benzene to phenol using hydrogen peroxide catalyzed by nickel complexes supported by pyridylalkylamine ligands, J Am Chem Soc, 137 (2015) 5867-5870.

[12] W. Wang, N. Li, L. Shi, Y. Ma, X. Yang, Vanadium-zirconium catalyst on different support for hydroxylation of benzene to phenol with O2 as the oxidant, Applied Catalysis A: General, 553 (2018) 117-125.

[13] X. He, C. Zhang, Recent advances in structure design for enhancing photocatalysis, Journal of

Materials Science, 54 (2019) 8831-8851.

[14] T.D. Bui, A. Kimura, S. Ikeda, M. Matsumura, Determination of Oxygen Sources for Oxidation of Benzene on TiO2 Photocatalysts in Aqueous Solutions Containing Molecular Oxygen, Journal of the American Chemical Society, 132 (2010) 8453–8458

[15] T.D. Bui, A. Kimura, S. Higashida, S. Ikeda, M. Matsumura, Two routes for mineralizing benzene by TiO2-photocatalyzed reaction, Applied Catalysis B: Environmental, 107 (2011) 119-127.

[16] H. Park, W. Choi, Photocatalytic conversion of benzene to phenol using modified TiO2 and polyoxometalates, Catalysis Today, 101 (2005) 291-297.

[17] G. Zhang, J. Yi, J. Shim, J. Lee, W. Choi, Photocatalytic hydroxylation of benzene to phenol over titanium oxide entrapped into hydrophobically modified siliceous foam, Applied Catalysis B: Environmental, 102 (2011) 132-139.

[18] O. Tomita, B. Ohtani, R. Abe, Highly selective phenol production from benzene on a platinum-loaded tungsten oxide photocatalyst with water and molecular oxygen: selective oxidation of water by holes for generating hydroxyl radical as the predominant source of the hydroxyl group, Catal. Sci. Technol., 4 (2014) 3850-3860.

[19] O. Tomita, T. Otsubo, M. Higashi, B. Ohtani, R. Abe, Partial Oxidation of Alcohols on Visible-Light-Responsive WO3 Photocatalysts Loaded with Palladium Oxide Cocatalyst, ACS Catalysis, 6 (2016) 1134-1144.

[20] J. Li, Y. Xu, Z. Ding, A.H. Mahadi, Y. Zhao, Y.-F. Song, Photocatalytic selective oxidation of benzene to phenol in water over layered double hydroxide: A thermodynamic and kinetic perspective, Chemical Engineering Journal, 388 (2020).

[21] P. Chen, L. Chen, Y. Zeng, F. Ding, X. Jiang, N. Liu, C.-T. Au, S.-F. Yin, Three-dimension hierarchical heterostructure of CdWO4 microrods decorated with Bi2WO6 nanoplates for high-selectivity photocatalytic benzene hydroxylation to phenol, Applied Catalysis B: Environmental, 234 (2018) 311-317.

[22] J.W. Han, J. Jung, Y.M. Lee, W. Nam, S. Fukuzumi, Photocatalytic oxidation of benzene to phenol using dioxygen as an oxygen source and water as an electron source in the presence of a cobalt catalyst, Chem Sci, 8 (2017) 7119-7125.

[23] S. Omwoma, C.T. Gore, Y. Ji, C. Hu, Y.-F. Song, Environmentally benign polyoxometalate materials,

Coordination Chemistry Reviews, 286 (2015) 17-29.

[24] S.S. Wang, G.Y. Yang, Recent advances in polyoxometalate-catalyzed reactions, Chem Rev, 115 (2015) 4893-4962.

[25] E.I. García-López, G. Marcì, F.R. Pomilla, A. Kirpsza, A. Micek-Ilnicka, L. Palmisano, Supported H3PW12O40 for 2-propanol (photo-assisted) catalytic dehydration in gas-solid regime: The role of the support and of the pseudo-liquid phase in the (photo)activity, Applied Catalysis B: Environmental, 189 (2016) 252-265.

[26] A.V. Ivanov, E. Zausa, Y.B. Taârit, N. Essayem, Mechanism of propene hydration over heteropolyacid catalysts, Applied Catalysis A: General, 256 (2003) 225-242.

[27] J. Macht, M.J. Janik, M. Neurock, E. Iglesia, Catalytic Consequences of Composition in Polyoxometalate Clusters with Keggin Structure, Angewandte Chemie, 119 (2007) 8010-8014.

[28] I.A. Weinstock, R.E. Schreiber, R. Neumann, Dioxygen in Polyoxometalate Mediated Reactions, Chem Rev, 118 (2018) 2680-2717.

[29] B.B. Sarma, R. Carmieli, A. Collauto, I. Efremenko, J.M.L. Martin, R. Neumann, Electron Transfer Oxidation of Benzene and Aerobic Oxidation to Phenol, ACS Catalysis, 6 (2016) 6403-6407.

[30] B. Yue, Y. Zhou, J. Xu, Z. Wu, X. Zhang, Y. Zou, S. Jin, Photocatalytic Degradation of Aqueous 4-Chlorophenol by Silica-Immobilized Polyoxometalates, Environ. Sci. Technol. , 36 (2002) 1325-1329.

[31] H. Hori, Decomposition of nonafluoropentanoic acid by heteropolyacid photocatalyst H3PW12O40 in aqueous solution, Journal of Molecular Catalysis A: Chemical, 211 (2004) 35-41.

# Chapter 2:

One-step oxidation of benzene to phenol with $H_3PW_{12}O_{40}$ under photoirradiation

# Chapter 2: One-step oxidation of benzene to phenol with $H_3PW_{12}O_{40}$ under photoirradiation

## 2.1 Introduction

As an important chemical intermediate, phenol is widely used in industry as a precursor for various chemical products including resins, dyes, pharmaceuticals, and pesticides [1, 2]. Industrial phenol production is based on a three-stage cumene process. Although this process achieved high success, it has several disadvantages including high energy consumption, hazardous intermediates, and the production of an equal amount of acetone as a byproduct [3]. For this reason, one-pot synthesis of phenol from benzene has been actively explored over the past decades [4, 5]. Most of the reported catalytic systems use $H_2O_2$, $N_2O$ as oxidants or generate these oxidants *in situ* from the oxidant $O_2$ and the reductants $H_2$, CO, and $NH_3$ [6-8]. Using $O_2$ only as an oxidant is ideal for the oxidation of benzene to phenol, especially when $O_2$ in air is directly available. However, since benzene is less reactive to $O_2$, the reported thermocatalytic reactions are generally carried out under high-temperature or high-pressure conditions [9-14].

In recent years, the photocatalytic technology for converting benzene to phenol with $O_2$ has emerged as a "green" alternative. The photosensitive materials can be photoactivated under mild conditions, including ambient reaction temperatures and pressures [15]. For example, one-pot phenol synthesis from benzene can be promoted since semiconductor photocatalysts can generate holes and radicals such as $^{\bullet}OH$, $^{\bullet}O_2^-$ or $^{\bullet}HO_2$ by light-irradiation under aerobic conditions [16-18]. However, due to the high reactivity and poor selectivity of these holes and radical species, the side reactions such as biphenyl formation and the benzene ring cleavage proceed easily. In addition, since the O−H bond energy of phenol ($\sim 371$ KJ/mol) is lower than the C−H bond energy of benzene ($\sim 473$ KJ/mol), the phenol product is more reactive than benzene [19, 20]. As a result, the oxidation of generated phenol to some unwanted phenolic compounds and $CO_2$ is inevitable [16, 17]. A limited number of examples on photocatalytic benzene oxidation to phenol that use only $O_2$ as an oxidant have been reported. Most of them were noble metal or non-noble metal catalysts with a cocatalyst or additional redox reagents [16,17,21-23]. To control the overoxidation process and minimize the
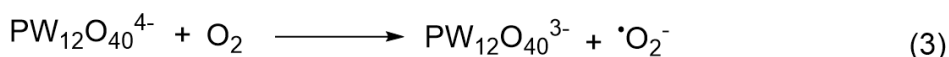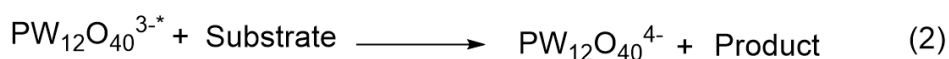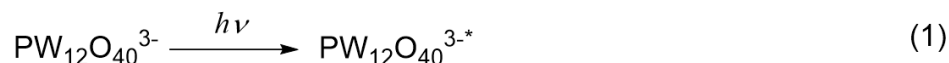
17

unwanted pathway, Choi and coworkers reported an enhanced phenol selectivity by entrapping titanium oxide nanoparticles into a hydrophobically modified mesocellular siliceous foam (TiO$_2$@MCF) as a non-noble metal catalyst [24]. Because the generated hydrophilic product was rapidly released out of the catalyst, the phenol overoxidation was suppressed, and phenol selectivity increased from 15.8% to 34.7%. Bi$_2$WO$_6$/CdWO$_4$ has also been reported for photocatalytic oxidation of benzene to phenol, which afforded 7.3% phenol yield with a selectivity of 99% [25].

Fukuzumi and coworkers published three organic photocatalysts for benzene oxidation in the past decade [22,23,26]. For example, they reported that 2,3-Dichloro-5,6- dicyano-*p*-benzoquinone (DDQ) showed a high yield (93%) and selectivity (98%) of phenol [23]. As mentioned above, additional redox reagents, *tert*-Butyl nitrite /HNO$_3$, were utilized to oxidize DDQH$_2$ to DDQ in the catalytic cycle. As a single catalyst without the need for additional redox reagents, quinolinium ion-based photocatalysts achieved oxidation of benzene to phenol using O$_2$ in high yields (30%) and selectivity (98%) [26]. Recently, Wei et al. reported the development of a quinolinium ion-based photocatalytic system for the oxidation of benzene to phenol using vanadium-substituted heteropolyacids as cocatalysts [27]. However, as with homogeneous organic photocatalysts in general, the recovery of quinolinium ion-based photocatalysts from the reaction medium and their reuse is very difficult. In this regard, it is important and challenging to develop inorganic photocatalysts that can hydroxylate benzene to phenol with O$_2$ with high selectivity and can be used repeatedly.

Heteropolyacids are anionic nanoclusters of early transition metal oxides which adopt a variety of structures. Due to their high oxidation stability, excellent water solubility, and unique structure-dependent reversible redox properties, they have been widely applied as homogeneous inorganic catalysts [28]. Furthermore, some of them are commercially available at a low price, reusable after the reaction, and even utilized on an industrial scale for some typical reactions such as oxidation of methacrolein and olefins (propene and butenes), polymerization of tetrahydrofuran [29]. A well-studied and commercially available heteropolyacid, H$_3$PW$_{12}$O$_{40}$, can be used for photocatalytic reactions [30,31]. Typically, the photoexcited state of H$_3$PW$_{12}$O$_{40}$ (PW$_{12}$O$_{40}^{3-*}$) can be used to activate the C−H bond via an electron transfer (ET) or hydrogen transfer (HT) process for the oxidation of organic substrates, resulting in the generation of product and heteropoly blue. The

heteropoly blue is readily reoxidized with $O_2$ to complete the catalytic cycle (Scheme 1) [32]. We hence hypothesized that if ET or HT process could occur to activate strong C−H bond such as those in benzene rings using $H_3PW_{12}O_{40}$, a new possibility would arise for the photocatalytic one-pot synthesis of phenol from benzene using only $O_2$. However, previous studies showed low phenol yield ( < 3%) over $PW_{12}O_{40}^{3-}$ as photocatalyst in a homogenous aqueous solution or biphasic solution [33,34].

$$PW_{12}O_{40}^{3-} \xrightarrow{h\nu} PW_{12}O_{40}^{3-*} \qquad (1)$$

$$PW_{12}O_{40}^{3-*} + \text{Substrate} \longrightarrow PW_{12}O_{40}^{4-} + \text{Product} \qquad (2)$$

$$PW_{12}O_{40}^{4-} + O_2 \longrightarrow PW_{12}O_{40}^{3-} + {}^{\bullet}O_2^- \qquad (3)$$

**Scheme 1.** General photocatalytic oxidation pathways of organic substrates over $H_3PW_{12}O_{40}$.

In this chapter, we show that photocatalytic oxidation of benzene to phenol by the heteropolyacid $H_3PW_{12}O_{40}$ using only $O_2$ as an oxidant in aqueous acetonitrile solution (50 vol%). This photocatalytic system exhibited 80 to 90% phenol selectivity with a 23 to 41% phenol yield. We found that the addition of acetonitrile to the reaction system in this process significantly prevented the overoxidation of phenol. Kinetic and UV-VIS spectroscopic studies and several controlled experiments were performed to demonstrate the reaction mechanism and explain why the addition of acetonitrile can inhibit phenol oxidation.

## 2.2 Material and Methods
### Materials and instruments

All solvents and reagents were purchased from Wako Pure Chemical Industries Ltd. $H_3PW_{12}O_{40}$, $H_3PMo_{12}O_{40}$, $H_4SiW_{12}O_{40}$, and $H_4SiMo_{12}O_{40}$ were purified by ether extraction and recrystallized in water before use. This purification process can remove insoluble impurities which can be formed by long-term storage [35-37]. The other reagents were used without further purification. The purified $H_3PW_{12}O_{40}$ were confirmed to have a Keggin-type structure by XRD and FTIR (Fig. 1). As shown in Fig. 1a, the position of the main characteristic peaks of $H_3PW_{12}O_{40}$ are observed in the $2\theta$ = 10.3, 25.4, and 34.6, which is consistent with previews studies [12,13]. As shown in Fig. 1b, the

obtained $H_3PW_{12}O_{40}$ shows IR bands approximately at 1,079 (stretching frequency of P–O in the central $PO_4$ tetrahedron of $H_3PW_{12}O_{40}$ molecules), 987 (terminal bands for W=O in the exterior $WO_6$ octahedron) and 890 and 806 cm$^{-1}$ (bands for the W–$O_b$–W and W–$O_c$–W bridge, respectively) corresponding to asymmetric vibration associated with Keggin ion [14-17].
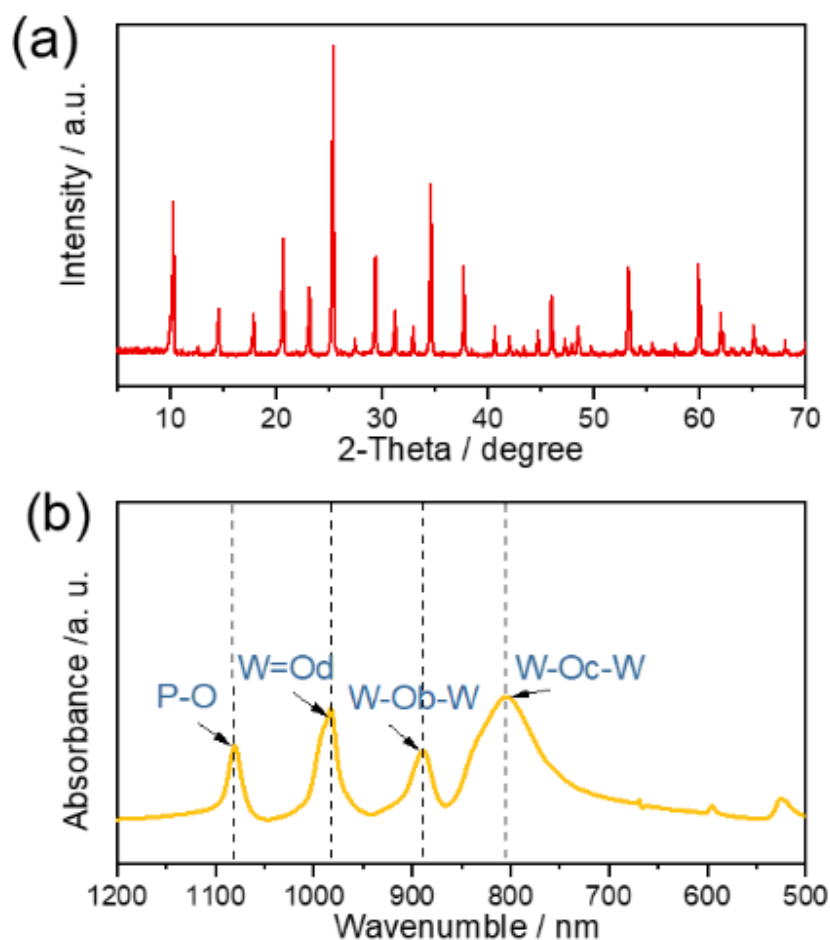


**Fig. 1.** XRD pattern, (b) FT-IR spectra of obtained $H_3PW_{12}O_{40}$

According to a previous study, graphitic carbon nitride (g-$C_3N_4$) was synthesized using urea as the precursor [38]. Typically, 10 g of urea was placed in a capped alumina crucible and then transferred into a muffle furnace. The crucible was annealed at 500 °C and maintained for 4 h to obtain g-$C_3N_4$ (scanning electron microscopy (SEM) images and X-ray diffraction (XRD) pattern shown in Fig. 2). Pt-$TiO_2$ was prepared using the photodeposition method reported earlier [39]. Typically, the commercially available P25 was stirred in an aqueous methanol solution (10 vol%) containing the required amount of $H_2PtCl_6$ as the platinum precursor. The suspended liquid was

irradiated with a 300 W xenon lamp. After washing several times with distilled water, the sample was dried in air at 70 °C for 24 h.
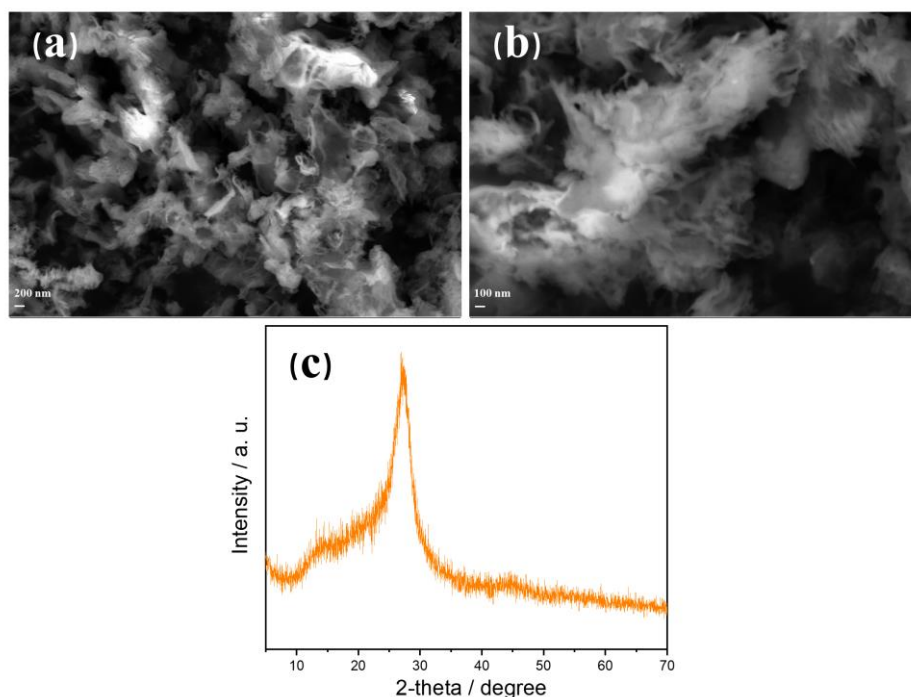


**Fig. 2.** SEM images (a and b) and XRD pattern (c) of g-$C_3N_4$

UV–VIS spectra were recorded on a UV-VIS spectrometer 3100 (Shimadzu, Japan). The samples were transferred into quartz cells (path length: 1.0 cm) and then subjected to measurements. XRD patterns were scanned at 40 kV and 40 mA (the step rate was 2°/min) by using a RINT 2200 diffractometer (RIGAKU, Japan) with Cu-Kα radiation (1.54 Å). The Fourier transform infrared (FTIR) spectra were obtained using an FT/IR-4100 spectrometer (JASCO, Japan). SEM images were obtained by an Ultra-55 instrument (Zeiss, Germany).

*Photocatalytic reaction under aerobic conditions*

Photocatalytic oxidation of benzene to phenol was conducted in a 100 mL photochemical reactor equipped with a water jacket for maintaining the temperature at 10 °C (Fig. 3). The illumination window on the top of the reactor is made of high-strength quartz glass. In a typical run, a 50 mL aqueous acetonitrile solution (50 vol%) containing 13 mM benzene, 5 mM catalyst was added into the reactor. The pH of the solution was adjusted to ~1 with $HClO_4$ to maintain the stability of the

catalysts. A 300W xenon lamp is used as the light source (emission spectrum: Fig. 4). The reaction solution was exposed to air atmosphere (1 atm) without bubbling for introducing oxygen as an oxidant. During the photocatalytic reaction, the reactor was kept at 10°C by circulating cooling water, which eliminated the thermal catalytic reaction caused by the heat radiation from the light source. Sample aliquots (10 μL) were withdrawn from the reactor after each time interval of irradiation and analyzed with reverse-phase high-performance liquid chromatography (HPLC) immediately. The mobile phase was composed of 65% phosphoric solution (0.2%) and 35% acetonitrile with a 1 cm$^3$/min flow rate.
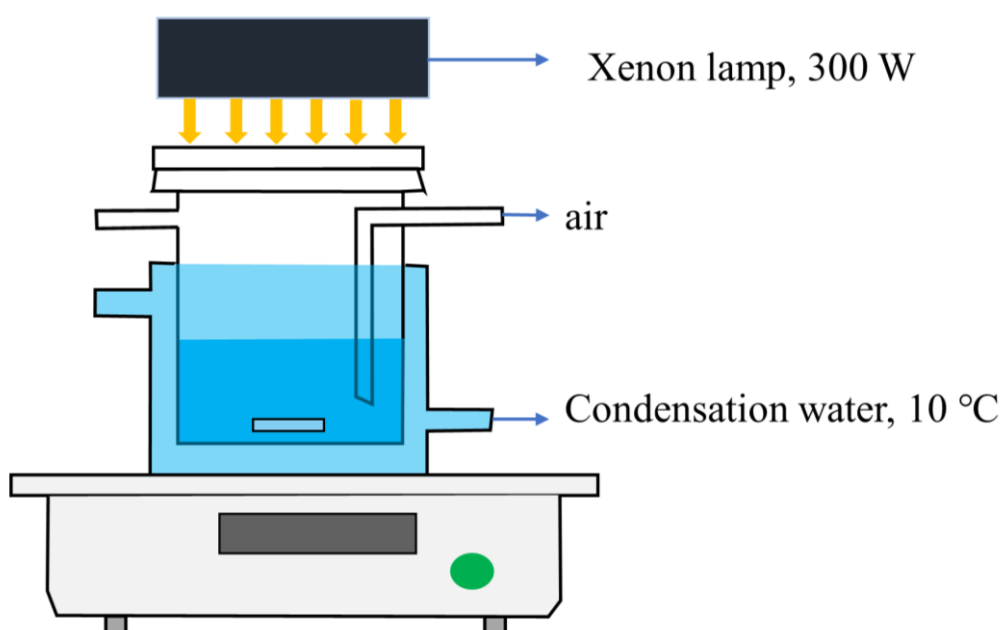


**Fig. 3.** Schematic representation of photocatalytic benzene oxidation setup
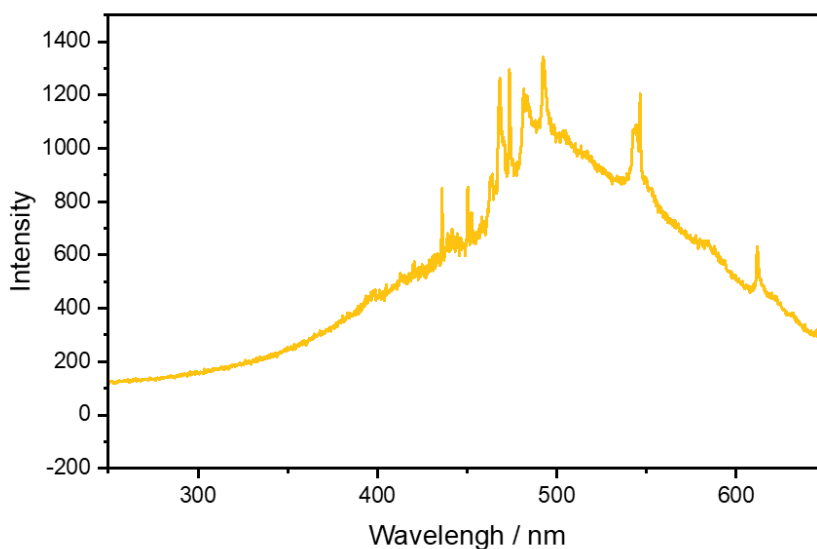
**Fig. 4.** The emission spectrum of the xenon lamp (300 W) in this study.

The conversion of benzene and yields of phenol were calculated using the following formulas.

$$Yield \ (phenol) = \frac{produced \ phenol \ concentration}{initial \ benzene \ concentration} \times 100\%$$

$$Conversion \ (benzene) = (1 - \frac{remained \ benzene \ concentration}{initial \ benzene \ concentration}) \times 100\%$$

$$Selectivity = \frac{yield \ (phenol)}{conversion \ (benzene)} \times 100\%$$

A control experiment using phenol as substrate was conducted under the same condition.

The amount of $H_2O_2$ produced during the reaction was determined spectroscopically [26]. After the photoreaction stopped, NaI (100 mM) was added to the reaction solution, and the absorption spectrum of $I_3^-$ species formed by the reaction of $I^-$ with $H_2O_2$ was measured. The concentration of $H_2O_2$ was determined from the absorbance at the absorption maximum (at 361 nm) of the $I_3^-$ species.

*Photocatalytic reaction under anaerobic conditions and reoxidation under the aerated condition*

The reaction solution is prepared with the same method as stated above. Before irradiation with the Xe lamp, the reaction solution was vigorously bubbled with argon for 15 min to remove the dissolved oxygen. Since the reaction solution was cooled to 10 °C and contained acetonitrile in which benzene dissolved, the amount of benzene vaporized during bubbling was only 1% of the amount of benzene in the reaction solution. In addition to HPLC analysis, the sample aliquots were also tested with UV-VIS spectroscopy to quantify heteropoly blue formation ($PW_{12}O_{40}^{4-}$).

After the above reaction, the xenon lamp was turned off, and the reaction solution was exposed to air. The sample aliquots were analyzed with HPLC and UV-VIS spectroscopy after the reaction solution changed to colorless again. All the reactions were conducted three times to assure reproducibility.
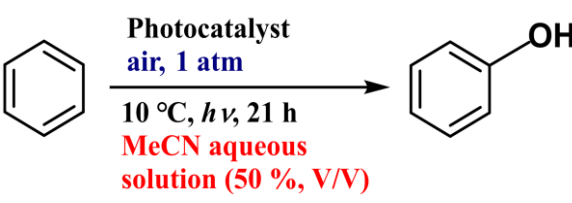
## 2.3 Results and discussion
*Photocatalytic oxidation of benzene to phenol.*

The catalytic activity of various photocatalysts for phenol formation under the typical condition in aerobic aqueous acetonitrile solution (50 vol%) has been compared, as shown in Table 1. The

phenol yield with $H_3PW_{12}O_{40}$ reached 36.9%, significantly higher than the other three kinds of heteropolyacids (Entries 1-4). The high activity of $H_3PW_{12}O_{40}$ over other heteropolyacids is related to two aspects: (1) It has a large energy gap between the $O^{2-}$-based HOMO and the $W^{6+}$-based LUMO, which endows it with high redox potential and reactivity [28]. (2) The heteropoly blue of molybdenum-containing heteropolyacids showed reluctant reoxidation with $O_2$ during the reaction. Above reasons explained why tungsten-containing heteropolyacids show higher activity than molybdenum-containing heteropolyacids. Also, $H_4SiW_{12}O_{40}$ showed a much lower phenol yield than $H_3PW_{12}O_{40}$. The low activity of $H_4SiW_{12}O_{40}$ may be due to its relatively mild photocatalytic oxidation reactivity. For comparison, $WO_3$, $TiO_2$ (P25), $Pt-TiO_2$, and graphite carbon nitride (g-$C_3N_4$), which are representative heterogeneous photocatalysts for benzene oxidation reported in recent years [16,21,33,40,41], resulted in lower phenol yields and selectivity compared to heteropolyacids (Entries 5–8).

**Table 1**
Benzene oxidation to phenol over different photocatalysts. [a]



| Entry | catalysts | Phenol yield (%) | Selectivity (%) | Type of photocatalysts |
|-------|-----------|------------------|-----------------|------------------------|
| 1 | $H_3PW_{12}O_{40}$ | 36.9 | 84.2 | Heteropolyacid |
| 2 | $H_3PMo_{12}O_{40}$ | 1.5 | 68.3 | Heteropolyacid |
| 3 | $H_4SiW_{12}O_{40}$ | 13.5 | 97.1 | Heteropolyacid |
| 4 | $H_4SiMo_{12}O_{40}$ | 1.0 | 81.4 | Heteropolyacid |
| 5 [b] | $WO_3$ | 2.7 | 23.2 | Semiconductor |
| 6 [b] | $TiO_2$ (P25) | 9.2 | 28.9 | Semiconductor |
| 7 [b, c] | $Pt-TiO_2$ | 5.5 | 7.8 | Semiconductor |
| 8 [b] | g- $C_3N_4$ [e] | <0.1 | - | Semiconductor |
| 9 [d] | No catalyst | _ | _ | _ |
| 10 [e] | $H_3PW_{12}O_{40}$ | 35.2 | 84.0 | Heteropolyacid |

[a] Reaction condition: aqueous acetonitrile solution (50 vol%); light source, 300 W xenon lamp; temperature, 10 °C; irradiation times, 21 h; catalyst concentration, 5 mM; benzene concentration, 13 mM; pH = 1 (adjusted by $HClO_4$), under ambient condition. [b] 500 mg

24

catalyst. [c] 1% Pt loaded. [d] Phenol was not detected. [e] Without adding HClO₄.

The structural stability of heteropoly anion is particularly dependent on pH [42]. The Keggin anion $PW_{12}O_{40}^{3-}$ is maintained at 1.0–2.5 and decomposes to lacunary polyanion $PW_{11}O_{39}^{7-}$ at a higher pH value. In this study, the pH value was adjusted to 1 with HClO₄ so that the Keggin structure would be stable and the byproduct organic acid, if formed in the benzene opening reaction, would not affect the pH value. The following two experiments confirmed that HClO4 was not involved in the benzene oxidation reaction as an oxidant. A control experiment without photocatalyst showed that the phenol concentration was below the detection limit (Entry 9), indicating that no direct oxidation of benzene with HClO₄ proceeded under irradiation. In addition, $H_3PW_{12}O_{40}$ showed 35.2% phenol yield without HClO₄, similar to the results with HClO₄ (Entry 10). This finding revealed that photooxidation of benzene to phenol with $PW_{12}O_{40}^{3-}$ was not promoted by HClO₄. Hence, benzene oxidation to phenol can be efficiently promoted by using $PW_{12}O_{40}^{3-}$ as inorganic homogenous photocatalyst.

Fig. 5a shows time course profiles for benzene oxidation reaction over $H_3PW_{12}O_{40}$ in 50% aqueous acetonitrile solution. The pH value was around 1 and unchanged during the reaction, indicating the effect of pH value on benzene oxidation was negligible. No product has been detected in the dark. After irradiation, benzene concentration gradually decreased with time. Phenol was produced as the main product and the phenol concentration monotonically increased. The phenol yield reached 40% in 24 hours. As the byproducts, we confirmed that there was a negligible amount of biphenyl (0.3%) and $CO_2$ ( < 0.1%). Other byproducts such as hydroquinone, catechol, and benzoquinone were also found (Fig. 5b), which are ascribed to the overoxidation of phenol [16,22]. However, the concentrations of these products were much lower than phenol concentration, indicating that the rate of phenol oxidation was much lower than that of phenol formation under our conditions. Thus, the overoxidation of phenol has been significantly inhibited in our reaction system.
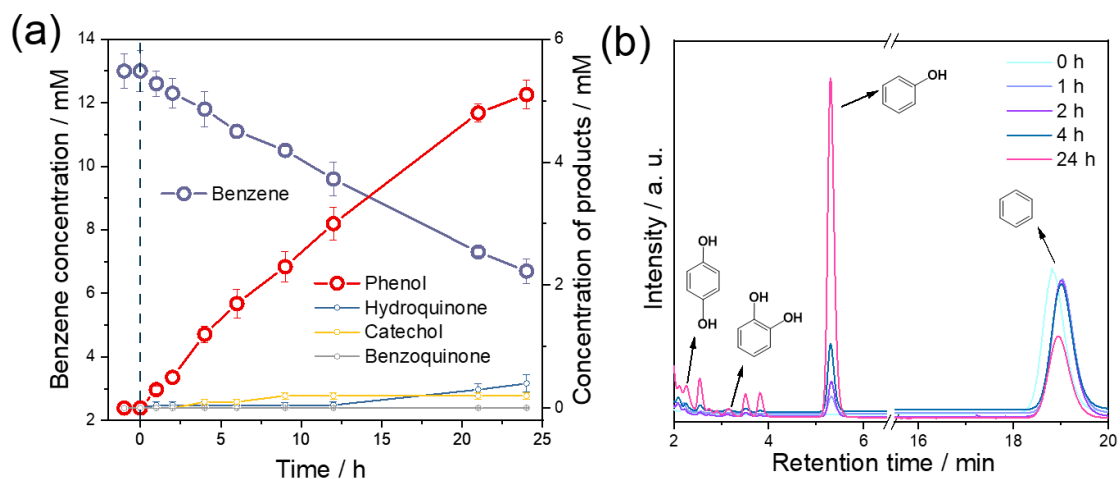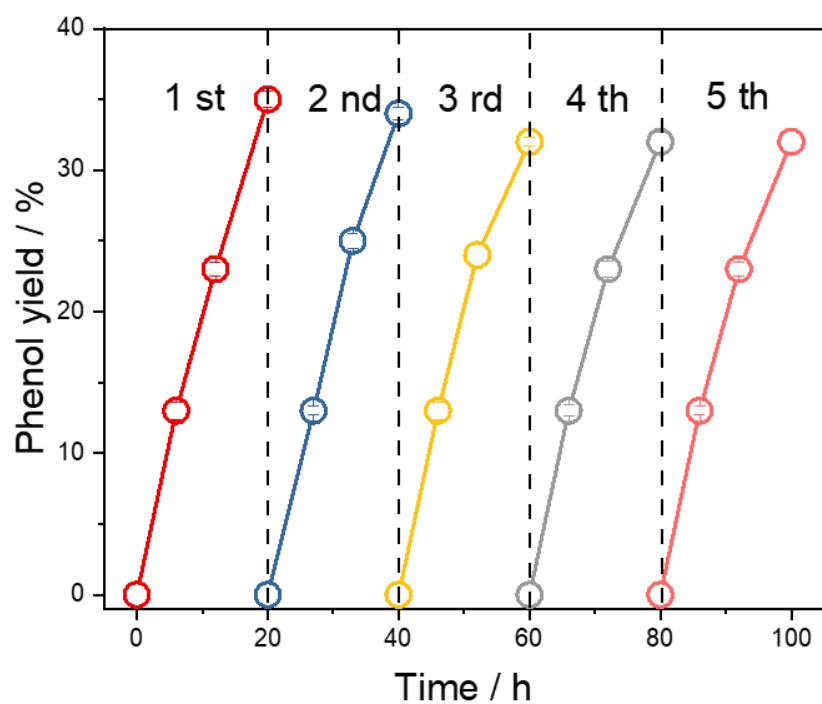
**Fig. 5.** (a) Time course of photocatalytic oxidation of benzene over $H_3PW_{12}O_{40}$. Reaction condition: solution, the mixture of water and acetonitrile (50 / 50); pH, 1; light source, 300 W xenon lamp; temperature, 10 °C; initial benzene concentration, 13 mM; catalyst concentration, 5 mM; under ambient condition. (b) HPLC result of photocatalytic benzene oxidation at a different time interval.

In addition, the UV-VIS absorption spectrum of the reaction solution after 24 h irradiation showed almost no change (Fig. 6), indicating that no catalyst degradation occurred. Thus, $H_3PW_{12}O_{40}$ exhibited high stability during the benzene photooxidation [43]. After the reaction, the phenol product and the solvent can be separated by low-temperature rotatory evaporation (under 50 °C). In this condition, phenol can be evaporated completely together with solvent in high purity. The residual solid contained catalyst and byproducts such as hydroquinone were remained. Then, the solid phase of the catalyst can be dissolved with an equal amount of solvent for next use. The results of five cycles of benzene photo-oxidation are shown in Fig. 7. After the fifth consecutive run, the phenol yield decreased by 8.6% compared to the first run, although the phenol yield was still above 30%. The decrease in the phenol yield could be attributed to residual byproducts from the previous cycle, which inhibited benzene oxidation with $H_3PW_{12}O_{40}$.
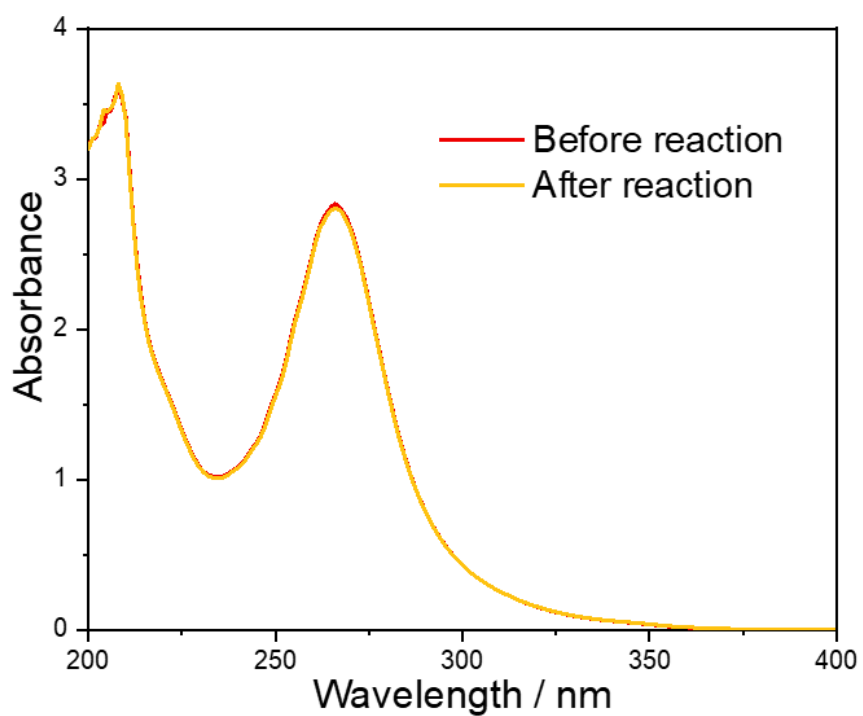
**Fig. 6.** UV-VIS spectra of the 100 times diluted reaction solution before reaction (black line) and after reaction (red line). Reaction condition: solution, mixture of water and acetonitrile (50 / 50); pH, 1; light source, 300 W xenon lamp; temperature, 10 °C; benzene amount, 13 mM; catalyst amount, 5 mM; reaction time, 24 h; under ambient condition. The reaction solution diluted with acetonitrile.

**Fig. 7.** Cycling use of $H_3PW_{12}O_{40}$ for photocatalytic benzene oxidation. Reaction condition: solution, the mixture of water and acetonitrile (50 / 50); pH, 1; light source, 300 W xenon lamp; temperature, 10 °C; initial benzene concentration, 13 mM; catalyst concentration, 5 mM; under ambient condition.

We optimized the phenol formation by varying the reaction conditions, including acetonitrile concentration (V/V), reaction time, and initial benzene concentration (mM). As shown in Table 2 (Entries 1–3), the selectivity can be optimized to 95% by increasing acetonitrile concentration (to 80%) and shorten reaction time (to 4 h). On the contrary, the phenol selectivity decreased to 39% at the same reaction time (4 h) when using pure water as a solvent (Entries 4–5). As discussed below, acetonitrile suppresses the complexation between $PW_{12}O_{40}^{3-}$ with phenol, resulting in high selectivity. Hereafter, based on both phenol yield and selectivity, 50% (V/V) of acetonitrile was used as the solvent. As shown in Fig. 8a, the amount of phenol produced continuously increased with the initial benzene concentration. There is no obvious impact on the phenol selectivity, ranging from 80 – 83% (Fig. 8b). As will be discussed in detail later, the oxidation of benzene produces the benzene cation radical, an intermediate in the formation of phenol, by electron transfer from benzene to the excited $PW_{12}O_{40}^{3-}$. When the benzene cation radical attacks another benzene, biphenyl is formed [44]. The result that phenol selectivity was almost independent of benzene concentration differed from our expectation that biphenyl formation, a bimolecular reaction, would be accelerated at higher benzene concentrations. On the other hand, the phenol yield slightly increased from 37% to 41% by decreasing the initial benzene concentration from 30 mM to 7 mM (Entries 6–8). Thus, the phenol yield increased with the increase in the relative concentration of $PW_{12}O_{40}^{3-}$.

**Table 2**
Controlled experiments on the photocatalytic oxidation of benzene to phenol.



| Entry | Initial benzene mM | Acetonitrile concentration / % | Time/ h | Phenol yield / % | Selectivity / % |
|-------|--------------------|--------------------------------|---------|------------------|-----------------|
| 1 | 30 | 80 | 4 | 4 | 95 |
| 2 | 30 | 50 | 4 | 9 | 92 |

28

| 3 | 30 | 50 | 12 | 23 | 90 |
|---|----|----|----|----|----|
| 4 | 30 | 0  | 1  | 7  | 51 |
| 5 | 30 | 0  | 4  | 18 | 39 |
| 6 | 7  | 50 | 24 | 41 | 80 |
| 7 | 13.5 | 50 | 24 | 40 | 81 |
| 8 | 30 | 50 | 24 | 37 | 83 |

Reaction condition: pH, 1; light source, 300 W xenon lamp; temperature, 10 °C; catalyst concentration, 5 mM; under ambient condition.
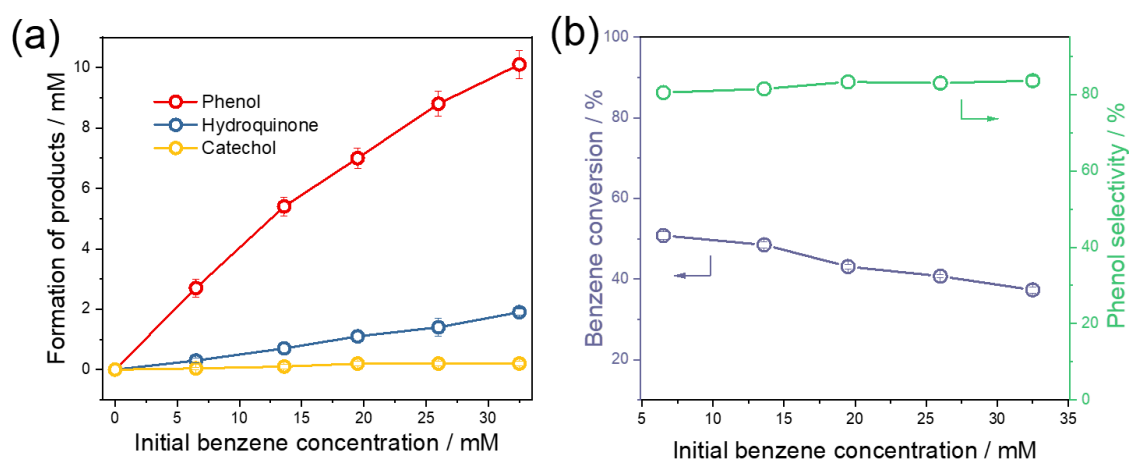


**Fig. 8.** Influence of initial benzene amount on (a)yield of products and (b) benzene conversion and phenol selectivity. Reaction condition: solution, mixture of water and acetonitrile (50 / 50); pH, 1; light source, 300 W xenon lamp; temperature, 10 °C; catalyst amount, 5 mM; reaction time, 24 h; under ambient condition.

Table 3 summarized the activities of photocatalysts for benzene oxidation to phenol reported so far [45,46]. There are several advantages of our reaction system. The current photocatalytic system showed higher phenol yield as compared with most reported aerobic systems, like Au-Pd/TiO$_2$ (30%) [17], TiO$_2$@MCF (14%) [24], Bi$_2$WO$_6$/CdWO$_4$ (7%) [25], Zn$_2$Ti-LDH (5%) [47], QuCN$^+$ (30%) [26] and [RuII(Me$_2$phen)$_3$]$^{2+}$ (30%) [22]. Unlike quinolinium ions and some other photocatalysts, H$_3$PW$_{12}$O$_{40}$ can be recycled after the reaction. Moreover, the phenol selectivity (80–90%) of the present photocatalytic system is comparable or higher than those of previously reported systems using Pt/WO$_3$ (69%)[16], TiO$_2$@MCF (35%) [24], Bi$_2$WO$_6$/CdWO$_4$ (99%) [25], Zn$_2$Ti-LDH (87%) [47], QuCN$^+$ (98%) [26].

**Table 3.**

Oxidation of benzene to phenol on different photocatalysts

| Entry | Catalyst | Oxidant | Noble metal | Reusability | Time (h) | Yield (%) | Sel. (%) | Ref. |
|---|---|---|---|---|---|---|---|---|
| 1 | Au-Pd/TiO$_2$ | O$_2$ | Yes | No | 6 | 30 | - | [17] |
| 2 | Pt/WO$_3$ | air | Yes | No | 4 | 51 | 69 | [16] |
| 3 | TiO$_2$@MCF | O$_2$ | None | No | 2 | 14 | 35 | [24] |
| 4 | Bi$_2$WO$_6$/CdWO$_4$ | O$_2$ | None | Yes | 3 | 7 | 99 | [25] |
| 5 | Zn$_2$Ti-LDH | air | None | Yes | 10 | 5 | 87 | [47] |
| 6 | QuCN$^{+\,a}$ | O$_2$ | None | No | 1 | 30 | 98 | [26] |
| 7 | [RuII(Me$_2$phen)$_3$]$^{2+\,a}$ | O$_2$ | None | No | 24 | 30 | - | [22] |
| 8 | H$_3$PW$_{12}$O$_{40}$$^b$ | **air** | None | Yes | 12 | 23 | 90 | This work |
| 9 | - | **air** | None | Yes | 24 | 41 | 80 | This work |

[a] Homogenous organic photocatalysts

[b] Homogenous inorganic photocatalyst

*Mechanism of photocatalytic benzene oxidation to phenol*

The above results prompted us to further investigate the mechanism of the reaction process. For this purpose, the benzene oxidation reaction under an anaerobic atmosphere was carried out to investigate the role of O$_2$ (Fig. 9). In this photoreaction, the catalyst color changes from colorless to blue, which visually indicates the reduction of H$_3$PW$_{12}$O$_{40}$. UV-VIS spectroscopic study revealed that strong intervalence charge-transfer (IVCT) absorption bands ($\lambda_{max}$: 498 nm, $\lambda_{max}$: 750 nm) appeared in the visible region, indicating the formation of heteropoly blue, the one-electron-reduced form of catalyst (PW$_{12}$O$_{40}$$^{4-}$) (Fig. 9) [48]. There was no formation of the two-electron-reduced form of H$_3$PW$_{12}$O$_{40}$, consistent with its much lower quantum yield than the one-electron-reduced form [49]. A saturation behavior was observed when the irradiation time is over 150 min. More importantly, the formation of PW$_{12}$O$_{40}$$^{4-}$ can be calculated from the molar absorption coefficient at 750 nm ($2 \times 10^3$ M$^{-1}$ cm$^{-1}$), as shown in Fig. 10. The time course profiles for phenol formation show that the phenol yield reached 1.7% at 240 min. The amount of phenol produced in this process was equivalent to half of the amount of PW$_{12}$O$_{40}$$^{4-}$ produced (Fig. 10). This result indicates that the two-electron-oxidation of benzene to phenol is associated with the formation of the one-electron reduced form of H$_3$PW$_{12}$O$_{40}$. The detailed reaction pathway will be discussed later.
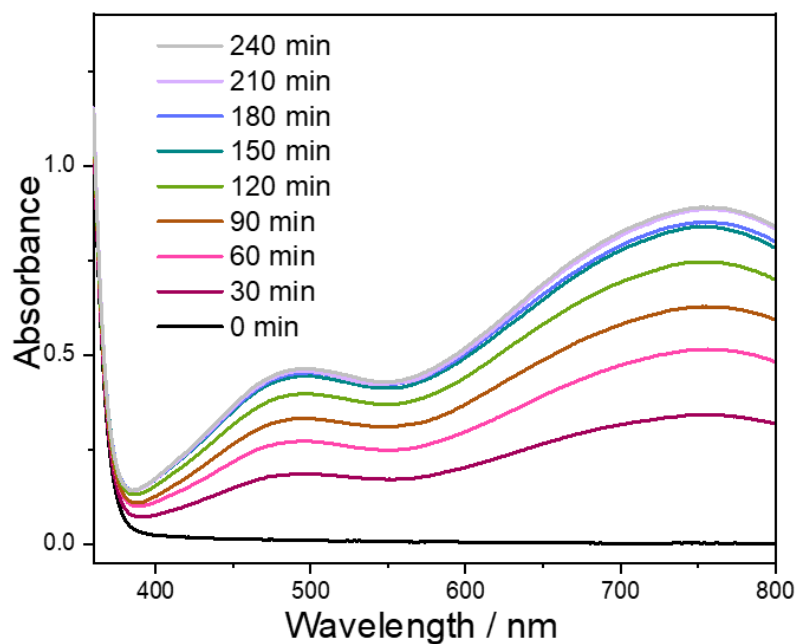
**Fig. 9.** UV–VIS spectra of the reaction solution after 30, 60, 90, 120, 150, 180, 210, 240 min of irradiation under argon. Solution: mixture of water and acetonitrile (50 / 50); pH, 1; light source, 300 W xenon lamp; temperature, 10 °C; initial benzene concentration: 13 mM, catalyst concentration: 5 mM.
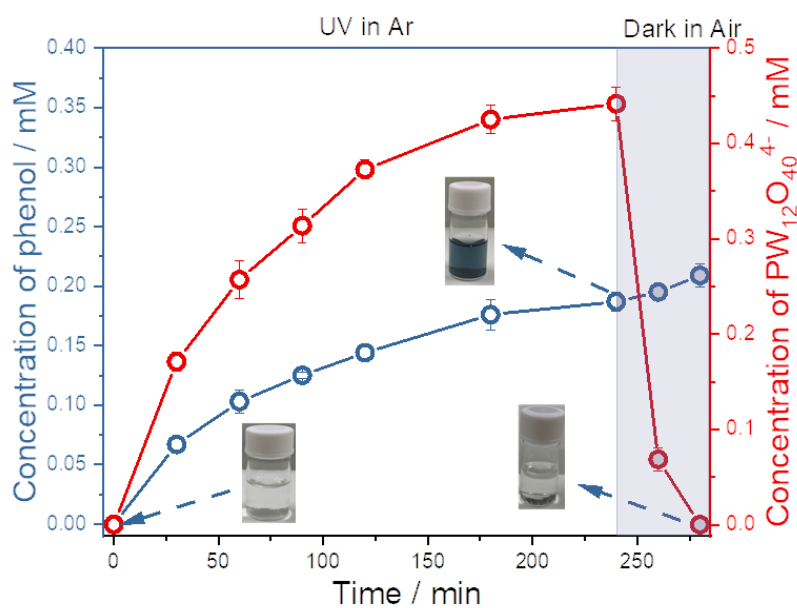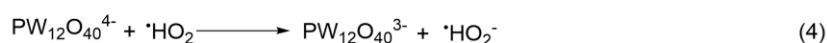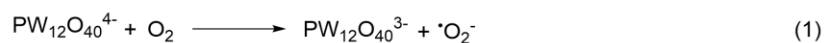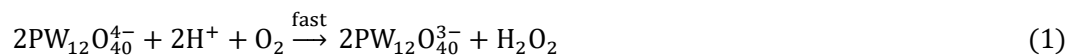


**Fig. 10.** Time course for the phenol formation under anaerobic condition. Reaction condition: solution, a mixture of water and acetonitrile (50 / 50); pH, 1; light source, 300 W xenon lamp; temperature, 10 °C; initial benzene concentration, 13 mM; catalyst concentration, 5 mM.

31
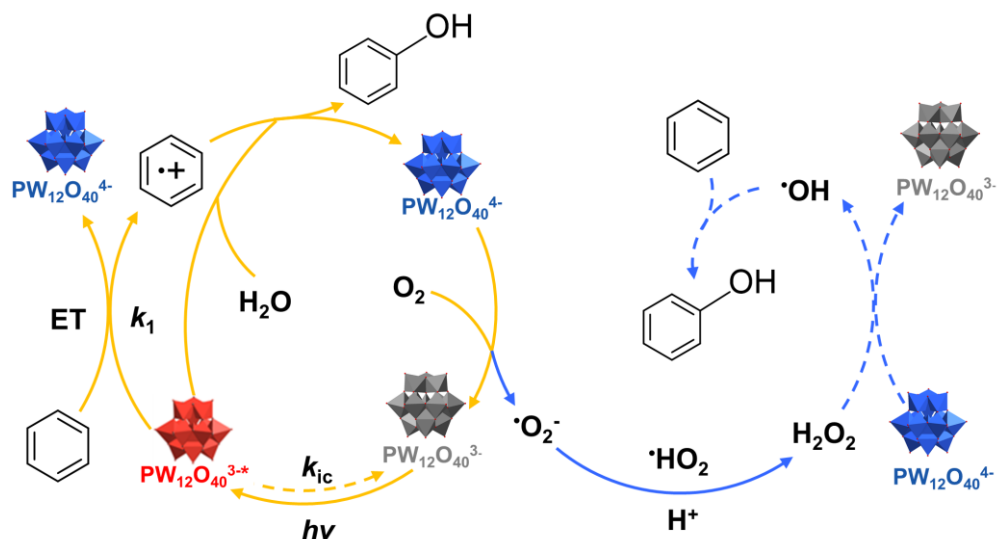
**Scheme 2.** Proposed mechanism of the photocatalytic oxidation of benzene to phenol with $O_2$.

In the absence of oxygen, no reoxidation of $PW_{12}O_{40}^{4-}$ to $PW_{12}O_{40}^{3-}$ was observed. However, $PW_{12}O_{40}^{4-}$ has been rapidly reoxidized to its original status in 40 min when the irradiation was stopped and the reaction system was exposed to air, as shown in Fig. 10. This reoxidation process of the catalyst was evidenced by the color change of the solution from blue to colorless and the disappearance of the IVCT bands in UV–visible spectra. The presence of oxygen can promote the reoxidation of $PW_{12}O_{40}^{4-}$, and this process can be described as follows (Scheme 2). According to previous studies, this reoxidation is a sequence of electron transfer steps with intermediate formation of $^{\bullet}O_2^-/^{\bullet}HO_2$ and $H_2O_2$, while comprehensive experimental and theoretical studies have unequivocally shown that the first step is electron transfer by an outer-sphere mechanism between $PW_{12}O_{40}^{4-}$ and $O_2$ (see in Eq. 1 and the detailed reaction pathway in Fig. 11) [50-52]. The proposed reaction pathway was shown in Fig.11, as supported by comprehensive experimental and theoretical studies in previous works. First, electron transfer between $PW_{12}O_{40}^{4-}$ and $O_2$ has been convincingly shown to occur by an outer-sphere mechanism to form superoxide radical ($^{\bullet}O_2^-$). Because the solution in our case is highly acidic (pH~1), the generated $^{\bullet}O_2^-$ can be rapidly transformed to a superoxide intermediate ($^{\bullet}HO_2$) in the presence of $H^+$. Subsequently, the $^{\bullet}HO_2$ can cause spontaneous disproportionation to give $H_2O_2$ and $O_2$. In addition, the $^{\bullet}HO_2$ could also reoxidize $PW_{12}O_{40}^{4-}$ to give $H_2O_2$. All these reactions showed the product of the reaction between $PW_{12}O_{40}^{4-}$ and $O_2$ to be $H_2O_2$, consist with the reaction stoichiometry.

Notably, the generation of $H_2O_2$ was confirmed in our system, consistent with previous work (Fig. 12).

$$2PW_{12}O_{40}^{4-} + 2H^+ + O_2 \xrightarrow{fast} 2PW_{12}O_{40}^{3-} + H_2O_2 \qquad (1)$$

$$PW_{12}O_{40}^{4-} + O_2 \longrightarrow PW_{12}O_{40}^{3-} + {}^\bullet O_2^- \qquad (1)$$

$${}^\bullet O_2^- + H^+ \longrightarrow {}^\bullet HO_2 \qquad (2)$$

$${}^\bullet HO_2 + {}^\bullet HO_2 \longrightarrow H_2O_2 + O_2 \qquad (3)$$

$$PW_{12}O_{40}^{4-} + {}^\bullet HO_2 \longrightarrow PW_{12}O_{40}^{3-} + {}^\bullet HO_2^- \qquad (4)$$

$${}^\bullet HO_2^- + H^+ \longrightarrow H_2O_2 \qquad (5)$$

$$2PW_{12}O_{40}^{4-} + 2H^+ + O_2 \longrightarrow 2PW_{12}O_{40}^{3-} + H_2O_2 \qquad (6)$$

**Fig. 11.** Schematic description of reaction route of reoxidation of $PW_{12}O_{40}^{4-}$ with $O_2$
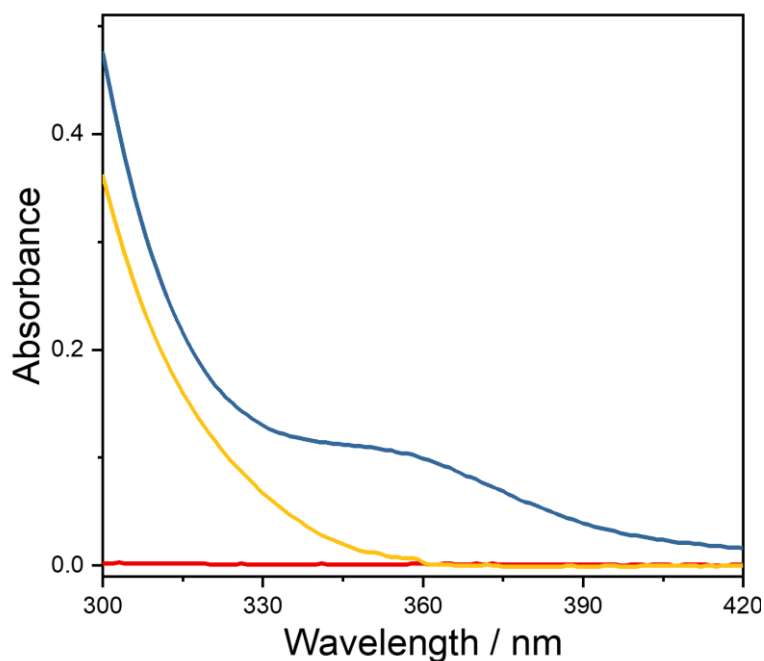


**Fig. 12.** UV-VIS spectra: aqueous solution of NaI (0.1 M) before (black line) and after (red) addition of a solution of the product mixture; diluted solution (blue line) of the product mixture

The generated $H_2O_2$ can accept an electron from $PW_{12}O_{40}^{4-}$ to give ${}^\bullet OH$ and $PW_{12}O_{40}^{3-}$ (Eq. 2). Then, generated ${}^\bullet OH$ can attack benzene to give phenol (Eq. 3) [12].

33

$$H_2O_2 + PW_{12}O_{40}^{4-} + H^+ \rightarrow \ ^\bullet OH + PW_{12}O_{40}^{3-} + H_2O \qquad (2)$$

$$Benzene + 2 \ ^\bullet OH \rightarrow Phenol + H_2O \qquad (3)$$
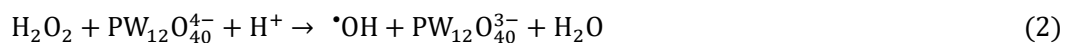
The phenol formation from competitive reaction with $PW_{12}O_{40}^{3-}$ (Eq. 4) was excluded because no phenol was generated in the mixture of benzene, $H_2O_2$ in $PW_{12}O_{40}^{3-}$ solution under dark.

$$PW_{12}O_{40}^{3-} + H_2O_2 + 3/2 Benzene \rightarrow PW_{12}O_{40}^{4-} + H^+ + 1/2H_2O + 3/2Phenol \qquad (4)$$

The reaction route of $H_2O_2$ in our system hence is believed to follow Eq.2 and 3. This $H_2O_2$ induced phenol formation process is generally involved in Fenton-like catalytic systems and the reported semiconductor-based photocatalytic systems, and organic homogenous photocatalytic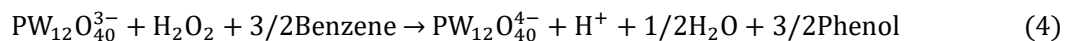 systems [22,25]. Hence, phenol is generated in both the photocatalyst reduction and reoxidation process in our system (Scheme 2), which is consistent with the result in Fig. 6. However, the amount of phenol produced in the reoxidation process was much less significant. The previous reports have shown that the reoxidation of $PW_{12}O_{40}^{4-}$ with $H_2O_2$ is kinetically slower than that with $O_2$ [50-52]. Hence, it is reasonable that the reoxidation with $O_2$ was dominated rather than that with $H_2O_2$ in the reoxidation process.

To investigate the contribution of benzene formation reaction in the reoxidation process from $PW_{12}O_{40}^{4-}$ to $PW_{12}O_{40}^{3-}$ in our system, we carried out photocatalytic benzene oxidation by adding $H_2O_2$ in an argon atmosphere instead of exposing it to air (Fig. 13). The result shows that the phenol generated with time, accompanied by the reoxidation of $PW_{12}O_{40}^{4-}$ to $PW_{12}O_{40}^{3-}$. However, the selectivity of phenol in this reaction (35%) was much lower than that of the reaction using $O_2$ as the oxidant. In the oxidation of aromatic hydrocarbons, $^\bullet OH$ radicals have been reported to exhibit high activity and low selectivity [53,54]. Therefore, in the presence of excess $^\bullet OH$ produced by the decomposition of $H_2O_2$, peroxidation and side reactions of phenol may have occurred, resulting in a lower yield and selectivity of phenol. The lower phenol selectivity using $H_2O_2$ as an oxidant confirms that the reoxidation of $PW_{12}O_{40}^{4-}$ with $O_2$, but not with $H_2O_2$, is the dominant route in our system.
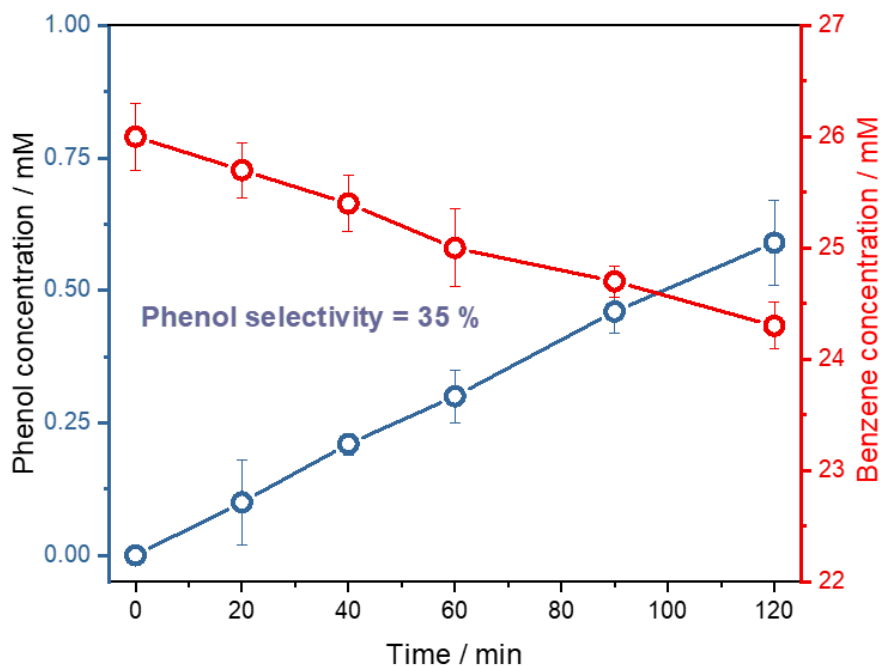
**Fig. 13.** Time course of photocatalytic oxidation of benzene over $H_3PW_{12}O_{40}$ using $H_2O_2$ as oxidant. Reaction condition: solution, 100 mM of $H_2O_2$ aqueous solution and acetonitrile (50 / 50); benzene concentration, 24 mM; pH, 1; light source, 300 W xenon lamp; temperature, 10 °C; concentration of catalyst, 5 mM; argon atmosphere.

*Effect of acetonitrile addition*

The proposed process for photocatalytic benzene oxidation using $H_3PW_{12}O_{40}$ is shown in Scheme 3a. As mentioned above, we have observed that our system produces negligible amounts of biphenyl and $CO_2$. More importantly, phenol oxidation was suppressed in the photoreaction with $H_3PW_{12}O_{40}$ in aqueous acetonitrile solutions. We suppose this suppressed overoxidation of phenol is ascribed to acetonitrile in the solution. To verify this assumption, we used phenol as the initial substrate instead of benzene.
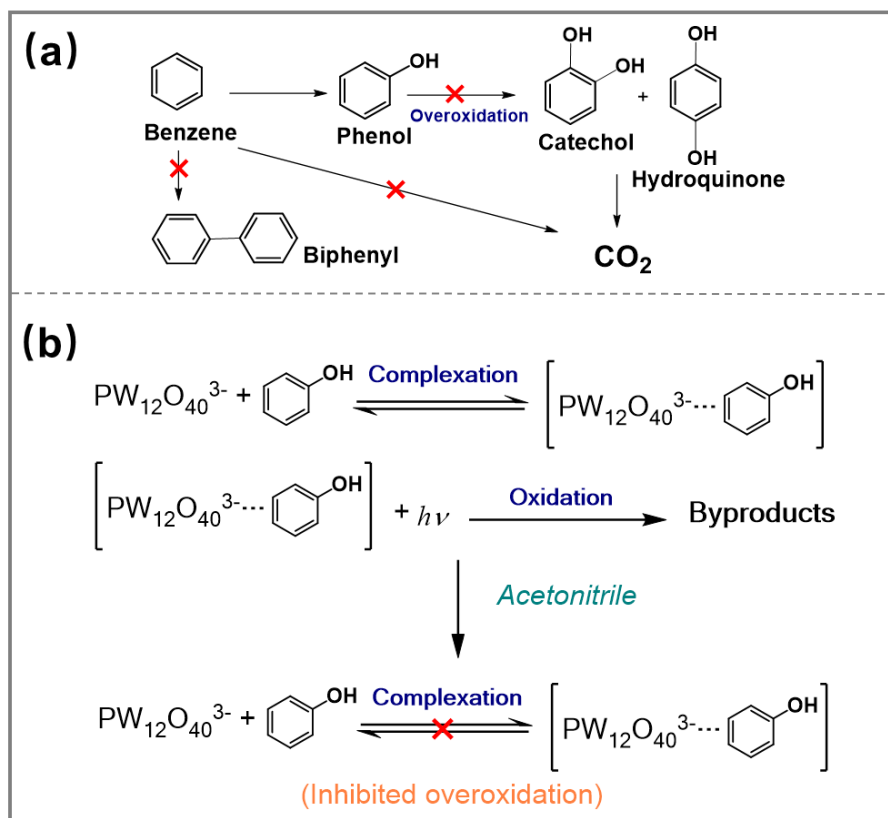
**Scheme 3.** (a) Photocatalytic oxidation pathways of benzene. (b) The inhibited overoxidation of phenol by adding acetonitrile. The crosses indicate the unwanted reaction pathways.

As shown in Fig.14a, there is no significant consumption of phenol even after 24 hours in an aerated aqueous acetonitrile solution (50 vol%, red line). As a comparison, 60% of phenol has been decomposed when using pure water as a solvent with no other conditions changed (blue line). The inhibited phenol oxidation by adding acetonitrile will be discussed as follows. Previous studies showed a strong complexation of $PW_{12}O_{40}^{3-}$ with several substrates, including alcohols, 4-chlorophenol, and trifluoroacetic acid, which is essential for the following photochemical oxidation reaction [49,55,56]. Herein, the complexation of $PW_{12}O_{40}^{3-}$ with phenol was also evidenced with the band in the $\lambda > 360$ nm region in UV-VIS spectra (Fig. 14b and Fig. 15), consistent with the assignment for the primary electronic transition as a ligand-to-metal charge-transfer (LMCT) band. This finding means that a precomplexation process is also an important step for phenol oxidation. However, the absorbance of these bands decreased with an increase in acetonitrile concentration, indicating that the addition of acetonitrile significantly inhibited the complexation of $PW_{12}O_{40}^{3-}$

with phenol (Scheme 3b).
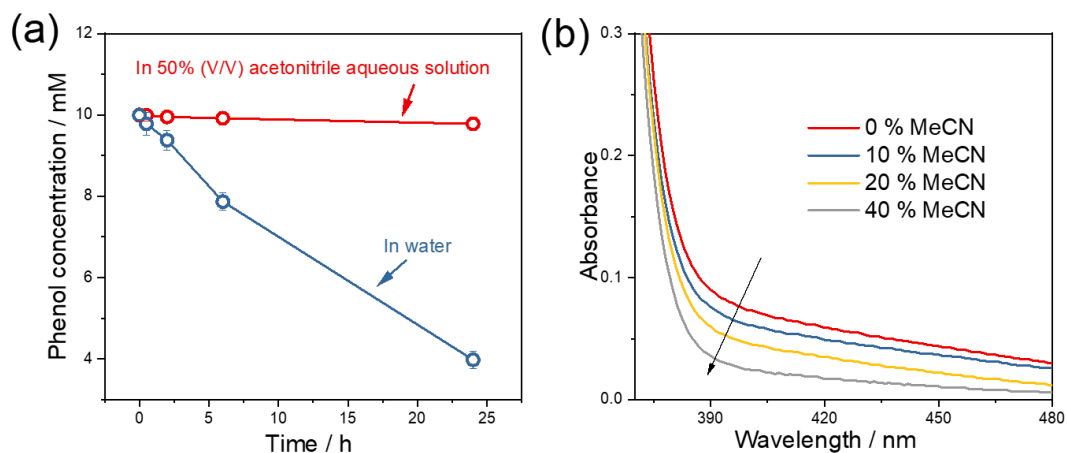


**Fig. 14.** (a) Time course for phenol decomposition in acetonitrile solution (50 vol%, red line) and water (blue line). Reaction condition: pH, 1; light source, 300 W xenon lamp; temperature, 10 °C; initial phenol concentration, 10 mM; catalyst concentration, 5 mM; under ambient condition. (b) Changes in the UV-VIS absorption spectra of $H_3PW_{12}O_{40}$ in aqueous solution on the concentration of acetonitrile. concentration of $H_3PW_{12}O_{40}$, 7.5 mM; concentration of phenol, 16.5 mM; concentration of acetonitrile (0, 10 %, 20 % and 40 %, V/V).
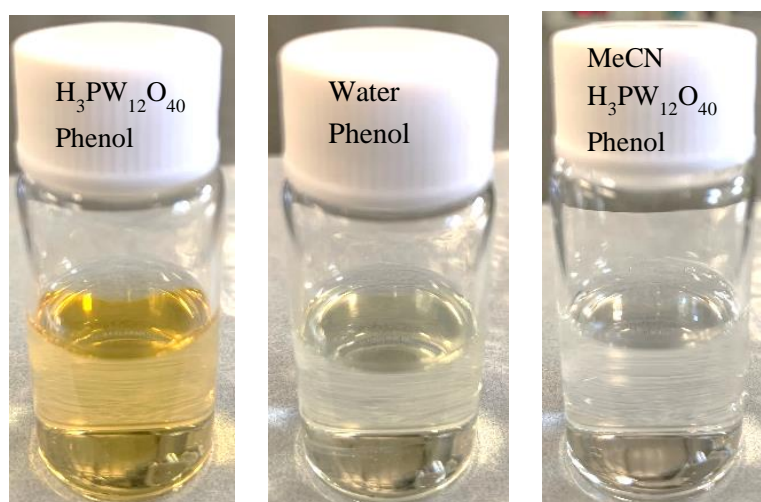


**Fig. 15.** Images of phenol in different aqueous solution

To further investigate the effect of acetonitrile on benzene photooxidation, we compared the reactivity of excited $PW_{12}O_{40}^{3-}$ in acetonitrile and aqueous solutions. The rate of ethanol oxidation with $PW_{12}O_{40}^{3-}$ was compared in an ethanol/water solution and ethanol/acetonitrile solution (50 % V/V) under argon atmosphere. In this reaction, the precomplexation process can be ignored because it can easily bind to $PW_{12}O_{40}^{3-}$. As shown in Fig. 16, the amount of generated heteropoly blue in

37

ethanol/acetonitrile solution is significantly lower than in ethanol/water. This finding suggests that the rate of electron transfer from substrate to excited $PW_{12}O_{40}^{3-}$ was greater in water than in acetonitrile. Another possibility about the suppressed reaction is that acetonitrile may decrease the lifetime of the excited state of $PW_{12}O_{40}^{3-}$ ($PW_{12}O_{40}^{3-*}$), because the solvents may have a great influence on the lifetime of excited states of reactants [57].
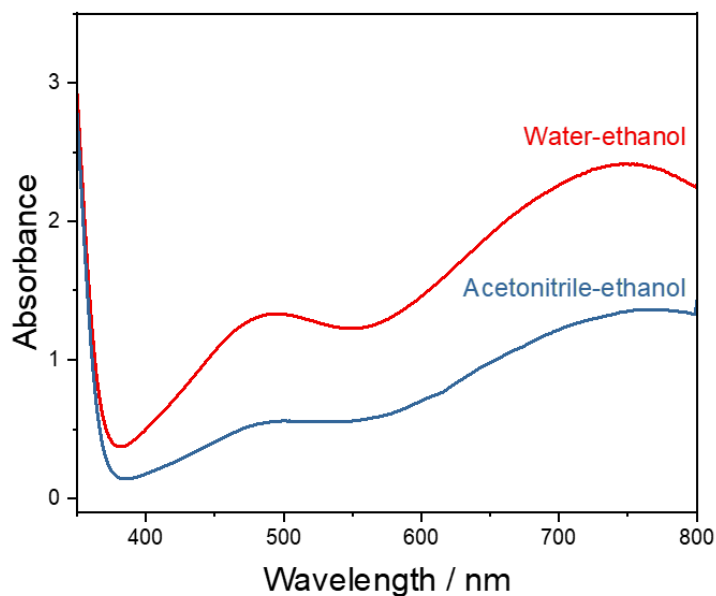


**Fig. 16.** UV–VIS spectra of the water-ethanol mixture and acetonitrile-water mixture after irradiation for 5 min. pH, 1; light source, 300 W xenon lamp; temperature, 10 °C; catalyst concentration: 5 mM; argon atmosphere.

*Kinetic analysis*

Fig. 17(a) shows the dependence of the initial rate for phenol formation ($r_0$) on the catalyst concentration at a certain initial benzene concentration ([benzene]$_0$). As the concentration of $H_3PW_{12}O_{40}$ increases, the amount of phenol produced increases monotonically. The result indicates that the increasing number of active sites promotes the oxidation of benzene to phenol. However, as the catalyst concentration increased above 5 mM, the initial rate was almost saturated. As the catalyst concentration increases, the amount of excited state of catalyst increased, and the rate of benzene oxidation increased. However, when the catalyst concentration was too high, all the light from the light source was absorbed, and the amount of photoexcited catalyst was saturated, resulting in a saturated reaction rate. The reaction rates also increased with [benzene]$_0$ and then almost

saturated at a concentration of 160 mM benzene (Fig. 17b). This kinetic tendency indicates the Langmuir–Hinshelwood (L-H) mechanism where precomplexation between heteropoly anion $PW_{12}O_{40}^{3-}$ and substrate occurs before excitation of the catalyst or diffusion encounter mechanism where photoexcited $PW_{12}O_{40}^{3-}$ encounters a benzene molecule and undertakes a redox reaction [58]. The reciprocal plots show a linear correlation, as shown in Fig. 17 (c and d), in which the linear dependence $R^2$ is greater than 0.98.
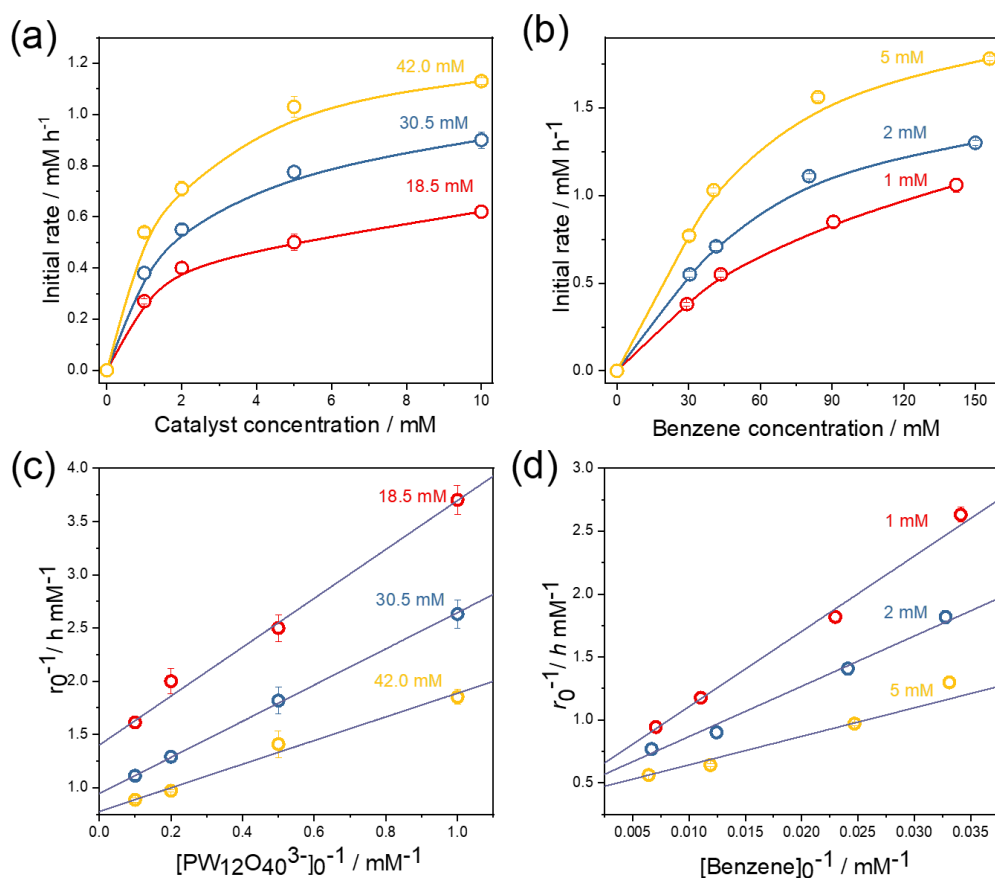


**Fig. 17.** (a) Dependence of initial rate $r_0$ on catalyst concentration $[PW_{12}O_{40}^{3-}]_0$ at 18.5 mM, 30.5 mM, and 42.5 mM of the initial benzene concentration $[benzene]_0$ (b) Dependence of initial rate $r_0$ on benzene concentration $[benzene]_0$ at 1 mM, 2 mM, and 5 mM of catalyst concentration $[PW_{12}O_{40}^{3-}]_0$. (c) Plot of $1/r_0$ versus $1/[benzene]_0$. (d) The plot of $1/r_0$ versus $1/[PW_{12}O_{40}^{3-}]_0$. Reaction condition: solution, mixture of water and acetonitrile (50 / 50); pH, 1; light source, 300 W xenon lamp; temperature, 10 °C; under ambient condition.

As stated above, phenol oxidation over $H_3PW_{12}O_{40}$ in an aqueous solution is initialed by a precomplexation, evidenced by an absorption band in UV-VIS spectra. However, no complexation process was observed when using benzene as substrate instead of phenol. Fox and coworkers

pointed out that the tightness of the association between substrates and $PW_{12}O_{40}^{3-}$ parallels their polarity [56]. The impact of substrate polarity is convincible, although the detailed mechanism for the complexation remains obscure. Hence, benzene showed no such complexation due to the lack of polar groups. Accordingly, the precomplexation mechanism based on L-H kinetics can be excluded, and the diffusion encounter mechanism can account for the none-precomplexation in benzene oxidation. Accordingly, benzene oxidation over $PW_{12}O_{40}^{3-}$ is initialed by the activation of $PW_{12}O_{40}^{3-}$ without precomplexation. In this step, O→M LMCT from the $O_2^-$ - based HOMO to the $W_6^+$ - based LUMO can be triggered under UV light irradiation, which leads to the formation of the photoexcited state of $PW_{12}O_{40}^{3-}$ ($PW_{12}O_{40}^{3-*}$) [59]. $PW_{12}O_{40}^{3-*}$ encounters benzene to form an exciplex before deactivation ($k_{ic}$), and subsequently, benzene is hydroxylated ($k_1$) according to the following equation (Eq. 5-7).

$$PW_{12}O_{40}^{3-} \xrightarrow{I\Phi,h\nu} PW_{12}O_{40}^{3-*} \tag{5}$$

$$PW_{12}O_{40}^{3-*} \xrightarrow{k_{ic}} PW_{12}O_{40}^{3-} \tag{6}$$

$$\text{Benzene} + PW_{12}O_{40}^{3-*} \xrightarrow{k_1,\text{ET}} \text{Benzene}^{\bullet+} + PW_{12}O_{40}^{4-} \tag{7}$$
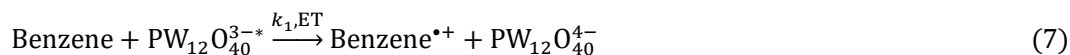
Here, $I$ refer to the quantity of light absorbed, $\Phi$ is the quantum efficiency for the catalyst excitation. Neumann and coworkers reported that the excited vanadium-substituted heteropolyacid could activate the C−H bond in benzene via the ET mechanism in the thermal catalytic system [60]. We propose a benzene oxidation reaction on $PW_{12}O_{40}^{3-*}$ also involved this ET step since this vanadate is structurally analogous to our tungstate. The electron transfer from benzene molecular to $PW_{12}O_{40}^{3-*}$ occurs, forming the benzene cation radical ($k_1$), which is rapidly hydroxylated to phenol (Eq. 8). The amount of reacted $PW_{12}O_{40}^{3-}$ is almost twice the amount of generated phenol from the stoichiometry of this pathway, showing a good agreement with the result in Fig. 10.

$$\text{Benzene}^{\bullet+} + PW_{12}O_{40}^{3-} + H_2O \xrightarrow{\text{fast}} \text{Phenol} + PW_{12}O_{40}^{4-} + 2H^+ \tag{8}$$
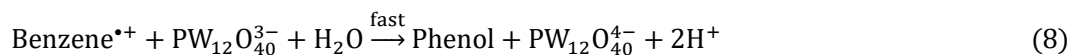
From reactions 5-7 (reactions 8 is too fast to interfere), applying the steady-state approximation for $PW_{12}O_{40}^{3-}$, we obtain rate expression from reaction 9:
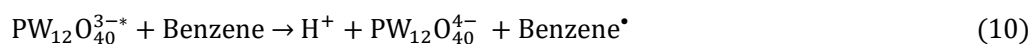
$$r = \frac{d[PW_{12}O_{40}^{3-}]}{dt} = \frac{k_1[benzene]_0 I\Phi}{k_{ic} + k_1[benzene]_0} \tag{9}$$

From the reciprocal plot in Fig. 17, the reaction parameters were obtained and summarized in Table 4.

**Table 4.** Kinetic parameters of benzene oxidation to phenol

| Entry | $[PW_{12}O_{40}{}^{3-}]$ / mM | $I\Phi$ / $h^{-1}$ | $k_{ic}{}^{-1} k_1$ / $mM^{-1}$ | $R^2$ |
|-------|-------|-------|-------|-------|
| 1 | 1 | 2.08 | 0.0079 | 0.997 |
| 2 | 2 | 2.27 | 0.1074 | 0.995 |
| 3 | 5 | 2.94 | 0.1259 | 0.989 |

Photoexcited heteropolyacids react with organic species by the HT mechanism, in which the abstraction of the hydrogen atom directly generates a radical intermediate. In this way, for example, a phenyl radical will be generated after the HT process, leading to the following oxidation reaction (Eq. 10,11).

$$PW_{12}O_{40}^{3-*} + Benzene \rightarrow H^+ + PW_{12}O_{40}^{4-} + Benzene^{\bullet} \tag{10}$$

$$Benzene^{\bullet} + PW_{12}O_{40}^{3-} + H_2O \rightarrow Phenol + PW_{12}O_{40}^{4-} + H^+ \tag{11}$$

Hence, to further confirm that the C−H bond activation by $PW_{12}O_{40}{}^{3-*}$ obeys the ET mechanism, we examined the kinetic isotope effect (KIE). The KIE was defined as $k_H/k_D$, in which $k_H$ ($k_1$) and $k_D$ are the rate constants for the benzene oxidation reaction conducted over benzene and benzene-$d_6$, respectively. Fig. 18 shows the dependence of initial rate $r_0$ on the initial benzene concentration $[benzene]_0$ by using benzene and benzene-$d_6$, respectively. From the reciprocal plots, as shown in Fig. 19, the KIE value was determined to be 1.15. This value might have been due to secondary kinetic isotope effects, indicating the ET mechanism dominated our reaction system. Comparably, Kochi and coworkers obtained a comparable value (1.05) in benzene oxidation with cobalt (III) trifluoroacetate by ET mechanism [44]. A reasonable explanation is that the HT is more likely involved in the oxidation of species with easily removable hydrogen atoms, e.g., alcohols. Since the C−H bond in benzene is so strong, ET to produce a radical cation from a benzene molecule is considered a more likely route than the direct abstraction of a hydrogen atom.
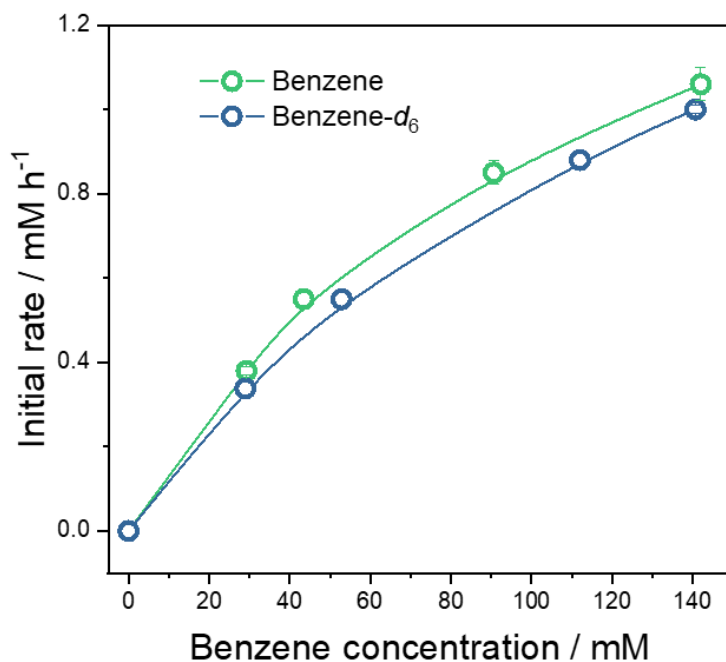
**Figure 18.** Dependence of initial rate $r_0$ on benzene amount [benzene]$_0$ Reaction condition: catalyst amount, 5 mM; solution, mixture of water and acetonitrile (50 / 50); pH, 1; light source, 300 W xenon lamp; temperature, 10 °C; under ambient condition.
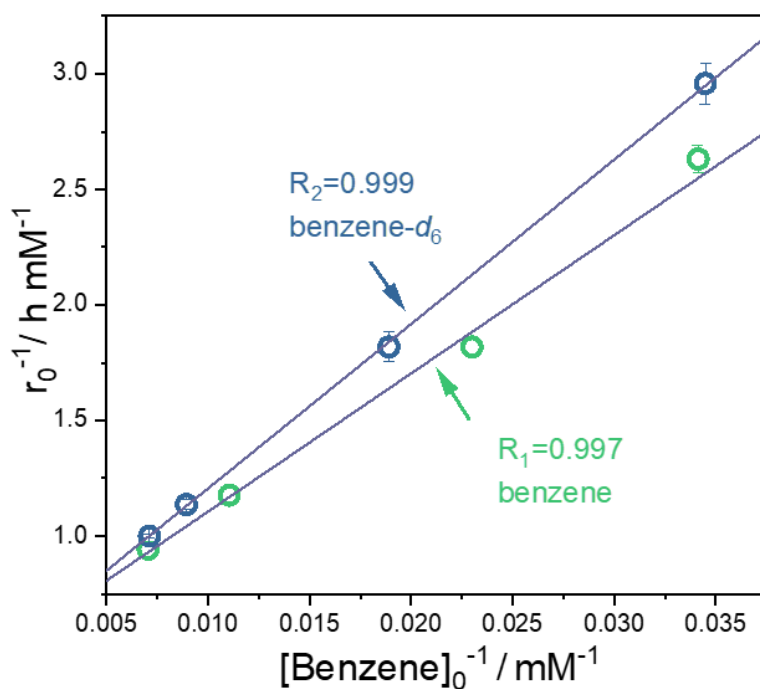


**Fig. 19.** Plot of $1/r_0$ versus 1/[benzene]$_0$. and 1/[benzene-$d_6$]$_0$. Reaction condition: catalyst concentration, 5 mM; solution, mixture of water and acetonitrile (50 / 50); pH, 1; light source, 300 W xenon lamp; temperature, 10 °C; under ambient condition.

Based on the above results, we can understand that the photochemical benzene oxidation over $H_3PW_{12}O_{40}$ in an aqueous solution is mechanically different from phenol oxidation. On the one hand, the precomplexation process of phenol and photocatalyst is essential for the following photochemical oxidation of phenol; on the other hand, it is not involved in the benzene oxidation reaction. This difference ensures that the phenol overoxidation has been significantly inhibited by adding acetonitrile into the solvent, although benzene oxidation is also suppressed to some extent. Hence, benzene can be oxidized, but phenol can not be oxidized over $H_3PW_{12}O_{40}$ in our system. As a result, a high phenol yield and unusual selectivity have been achieved.

**2.4 Conclusion**

In summary, we found that benzene can directly and significantly be oxidized to phenol with $O_2$ under ambient conditions by using heteropolyacid $H_3PW_{12}O_{40}$ as an inorganic photocatalyst. The addition of acetonitrile into solvent can significantly inhibit the overoxidation of phenol. Mechanic studies and control experiments revealed the different reaction processes are involved in benzene oxidation and phenol oxidation, which plays a key role in this unusual selective oxidation of benzene to phenol. This study highlights heteropolyacid $H_3PW_{12}O_{40}$ as promising photocatalysts for benzene oxidation due to several merits, including commercial availability with low price, utilization of air, high stability, easy recyclability, and high performance. The present work reported a superior inorganic photocatalyst for benzene oxidation to phenol with $O_2$ and opened a new avenue to apply heteropolyacid in photocatalytic organic synthesis.

**References**

[1] R. Molinari, T. Poerio, Remarks on studies for direct production of phenol in conventional and membrane reactors, Asia-Pac J. Chem. Eng. 5 (2010) 191–206, https://doi.org/10.1002/apj.369.

[2] Y. Morimoto, S. Bunno, N. Fujieda, H. Sugimoto, S. Itoh, Direct hydroxylation of benzene to phenol using hydrogen peroxide catalyzed by nickel complexes supported by pyridylalkylamine ligands, J. Am. Chem. Soc. 137 (2015) 5867–5870, https://doi.org/10.1021/jacs.5b01814.

[3] S. Muthuramalingam, K. Anandababu, M. Velusamy, R. Mayilmurugan, One step phenol synthesis from benzene catalysed by nickel(ii) complexes, Catal. Sci. Technol. 9 (2019) 5991–6001, https://doi.org/10.1039/C9CY01471C.

[4] J.-H. Yang, G. Sun, Y. Gao, H. Zhao, P. Tang, J. Tan, A.-H. Lu, D. Ma, Direct catalytic oxidation of benzene to phenol over metal-free graphene-based catalyst, Energ. & Environ. Sci. 6 (2013), https://doi.org/10.1039/C3EE23623D.

[5] L. Meng, X. Zhu, E.J.M. Hensen, Stable Fe/ZSM-5 nanosheet zeolite catalysts for the oxidation of benzene to phenol, ACS Catal. 7 (2017) 2709–2719, https://doi.org/10.1021/acscatal.6b03512.

[6] Y. Leng, J. Liu, P. Jiang, J. Wang, Organometallic-polyoxometalate hybrid based on V-Schiff base and phosphovanadomolybdate as a highly effective heterogenous catalyst for hydroxylation of benzene, Chem. Eng. J. 239 (2014) 1–7, https://doi.org/10.1016/j.cej.2013.10.092.

[7] S. Gopalakrishnan, J. Munch, R. Herrmann, W. Schwieger, Effects of microwave radiation on one-step oxidation of benzene to phenol with nitrous oxide over Fe-ZSM-5 catalyst, Chem. Eng. J. 120 (2006) 99–105, https://doi.org/10.1016/j.cej.2006.03.017.

[8] X. Chen, J. Zhang, X. Fu, M. Antonietti, X. Wang, Fe-g-$C_3N_4$-catalyzed oxidation of benzene to phenol using hydrogen peroxide and visible light, J. Am. Chem. Soc. 131 (2009) 11658–11659, https://doi.org/10.1021/ja903923s.

[9] C. Guo, W. Du, G. Chen, L. Shi, Q. Sun, Influence of temperature on hydroxylation of benzene to phenol using molecular oxygen catalyzed by $V/SiO_2$, Catal. Commun. 37 (2013) 19–22, https://doi.org/10.1016/j.catcom.2013.03.018.

[10] A. Okemoto, Y.-h. Tsukano, A. Utsunomiya, K. Taniya, Y. Ichihashi, S. Nishiyama, Selective catalytic oxidation of benzene over Cu/Ti/HZSM-5 under low oxygen pressure for one step synthesis of phenol, J. Mol. Catal. A: Chem. 411 (2016) 372–376, https://doi.org/10.1016/j.molcata.2015.11.007.

[11] W. Wang, N. Li, L. Shi, Y. Ma, X. Yang, Vanadium-zirconium catalyst on different support for hydroxylation of benzene to phenol with $O_2$ as the oxidant, Appl. Catal. A: Gen. 553 (2018) 117–125, https://doi.org/10.1016/j.apcata.2018.01.005.

[12] W. Wang, H. Tang, X. Jiang, F.E. Huang, Y. Ma, Quinone-amine polymers as metal-free and reductant-free catalysts for hydroxylation of benzene to phenol with molecular oxygen, Chem. Commun. 55 (2019) 7772–7775, https://doi.org/10.1039/C9CC03623G.

[13] Z. Long, G. Chen, S. Liu, F. Huang, L. Sun, Z. Qin, Q. Wang, Y. Zhou, J. Wang, Synergistic combination of graphitic $C_3N_4$ and polyoxometalate-based phase-transfer catalyst for highly efficient reductant-free aerobic hydroxylation of benzene, Chem. Eng. J. 334 (2018) 873–881, https://doi.org/10.1016/j.cej.2017.10.083.

[14] Z. Long, Y. Zhou, G. Chen, P. Zhao, J. Wang, 4,4′-Bipyridine-modified molybdovanadophosphoric acid: A reusable heterogeneous catalyst for direct hydroxylation of benzene with $O_2$, Chem. Eng. J. 239 (2014) 19–25, https://doi.org/10.1016/j.cej.2013.10.103.

[15] Y. Ide, M. Torii, T. Sano, Layered silicate as an excellent partner of a $TiO_2$ photocatalyst for efficient and selective green fine-chemical synthesis, J. Am. Chem. Soc. 135 (2013) 11784–11786, https://doi.org/10.1021/ja406855e.

[16] O. Tomita, B. Ohtani, R. Abe, Highly selective phenol production from benzene on a platinum-loaded tungsten oxide photocatalyst with water and molecular oxygen: selective oxidation of water by holes for generating hydroxyl radical as the predominant source of the hydroxyl group, Catal. Sci. Technol. 4 (2014) 3850–3860, https://doi.org/10.1039/C4CY00445K.

[17] R. Su, L. Kesavan, M.M. Jensen, R. Tiruvalam, Q. He, N. Dimitratos, S. Wendt, M. Glasius, C.J. Kiely, G.J. Hutchings, F. Besenbacher, Selective photocatalytic oxidation of benzene for the synthesis of phenol using engineered Au-Pd alloy nanoparticles supported on titanium dioxide, Chem. Commun. 50 (2014) 12612–12614, https://doi.org/10.1039/C4CC04024D.

[18] P. Devaraji, N.K. Sathu, C.S. Gopinath, Ambient oxidation of benzene to phenol by photocatalysis on $Au/Ti_{0.98}V_{0.02}O_2$: role of holes, ACS Catal. 4 (2014) 2844–2853, ttps://doi.org/10.1021/cs500724z.

[19] O.V. Dorofeeva, O.N. Ryzhova, Enthalpy of formation and O–H bond dissociation enthalpy of phenol: inconsistency between theory and experiment, J. Phys. Chem. A 120 (2016) 2471–2479, https://doi.org/10.1021/acs.jpca.6b02233.

[20] G.E. Davico, V.M. Bierbaum, C.H. DePuy, G. B. Ellison, R.R. Squires, The C—H bond energy of benzene, J. Am. Chem. Soc. 117 (1995) 2590–2599, https://doi.org/10.1021/ja00114a023.

[21] Z. Zheng, B. Huang, X. Qin, X. Zhang, Y. Dai, M.-H. Whangbo, Facile in situ synthesis of visible-light plasmonic photocatalysts $M@TiO_2$ (M = Au, Pt, Ag) and evaluation of their photocatalytic oxidation of benzene to phenol, J. Mater. Chem. 21 (2011) 9079–9087,

https://doi.org/10.1039/C1JM10983A.

[22] J.W. Han, J. Jung, Y.M. Lee, W. Nam, S. Fukuzumi, Photocatalytic oxidation of benzene to phenol using dioxygen as an oxygen source and water as an electron source in the presence of a cobalt catalyst, Chem. Sci. 8 (2017) 7119–7125, https://doi.org/10.1039/C7SC02495A.

[23] K. Ohkubo, A. Fujimoto, S. Fukuzumi, Visible-light-induced oxygenation of benzene by the triplet excited state of 2,3-dichloro-5,6-dicyano-p-benzoquinone, J. Am. Chem. Soc. 135 (2013) 5368–5371, https://doi.org/10.1021/ja402303k.

[24] G. Zhang, J. Yi, J. Shim, J. Lee, W. Choi, Photocatalytic hydroxylation of benzene to phenol over titanium oxide entrapped into hydrophobically modified siliceous foam, Appl. Catal. B: Environ. 102 (2011) 132–139, https://doi.org/10.1016/j.apcatb.2010.11.034.

[25] P. Chen, L. Chen, Y. Zeng, F. Ding, X. Jiang, N. Liu, C.-T. Au, S.-F. Yin, Three-dimension hierarchical heterostructure of $CdWO_4$ microrods decorated with $Bi_2WO_6$ nanoplates for high-selectivity photocatalytic benzene hydroxylation to phenol, Appl. Catal. B: Environ. 234 (2018) 311–317, https://doi.org/10.1016/j.apcatb.2018.04.028.

[26] K. Ohkubo, T. Kobayashi, S. Fukuzumi, Direct oxygenation of benzene to phenol using quinolinium ions as homogeneous photocatalysts, Angew. Chem. Int. Edit. 50 (2011) 8652–8655, https://doi.org/10.1002/ange.201102931.

[27] Y. Gu, Q. Li, D. Zang, Y. Huang, H. Yu, Y. Wei, Light-induced efficient hydroxylation of benzene to phenol by quinolinium and polyoxovanadate-based supramolecular catalysts, Angew. Chem. Int. Edit. 59 (2020) 2–9, https://doi.org/10.1002/anie.202011164.

[28] E. Coronado, C.J. Go´mez-Garcı´a, Polyoxometalate-based molecular materials, J. Am. Chem. Soc. 98 (1998) 273−296, https://doi.org/10.1021/cr970471c.

[29] S.S. Wang, G.Y. Yang, Recent advances in polyoxometalate-catalyzed reactions, Chem. Rev. 115 (2015) 4893–4962, https://doi.org/10.1021/cr500390v.

[30] G. Marcì, E.I. García-López, L. Palmisano, Heteropolyacid-based materials as heterogeneous photocatalysts, Eur. J. Inorg. Chem. 2014 (2014) 21–35, https://doi.org/10.1002/ejic.201300883.

[31] E. Papaconstantinou, Photochemistry of polyoxometallates of molybdenum and tungsten and/or vanadium, Chem. Soc. Rev. 18 (1989) 1–31, https://doi.org/10.1039/CS9891800001.

[32] B. Yang, J.J. Pignatello, D. Qu, B. Xing, Reoxidation of photoreduced polyoxotungstate ($[PW_{12}O_{40}]^{4-}$) by different oxidants in the presence of a model pollutant. Kinetics and reaction mechanism, J. Phys. Chem. A 119 (2015) 1055–1065, https://doi.org/10.1021/jp510036x.

[33] H. Park, W. Choi, Photocatalytic conversion of benzene to phenol using modified $TiO_2$ and polyoxometalates, Catal. Today 101 (2005) 291–297, https://doi.org/10.1016/j.cattod.2005.03.014.

[34] M. Schulz, C. Paulik, G. Knör, Studies on the selective two-electron photo-oxidation of benzene to phenol using polyoxometalates, water and simulated solar radiation, J. Mol. Catal. A: Chem. 347 (2011) 60–64, https://doi.org/10.1016/j.molcata.2011.07.011.

[35] Y. Li, Z. Zhao, Preparation of phosphor-tungstic acids ($H_3PW_{12}O_{40}$) by solvent extraction with 2-octanol, Hydrometallurgy 185 (2019) 291–296, https://doi.org/10.1016/j.hydromet.2019.03.005.

[36] K.Y. Lee, T.Arai, S. Nakata, S. Asaoka, T. Okuhara, M. Misono, Catalysis by heteropoly compounds. 20. An NMR study of ethanol dehydration in the pseudoliquid phase of 12-tungstophosphoric acid, J. Am. Chem. Soc. 114 (1992) 2836–2842, https://doi.org/10.1021/ja00034a013.

[37] O. Toshio, K. Atsushi, H. Nobukiyo, M. Makoto, Y. Yukio, The important role of the bulk of 12-tungustophosphoric acid in the catalytic dehydration of alcohols to olefins, Chem. Lett. 10 (1981) 391–394, https://doi.org/10.1246/cl.1981.391.

[38] C. Lu, P. Zhang, S. Jiang, X. Wu, S. Song, M. Zhu, Z. Lou, Z. Li, F. Liu, Y. Liu, Y. Wang, Z. Le, Photocatalytic reduction elimination of $UO_2^{2+}$ pollutant under visible light with metal-free sulfur doped g-$C_3N_4$ photocatalyst, Appl. Catal. B: Environ. 200 (2017) 378–385, https://doi.org/10.1016/j.apcatb.2016.07.036.

[39] R. Abe, H. Takami, N. Murakami, B. Ohtani, Pristine simple oxides as visible light driven photocatalysts: highly efficient decomposition of organic compounds over platinum-loaded tungsten oxide, J. Am. Chem. Soc. 130 (2008) 7780–7781, https://doi.org/10.1021/ja800835q.

[40] S.M. Hosseini, M. Ghiaci, S.A. Kulinich, W. Wunderlich, H. Farrokhpour, M. Saraji, A. Shahvar, Au-Pd@g-$C_3N_4$ as an efficient photocatalyst for visible-light oxidation of benzene to phenol: experimental and mechanistic study, J. Phys. Chem. C 122 (2018) 27477–27485,

https://doi.org/10.1021/acs.jpcc.8b08788.

[41] Y. Zhang, S.-J. Park, Stabilizing CuPd bimetallic alloy nanoparticles deposited on holey carbon nitride for selective hydroxylation of benzene to phenol, J. Catal. 379 (2019) 154–163, https://doi.org/10.1016/j.jcat.2019.09.032.

[42] Z. Zhu, R. Tain, C. Rhodes, A study of the decomposition behaviour of 12-tungstophosphate heteropolyacid in solution, Can. J. Chem. 81 (2003) 1044–1050, https://doi.org/10.1139/v03-129.

[43] H. Hori, Decomposition of nonafluoropentanoic acid by heteropolyacid photocatalyst $H_3PW_{12}O_{40}$ in aqueous solution, J. Mol. Catal. A: Chem. 211 (2004) 35–41, ttps://doi.org/10.1016/j.molcata.2003.09.029.

[44] J.K. Kochi, R.T. Tang, T. Bernath, Mechanisms of aromatic substitution. role of cation-radicals in the oxidative substitution of arenes by cobalt(III), J. Am. Chem. Soc. 94 (1972) 7114–7123, https://doi.org/10.1021/ja00775a041.

[45] S. Fukuzumi, K. Ohkubo, One-step selective hydroxylation of benzene to phenol, Asian J. Org. Chem. 4 (2015) 836–845, https://doi.org/10.1002/ajoc.201500187.

[46] A. Mancuso, O. Sacco, D. Sannino, V. Venditto, V. Vaiano, One-step catalytic or photocatalytic oxidation of benzene to phenol: possible alternative routes for phenol synthesis? Catalysts 10 (2020) 1424, https://doi.org/10.3390/catal10121424.

[47] J. Li, Y. Xu, Z. Ding, A.H. Mahadi, Y. Zhao, Y.-F. Song, Photocatalytic selective oxidation of benzene to phenol in water over layered double hydroxide: A thermodynamic and kinetic perspective, Chem. Eng. J. 388 (2020) 124248, https://doi.org/10.1016/j.cej.2020.124248.

[48] H. Hori, Y. Takano, K. Koike, S. Kutsuna, H. Einaga, T. Ibusuki, Photochemical decomposition of pentafluoropropionic acid to fluoride ions with a water-soluble heteropolyacid photocatalyst, Appl. Catal. B: Environ. 46 (2003) 333–340, https://doi.org/10.1016/S0926-3373(03)00225-X.

[49] H. Hori, Y. Takano, K. Koike, K. Takeuchi, H. Einaga, Decomposition of environmentally persistent trifluoroacetic acid to fluoride ions by a homogeneous photocatalyst in water, Environ. Sci. Technol. 37 (2003) 418–422, https://doi.org/10.1021/es025783y.

[50] O. Snir, Y. Wang, M.E. Tuckerman, Y.V. Geletii, I.A. Weinstock, Concerted proton-electron transfer to dioxygen in water, J. Am. Chem. Soc. 132 (2010) 11678–11691.

ttps://doi.org/10.1021/ja104392k.

[51] M. Kim, I.A. Weinstock, Y.V. Geletii, C.L. Hill, Oxidation of reduced Keggin heteropolytungstates by dioxygen in water catalyzed by Cu(II), ACS Catal. 5 (2015) 7048−7054. https://doi.org/10.1021/acscatal.5b01771.

[52] Y.V. Geletii, C.L. Hill, R.H. Atalla, I.A. Weinstock, Reduction of $O_2$ to superoxide anion ($O_2$•⁻) in water by heteropolytungstate cluster-anions, J. Am. Chem. Soc. 128 (2006) 7033–17042, https://doi.org/10.1021/ja064244g.

[53] L. Chen, J. Tang, L.N. Song, P. Chen, J. He, C.T. Au, S.F. Yin, Heterogeneous photocatalysis for selective oxidation of alcohols and hydrocarbons, Appl. Catal. B: Environ. 242 (2019) 379–388, https://doi.org/10.1016/j.apcatb.2018.10.025.

[54] L. Xiong, J. Tang, Strategies and challenges on selectivity of photocatalytic oxidation of organic substances, Adv. Energy Mater. 11 (2021) 2003216. https://doi.org/10.1002/aenm.202003216.

[55] H. Einaga, M. Misono, Photocatalyzed decomposition of 4-chlorophenol by Keggin-type heteropolytungstate, B. Chem. Soc. Jpn. 70 (1997) 1551–1557, https://doi.org/10.1246/bcsj.70.1551.

[56] M.A. Fox, R. Cardona, E. Gaillard, Photoactivation of metal oxide surfaces: photocatalyzed oxidation of alcohols by heteropolytungstates, J. Am. Chem. Soc. 109 (1987) 6347–6354, https://doi.org/10.1021/ja00255a019.

[57] X.Shi,S. Liu, C. Duanmu, M. Shang, M. Qiu, C. Shen, Y. Yang, Y. Su, Visible-light photooxidation of benzene to phenol in continuous-flow microreactors, Chem. Eng. J. 420 (2021) 129976. https://doi.org/10.1016/j.cej.2021.129976.

[58] D.F. Ollis, Kinetics of liquid phase photocatalyzed reactions: an illuminating approach, J. Phys. Chem. B 109 (2005) 2439–2444, https://doi.org/10.1021/jp040236f.

[59] C. Streb, New trends in polyoxometalate photoredox chemistry: from photosensitisation to water oxidation catalysis, Dalton Trans. 41 (2012) 1651–1659, https://doi.org/10.1039/C1DT11220A.

[60] B.B. Sarma, R. Carmieli, A. Collauto, I. Efremenko, J.M.L. Martin, R. Neumann, Electron transfer oxidation of benzene and aerobic oxidation to phenol, ACS Catal. 6 (2016) 6403–6407,

https://doi.org/10.1021/acscatal.6b02083.

# Chapter 3:

Photocatalytic hydroxylation of benzene to phenol with dioxygen using sodium decatungstate

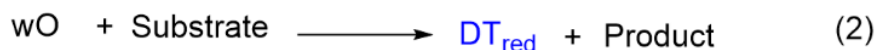# Chapter 3: Photocatalytic hydroxylation of benzene to phenol with dioxygen using sodium decatungstate

## 3.1 Introduction

Phenol is an important chemical intermediate for synthesizing petrochemicals, agrochemicals, pharmaceuticals, and plastics [1-3]. Recently, the worldwide production of phenol has been as high as 9.5 megatons, with approximately 90% of the phenol produced being obtained by the three-step cumene process [4-8]. This process is energy intensive, produces toxic intermediates, and generates an equal amount of acetone as a byproduct [9, 10]. For this reason, much effort has been devoted to the one-pot synthesis of phenol from benzene with various oxidants (e.g., $H_2O_2$, $N_2O$, $O_2$) in the past few decades [11-13]. Among these oxidants, oxygen ($O_2$) is ideal because it is inexpensive and readily available, especially because $O_2$ in the air can be used directly. However, due to the low reactivity of benzene with $O_2$, current thermal catalytic oxidation systems generally require a high temperature and pressure [14]. These harsh reaction conditions lead to a low selectivity, since phenol is more reactive than benzene. Therefore, additional reductants, such as $H_2$, CO, and ascorbic acid, have been utilized to activate $O_2$ under mild conditions [15-18].

Photocatalytic processes can provide a green route to hydroxylate benzene to phenol at room temperature [19, 20]. Several semiconductor-based photocatalysts, including $TiO_2$, have been employed in this process [21, 22]. In these processes, the photoinduced holes or hydroxyl radicals (•OH) from these photocatalysts can activate C–H in benzene molecules for phenol synthesis [23]. For example, Tomita *et al.* reported that particles of tungsten oxide loaded with noble-metal platinum (Pt/$WO_3$) photocatalytically produced phenol from benzene with a 75% selectivity at a 69% benzene conversion [24]. Chen *et al.* synthesized three-dimensional $Bi_2WO_6$/$CdWO_4$, which exhibited a phenol yield of 7.3% [25]. Li *et al.* reported that a $Zn_2Ti$-layered double hydroxide ($Zn_2Ti$-LDH) photocatalyst showed one-step oxidation of benzene to phenol with a phenol yield of 4.6% [26]. Recently, quinolinium ions and $[Ru^{II}(Me_2phen)_3]^{2+}$ have been reported to be highly active as organic photocatalysts [27, 28]. However, developing a highly active and low-cost inorganic photocatalyst for the oxidation of benzene to phenol with oxygen is a difficult but important

challenge.

Polyoxometalates (POMs) are metal-oxygen clusters with various properties, such as redox and acid-base properties. As described in the chapter 2, a heteropolyacid ($H_3PW_{12}O_{40}$) showed high activity for benzene oxidation to phenol in an aqueous acetonitrile solution. As another important POMs, the decatungstate (DT) anion ($W_{10}O_{32}^{4-}$) has been frequently used for organic synthesis and water purification due to its excellent photocatalytic activity [29]. Its absorption spectrum presents a useful overlap with the solar emission spectrum, with a maximum absorption at 323 nm [30]. This wavelength of light is more longer than that of $PW_{12}O_{40}^{3-}$, indicating $W_{10}O_{32}^{4-}$ maybe showed higher photocatalytic activity. Furthermore, the solubility of the decatungstate in organic solvents and water can be controlled by changing the type of countercation. Due to its unique photocatalytic properties, $W_{10}O_{32}^{4-}$ has been used in the photocatalytic oxidation of a variety of organic substrates in organic and aqueous media at ambient temperature and pressure [31-33]. For example, Fu $et$ $al.$ reported on the selective oxidation of cyclohexane to cyclohexanol and cyclohexanone with ($n$Bu$_4$N)$_4$W$_{10}$O$_{32}$ in an acetonitrile solution [34]. On the other hand, sodium decatungstate ($W_{10}O_{32}^{4-}$) was utilized in the degradation of various pollutants, such as pesticides and halogenated hydrocarbons, due to its high water solubility [35]. In these systems, the reaction begins by forming very reactive transient species after photoexcitation of DT, as shown in Scheme 1 [31]. Then, this reactive species can activate substrates with a hydrogen atom abstraction (HAT) or electron transfer (ET) process, resulting in a wide scope products and reduced species of DT (DT$_{red}$). Then, the reduced species is readily reoxidized with O$_2$ to complete the catalytic cycle (Scheme 1) [29]. Thus, $W_{10}O_{32}^{4-}$ shows a much different oxidative behavior compared with TiO$_2$. In TiO$_2$-catalyzed photooxidation, hydroxyl radicals ($^\bullet$OH) are the reactive oxidant species, which show a high activity for the degradation of both initial substrates and intermediates with a low selectivity. On the other hand, the oxidation rate of the intermediates was much slower than that of the initial substrates in photooxidation with $W_{10}O_{32}^{4-}$ systems, resulting in much slower mineralization [36-38]. We hypothesized that this reluctant mineralization behavior of $W_{10}O_{32}^{4-}$ is promising for the selective oxidation of benzene.

$$DT_{ox} \xrightarrow{h\nu} wO \qquad (1)$$

$$wO + Substrate \longrightarrow DT_{red} + Product \qquad (2)$$

$$DT_{red} + 2 H^+ + 1/2 O_2 \longrightarrow DT_{ox} + {}^\bullet O_2^- \qquad (3)$$

**Scheme 1.** General photocatalytic oxidation pathways of organic substrates over DT.

In this chapter, we show that benzene can be efficiently hydroxylated to phenol with $O_2$ using DT as a photocatalyst in an aqueous solution. In addition, the photocatalytic performance is further improved by adding a small amount of acetic acid as a co-solvent (water/acetic acid = 5/1, V/V). As a result, a high phenol yield (17–41%) and selectivity (76–82%) are achieved within 60 min under ambient conditions (1 atm, 10 °C). The use of acetic acid as a cosolvent enhanced the solubility of benzene and inhibited the vaporization of benzene. Furthermore, the solvent may affect the lifetime of the excited state of the reactants, which affects the catalytic performance of the organic synthesis [39]. Benzene hydroxylation under anaerobic conditions is also conducted to understand the role of oxygen and propose a phenol formation mechanism. In addition, the mechanistic difference between $W_{10}O_{32}^{4-}$ and semiconductor-based photocatalysts, such as $TiO_2$, is discussed, which provides helpful insight into the highly selective benzene hydroxylation of phenol.

## 3.2 Experimental

### Materials and Instruments

Sodium tungstate(VI) dihydrate ($Na_2WO_4 \cdot 2H_2O$), benzene, phenol, and other reagents were purchased from Wako Pure Chem. Ind. (Japan). According to the literature, sodium decatungstate ($Na_4W_{10}O_{32}$) was synthesized with a small modification [40]. The structure of decatungstate was confirmed via UV-VIS spectra (extinction coefficients of 13500 $M^{-1}$ $cm^{-1}$ for $W_{10}O_{32}^{4-}$ at 324 nm) and Fourier transform Infrared (FTIR) spectra (Fig. 1) [41]. Graphitic carbon nitride (g-$C_3N_4$) was synthesized using urea as the precursor [42].
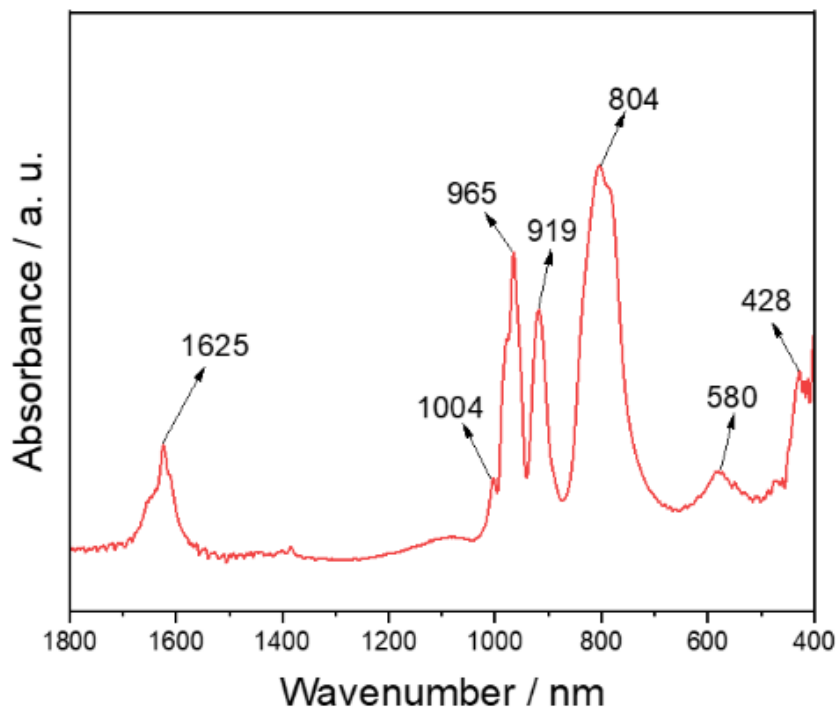
**Fig. 1.** FT-IR spectra of $Na_4W_{10}O_{32}$

The UV–VIS spectra were recorded on a UV-VIS spectrometer 3100 (Shimadzu, Japan). The samples were transferred into quartz cells (path length: 1.0 cm) and then subjected to measurements. Fourier transform infrared (FTIR) spectra were obtained using an FT/IR-4100 spectrometer (JASCO, Japan).

*Photocatalytic performance study under aerobic conditions*

Photocatalytic benzene oxidation to phenol over $W_{10}O_{32}^{4-}$ was conducted under an air atmosphere (1 atm) and low temperature (10 °C) in an aqueous solution. The reaction was conducted in a 100 mL photochemical reactor equipped with a water jacket to maintain the temperature at 10 °C, as shown in Fig. 2. The illumination window on the top of the reactor is made of high-strength quartz glass. In a typical run, a mixture of 25 mL of water and 5 mL of acetic acid containing 4 mM benzene was added into the reactor. Then, 0.136 mM photocatalyst was added to the solution. Photoirradiation was performed for the reaction solution under continuous stirring in air (1 atm) with a 300 W xenon lamp. Sample aliquots were withdrawn with a syringe from the reactor after reaction and immediately analyzed with reverse-phase high-performance liquid chromatography (HPLC). The mobile phase was composed of 65% phosphoric solution (0.2%) and 35% acetonitrile

55

with a flow rate of 1 cm$^3$/min.
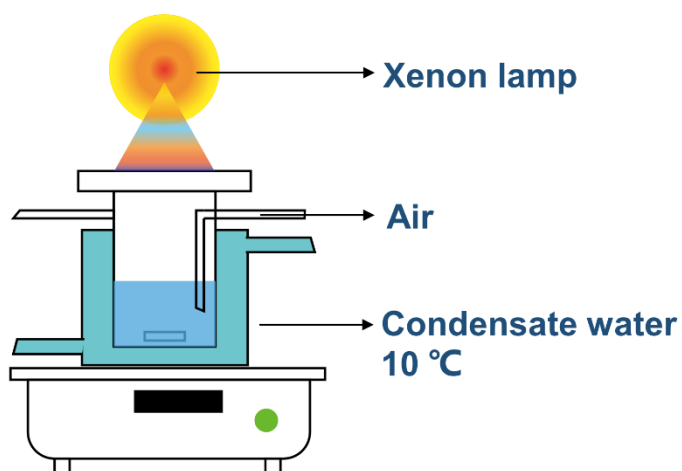


**Fig. 2.** Schematic representation of photocatalytic benzene hydroxylation setup

The benzene conversion, phenol yield, and selectivity were calculated using the following formulas.

$$Benzene\ conversion = (1 - \frac{remained\ benzene\ concentration}{initial\ benzene\ concentration}) \times 100\%$$

$$Phenol\ yield = \frac{produced\ phenol\ concentration}{initial\ benzene\ concentration} \times 100\%$$

$$Phenol\ selectivity = \frac{Phenol\ yield}{Benzene\ conversion} \times 100\%$$

*Photocatalytic reaction under anaerobic conditions and reoxidation under aerated conditions*

The reaction solution was prepared using the same method as stated above, but with excess benzene substrate. Before irradiation with the Xenon lamp, the reaction solution was vigorously bubbled with argon for 15 min to remove the dissolved oxygen. In addition to the HPLC analysis, the UV-VIS spectra of the sample aliquots were also measured to examine the decatungstate. After the reaction, the xenon lamp was turned off and the reaction solution was exposed to air. The sample aliquots were then analyzed again with HPLC and UV-VIS spectroscopy after the reaction solution became colorless.

### 3.3 Results and discussion
*Photocatalytic properties of $W_{10}O_{32}{}^{4-}$*

The time course of the photooxidation reaction of benzene to phenol catalyzed by $W_{10}O_{32}{}^{4-}$ in

water-acetic acid solution in air atmosphere (1 atm) and low temperature (10 °C) is shown in Fig. 3. First, it was confirmed that no products were detected under the reaction conditions before irradiation in the dark. In addition, the pH of the reaction solution was approximately 2 and did not change during the reaction. The phenol yield increased with time and reached a maximum (31%) at 120 min, but the selectivity decreased to 74% with the reaction time. Subsequently, when the time was extended to 180 min, the selectivity further decreased to 66%, but the reaction did not stop. This decrease in selectivity was due to the excessive oxidation of phenolic products, as evidenced by the small amount of benzoquinone observed as a byproduct. However, the byproduct concentration was much lower than the phenol concentration, resulting in the selective formation of phenol in this system.
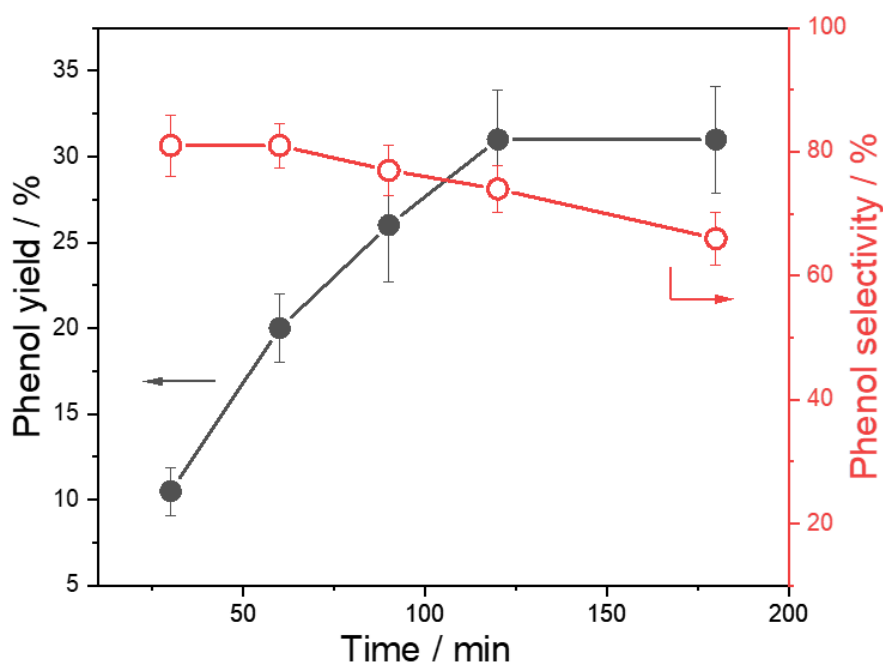


**Fig. 3** Effect of reaction time on photocatalytic benzene hydroxylation. Reaction condition: water/acetic acid, 5/1 (V/V); pH = 2; light source, 300 W xenon lamp; temperature, 10 °C; initial benzene concentration: 4 mM, photocatalyst concentration: 0.068 mM, air atmosphere (1 atm).

UV-VIS spectra were utilized to investigate the structural stabilization of $W_{10}O_{32}{}^{4-}$ polyanion in photocatalytic benzene hydroxylation in the water-acetic acid solution. As shown in Fig. 4a, the band at = 323 nm was assigned to the oxygen-to-tungsten charge transfer of four linear W–O–W

bridge bonds in the $W_{10}O_{32}{}^{4-}$ structure [43]. The Fig. 4b shows that both benzene and phenol exhibited a light absorption band in the 250-350 nm region. After the reaction, the absorption band extended to 300 nm due to the generation of phenol products. The absorbance at 323 nm was unchanged after the reaction, indicating no decomposition of the photocatalyst during the reaction, thereby confirming the high stability of $W_{10}O_{32}{}^{4-}$. The catalysts can be separated from the products in heterogeneous solid-liquid systems [44, 45] while isolating products in homogenous systems is more difficult. In our study, phenol could be separated from the reaction solution by ether extraction and rotary evaporation after the reaction. We also tried to recover the catalyst by the same method, but about 30% of the $W_{10}O_{32}{}^{4-}$ catalyst was lost during the separation process.
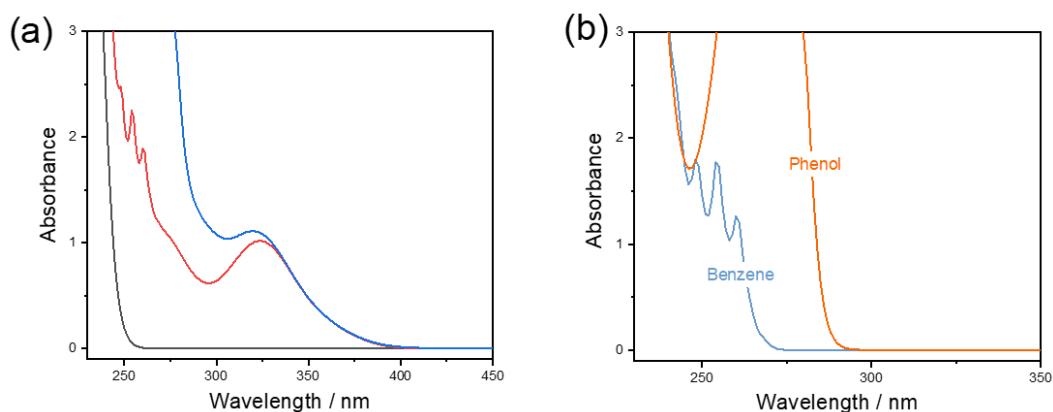


**Fig. 4** (a) UV-VIS spectra of the water-acetic acid mixture (black line), benzene (8 mM) and $W_{10}O_{32}{}^{4-}$ (0.068 mM) in the water-acetic acid mixture (red line), benzene (8 mM), and $W_{10}O_{32}{}^{4-}$ (0.068 mM) in the water-acetic acid mixture after irradiation for 120 min (blue line). (b) the UV-VIS spectra of benzene and phenol in the water-acetic acid mixture. The ratio of water and acetic acid is 5/1; pH = 2.

The results of the benzene photooxidation reaction in various solvents are shown in Table 1. A binary solvent consisting of either acetic acid, acetonitrile, or DMF added to water was used as the solvent because these solvents can suppress benzene vaporization. When this photocatalytic reaction was conducted in a mixture of water and acetic acid (5/1, V/V), the phenol yield and selectivity were 17% and 81%, respectively (Entries 1). The addition of the co-solvent significantly affects phenol formation in our system. In the reaction in pure water without the co-solvent, which was performed as a comparison, $W_{10}O_{32}{}^{4-}$ achieved a phenol yield of 16% and selectivity of 70% after

60 min of irradiation, with a phenol formation rate of 1.36 mM h$^{-1}$ (Entry 2). These values are lower than those in the water-acetic acid mixture. The low yield of phenol in the photoreaction in an aqueous solution was probably due to the low solubility of benzene in water and the tendency of benzene to volatilize. Another possible reason was the suppression of phenol oxidation by acetic acid. To confirm this assumption, we investigated photocatalytic phenol oxidation in pure water and a water-acetic acid mixture (5/1, V/V), as shown in Fig. 5. In pure water, 20% phenol was decomposed after 120 min irradiation, which decreased to 14% after adding acetic acid as a cosolvent.
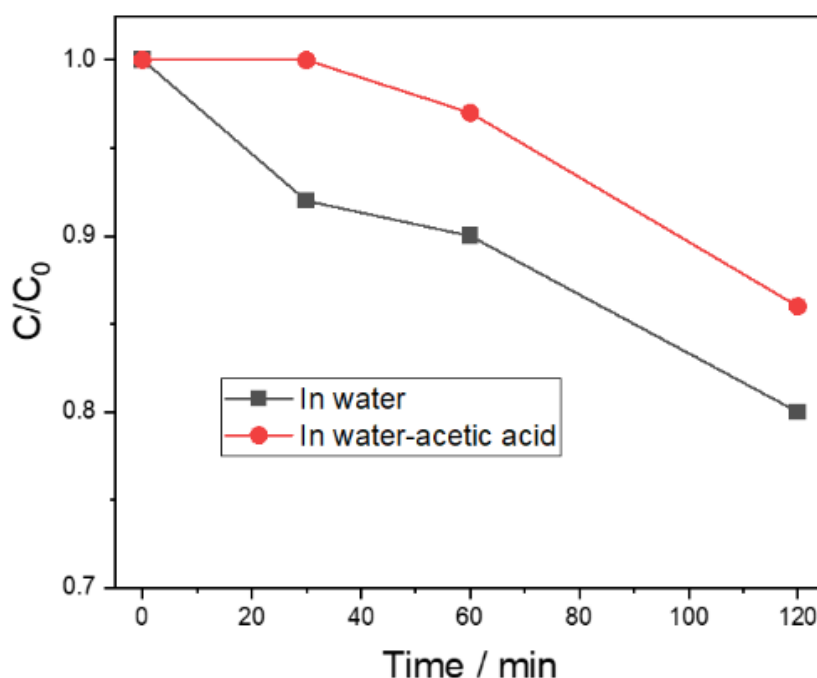


**Fig. 5** Photocatalytic oxidation of phenol in water and water-acetic mixture. Reaction condition: water/acetic acid, 5/1 (V/V); pH = 2; light source, 300 W xenon lamp; temperature, 10 °C; reaction time, 60 min; photocatalyst concentration: 0.136 mM, air atmosphere (1 atm).

On the other hand, the benzene yield decreased when the benzene oxidation reaction was conducted in a water-acetonitrile solution (Entry 3). Furthermore, the phenol yield was lower than 0.1% when using DMF as a co-solvent (Entry 4). Even under oxidative conditions (air atmosphere at 1 atm), the color of the reaction solution changed to blue after irradiation, indicating the accumulation of reduced catalyst in the DMF system, which was not observed in the other systems.

59

These results suggest that the oxidation of DMF was facilitated by the excited DT, which was even faster than the oxidation of benzene. These findings prompted us to investigate the oxidizability of cosolvent by excited DT.

First, we confirmed that the UV-VIS absorption spectra of $W_{10}O_{32}{}^{4-}$ did not change when the solution was changed from water-acetic acid and water, which had been adjusted to pH=2. Thus, the structure did not change when the cosolvent was changed. Hence, we performed a control experiment in which the photocatalyst in an aqueous solution (no benzene) with different cosolvents was irradiated under an argon atmosphere. The reduction in the catalyst after irradiation was visually observed by the color change to blue after irradiation. A UV-VIS spectroscopic study revealed that strong absorption bands (λmax: 630 nm, λmax: 780 nm) appeared in the visible region, indicating the formation of heteropoly blue ($W_{10}O_{32}{}^{5-}$ or $W_{10}O_{32}{}^{6-}$) (Fig. 6) [41].
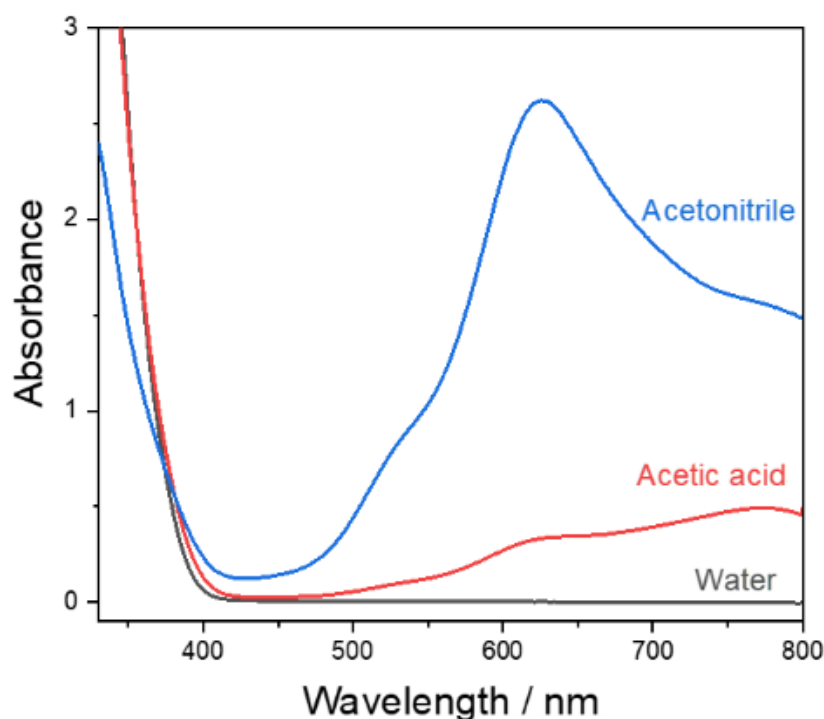


**Fig. 6** UV-VIS spectra of the $W_{10}O_{32}{}^{4-}$ (0.136 mM) in aqueous solution with different co-solvent after 60 min of irradiation under argon. Water/co-solvent, 5/1 (V/V); pH = 2; light source, 300 W xenon lamp; temperature, 10 °C.

The oxidation of water with excited DT is not observed according to UV-VIS spectra in a control

experiment. As shown in Fig. 6, the amount of heteropoly blue in an aqueous acetonitrile solution is much higher than that in aqueous acetic acid solution, indicating that the oxidation of acetonitrile by excited DT is much faster than that of acetic acid. This result can explain why the phenol yield decreases when acetonitrile is used as a cosolvent. The excited DT can attack both benzene and acetonitrile to proceed with the redox reaction. The change in the catalytic performance when acetonitrile was used as a cosolvent may be due to the competition of the solvent with excited DT for oxidation. On the other hand, when the behavior of $W_{10}O_{32}^{4-}$ in water-acetic acid solution was compared, the formation of the reduced form was significantly suppressed compared to the case using acetonitrile. This suggests that the inhibitory effect of $W_{10}O_{32}^{4-}$ on the benzene photooxidation reaction is smaller for acetic acid than for acetonitrile.

*Effect of polyanion structures*

Reportedly, the stability of $W_{10}O_{32}^{4-}$ polyanion in water strongly depended on pH [35]. Fig. 7 shows the UV-VIS spectra of solutions of $W_{10}O_{32}^{4-}$ polyanions dissolved in a water-acetonitrile solution and then adjusted to various pH values using $HClO_4$ or NaOH. To maintain the $W_{10}O_{32}^{4-}$ structure in an aqueous solution, it is necessary to keep the pH of the solution below 6.9 [46,47]. The peak at 323 nm in the UV-VIS spectra showed no change when the pH increased from 2 to 6, which is consistent with the stability of $W_{10}O_{32}^{4-}$ in the acidic solution [46]. When the pH was further increased, polyanions decomposed to form monomeric $WO_4^{2-}$ species. As a result, the peak at 323 nm decreased and even disappeared. The pH dependence of hydroxylation from benzene to phenol is strongly related to the structural stability of the polyanion. As shown in Table 1 (Entries 3 and 5), the phenol yield and formation rate showed almost no change when the pH value increased from 2 to 6. However, no phenol was generated in a basic solution (pH = 8, 10, or 12) (Entry 6-8). Furthermore, we confirmed that the phenol formation reaction did not proceed in the control experiment at a pH of 2 with no catalyst (Entry 9). These findings indicated that $W_{10}O_{32}^{4-}$ polyanions were the active species for benzene hydroxylation.
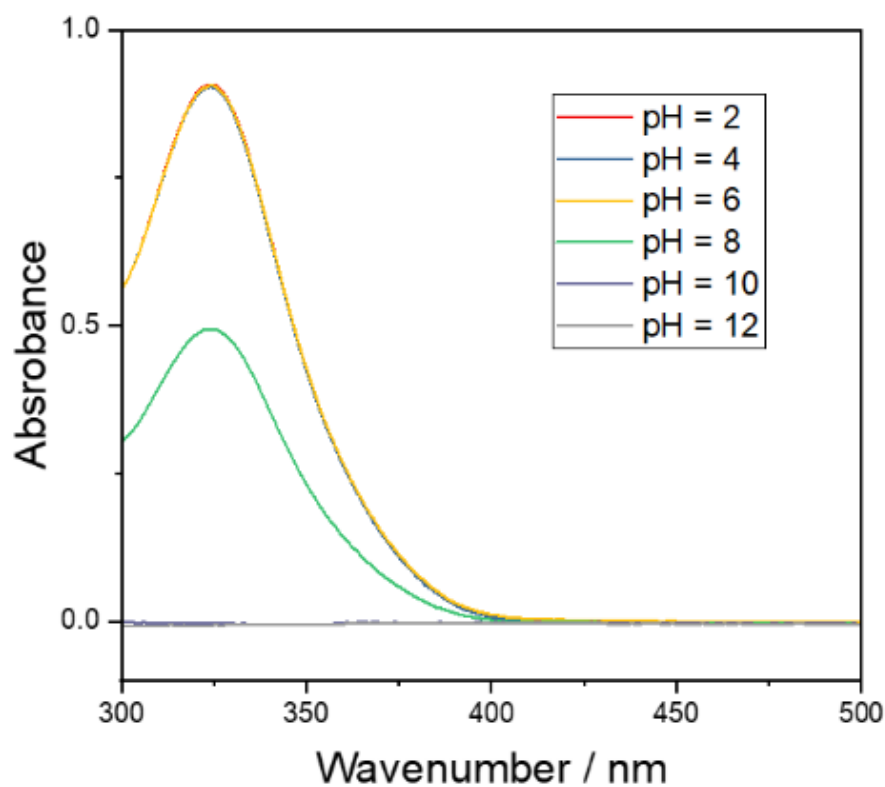
**Fig. 7** UV-VIS spectra of $W_{10}O_{32}^{4-}$ (0.068 mM) in water-acetonitrile (5/1, V/V) at different pH value

**Table 1** Photocatalytic benzene oxidation to phenol with $W_{10}O_{32}$ in various solvents [a]
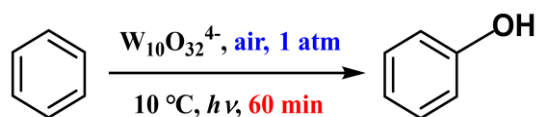


| Entry | Solvent | pH value | Phenol yield (%) | Selectivity (%) | Rate (mM h⁻¹) [b] |
|---|---|---|---|---|---|
| 1 | Water-acetic acid (5/1) | 2 | 17 | 81 | 1.45 |
| 2 | Pure water (1/0) | 2 | 16 | 70 | 1.36 |
| 3 | Water-acetonitrile (5/1) | 2 | 13 | 78 | 1.11 |
| 4 | Water-DMF (5/1) | 2 | < 0.1 | - | - |
| 5 | Water-acetonitrile (5/1) | 6 | 12 | 77 | 1.10 |
| 6 | Water-acetonitrile (5/1) | 8 | < 0.1 | - | - |
| 7 | Water-acetonitrile (5/1) | 10 | 0 | - | - |
| 8 | Water-acetonitrile (5/1) | 12 | 0 | - | - |

| | | | | | |
|---|---|---|---|---|---|
| 9 | Water-acetonitrile (5/1) [c] | 2 | 0 | - | - |
| 10 | Water-acetic acid (5/1) [c] | 2 | 0 | - | - |
| 11 | Water-acetic acid (2/1) | 2 | 11 | 81 | 0.94 |
| 12 | Water-acetic acid (1/2) | 2 | 3 | 82 | 0.26 |
| 13 | Water-acetic acid (0/1) | 2 | < 0.1 | - | - |

[a] Reaction condition: light source, 300 W xenon lamp; temperature, 10 °C; irradiation times, 60 min; catalyst concentration, 0.136 mM; benzene concentration, 8.5 mM; under ambient condition; [b] based on phenol formation; [c] without photocatalyst
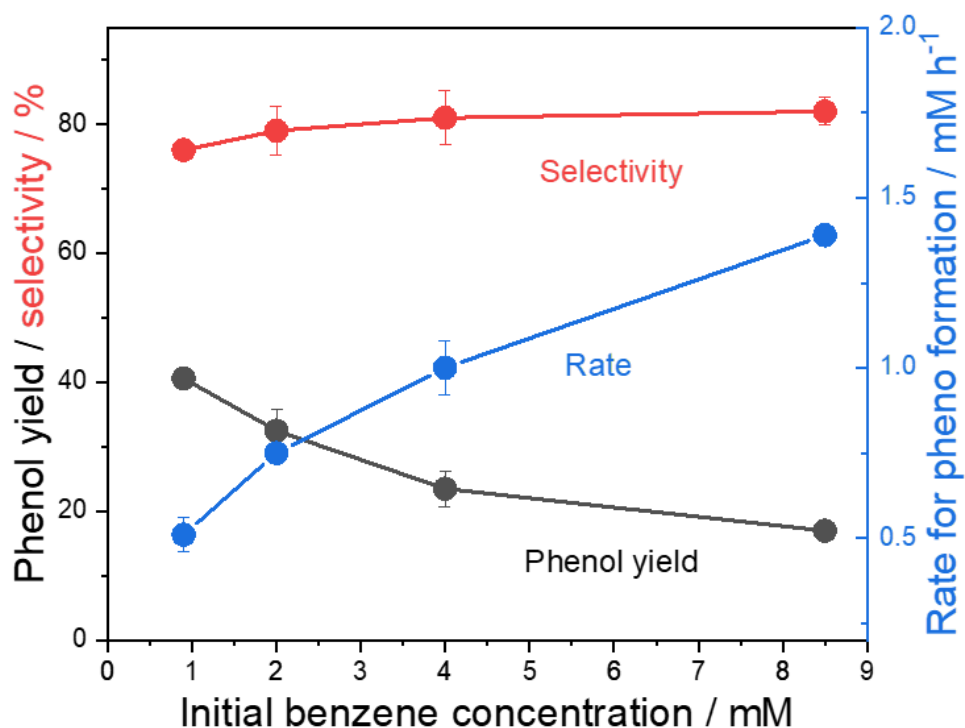
*Effect of reaction conditions*

The effect of the volume ratio of water to acetic acid on benzene oxidation was investigated. We first confirmed that no phenol was generated without a catalyst in the water-acetic acid system (pH = 2) in a control experiment (Entry 10, Table 1). As demonstrated above, the phenol yield and selectivity increased from 16% and 70% to 17% and 81%, respectively, when decreasing the ratio from 1/0 to 5/1 (Entries 1 and 2). However, the phenol yield continuously decreased to 3% by further increasing the ratio to 1/2, while the phenol selectivity showed no obvious changes (Entries 11 and 12). Notably, no measurable phenol was generated when the water and acetic acid ratio decreased to 0:1 (Entry 13). In addition, the phenol formation rate continuously decreased when the amount of acetic acid was increased. Thus, benzene oxidation and phenol formation were significantly suppressed when acetic acid was present in excess. Consequently, the maximum yield of phenol was obtained when the water and acetic acid ratio was 5/1.
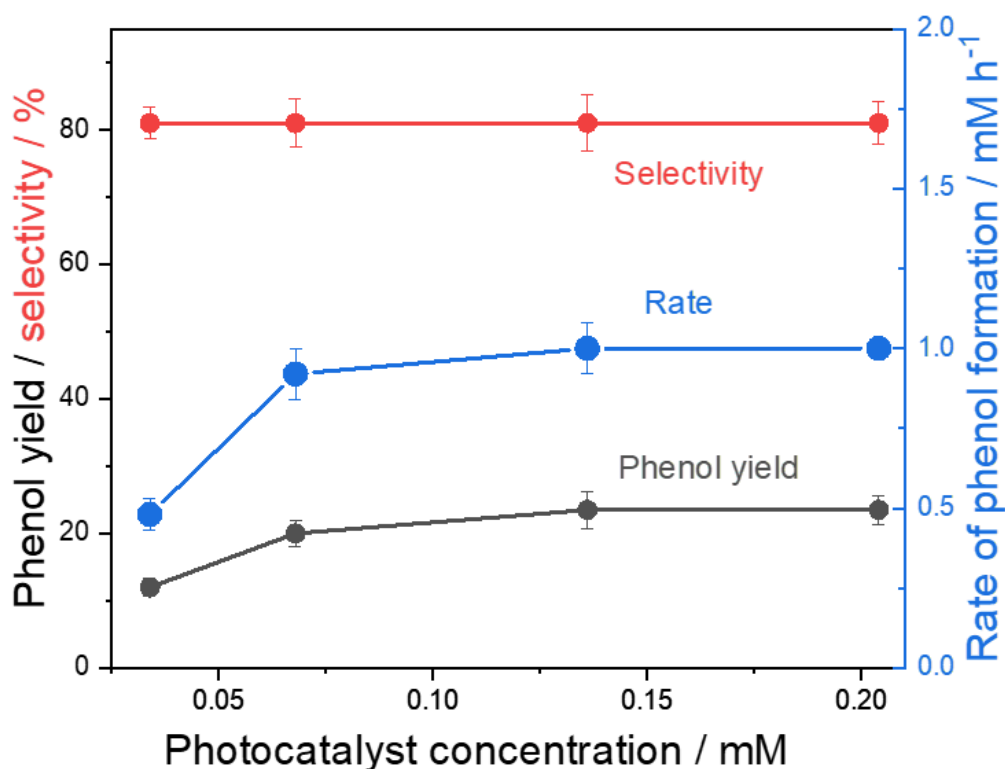
The effect of the benzene concentration on photocatalytic benzene hydroxylation was investigated. As demonstrated in Fig. 8, the phenol selectivity and phenol formation rate gradually increased from 76% and 0.51 mM h$^{-1}$ to 82% and 1.39 mM h$^{-1}$ when the initial benzene concentration increased from 0.9 mM to 8.5 mM. This increased phenol formation indicates an improved benzene hydroxylation, which may be ascribed to an increase in benzene radical cations at higher benzene concentrations [39]. The higher selectivity in the increased benzene concentration indicates suppressed overoxidation. However, the phenol yield continuously decreased from 41% to 17% when the benzene concentration increased from 0.9 mM to 8.5 mM. This decrease is likely

63

due to an insufficient interaction between substrates and an excited photocatalyst in excess benzene concentration.



**Fig. 8** Effect of initial benzene concentration on photocatalytic benzene hydroxylation. Reaction condition: water/acetic acid, 5/1 (V/V); pH = 2; light source, 300 W xenon lamp; temperature, 10 °C; reaction time, 60 min; photocatalyst concentration: 0.136 mM, air atmosphere (1 atm).

The benzene hydroxylation reaction was performed using different photocatalyst concentrations, as displayed in Fig. 9. The results demonstrated that when the photocatalyst concentration was between 0.034 mM and 0.136 mM, the phenol yield and formation rate increased from 12% and 0.48 mM h$^{-1}$ to 24% and 1.0 mM h$^{-1}$, respectively, with no obvious selectivity change. This improved effect is due to the increase in the light absorption by the photocatalyst at higher concentrations. However, this effect of the photocatalyst concentration on the phenol yield was nearly neglected when the photocatalyst concentration was beyond 0.136 mM, which is likely due to light absorption saturation. Hence, a concentration of 0.136 mM was utilized as the optimized concentration of the photocatalyst in our system.

**Fig. 9** Effect of photocatalyst concentration on photocatalytic benzene hydroxylation. Reaction condition: water/acetic acid, 5/1 (V/V); pH = 2; light source, 300 W xenon lamp; temperature, 10 °C; photocatalyst concentration: 0.136 mM, benzene concentration: 4 mM, air atmosphere (1 atm).

*Proposed mechanism for photocatalytic benzene hydroxylation*

According to previous works, $W_{10}O_{32}^{4-}$ can absorb light and result in a singlet excited state, transferring to a relatively stable intermediate (wO) [16]. This transformation occurs through a reorganization of the singly occupied orbital centered on oxygen atoms, leading to the formation of highly electrophilic oxygen centers in wO. The reaction between wO and organic compounds can occur through a HAT or ET process for organic synthesis or pollutant degradation. Hence, in order to understand the reaction mechanism of benzene oxidation with $W_{10}O_{32}^{4}$, it is important to confirm that this HAT or ET can occur using benzene as a substrate.

As described above, photocatalysts and light irradiation are necessary for benzene oxidation to phenol in our reaction system. Therefore, the formation of phenol is undoubtedly due to photocatalytic benzene oxidation with $W_{10}O_{32}^{4-}$. We performed the benzene oxidation reaction under an anaerobic atmosphere in a control experiment to investigate this process in more detail.

After irradiation, the generation of heteropoly blue was visually observed because the reaction solution changed from colorless to blue (inset of Fig. 10a). The absorption band in the visible region is significantly stronger than that without a benzene substrate, as shown in Fig. 10a, indicating the occurrence of benzene oxidation with wO. The formation of these reduced species can be calculated using the extinction coefficients of $W_{10}O_{32}^{5-}$ (3300 and 7000 $M^{-1}$ $cm^{-1}$ for $W_{10}O_{32}^{5-}$ at 630 and 780 nm, respectively) and $W_{10}O_{32}^{6-}$ (14000 and 5390 $M^{-1}$ $cm^{-1}$ for at 630 and 780 nm, respectively), as shown in Fig. 10b [41]. Accordingly, there is the generation of both one-electron-reduced forms ($W_{10}O_{32}^{5-}$) and two-electron-reduced forms ($W_{10}O_{32}^{6-}$) of $W_{10}O_{32}^{4-}$. The time course profiles for phenol formation showed that the phenol concentration increased to 0.12 mM at 30 min and then remained saturated. As described above, the co-solvent may also be oxidized, which will result in the generation of $W_{10}O_{32}^{5-}$ and $W_{10}O_{32}^{6-}$. We performed this anaerobic benzene oxidation reaction in pure water without acetic acid to further exclude this effect. As shown in Fig. 10c, the peak at 780 nm dominated, indicating that $W_{10}O_{32}^{5-}$ dominated, while almost no $W_{10}O_{32}^{6-}$ was generated according to the extinction coefficients of $W_{10}O_{32}^{5-}$ and $W_{10}O_{32}^{6-}$. This result is different from that in an aqueous acetic acid solution that showed the generation of $W_{10}O_{32}^{5-}$ and $W_{10}O_{32}^{6-}$ (Fig. 6a). Notably, the amount of phenol produced in pure water (0.11 mM) was equivalent to half of the amount of $W_{10}O_{32}^{5-}$ produced (Fig. 10d), indicating that the two-electron oxidation of benzene to phenol is associated with the formation of $W_{10}O_{32}^{5-}$.
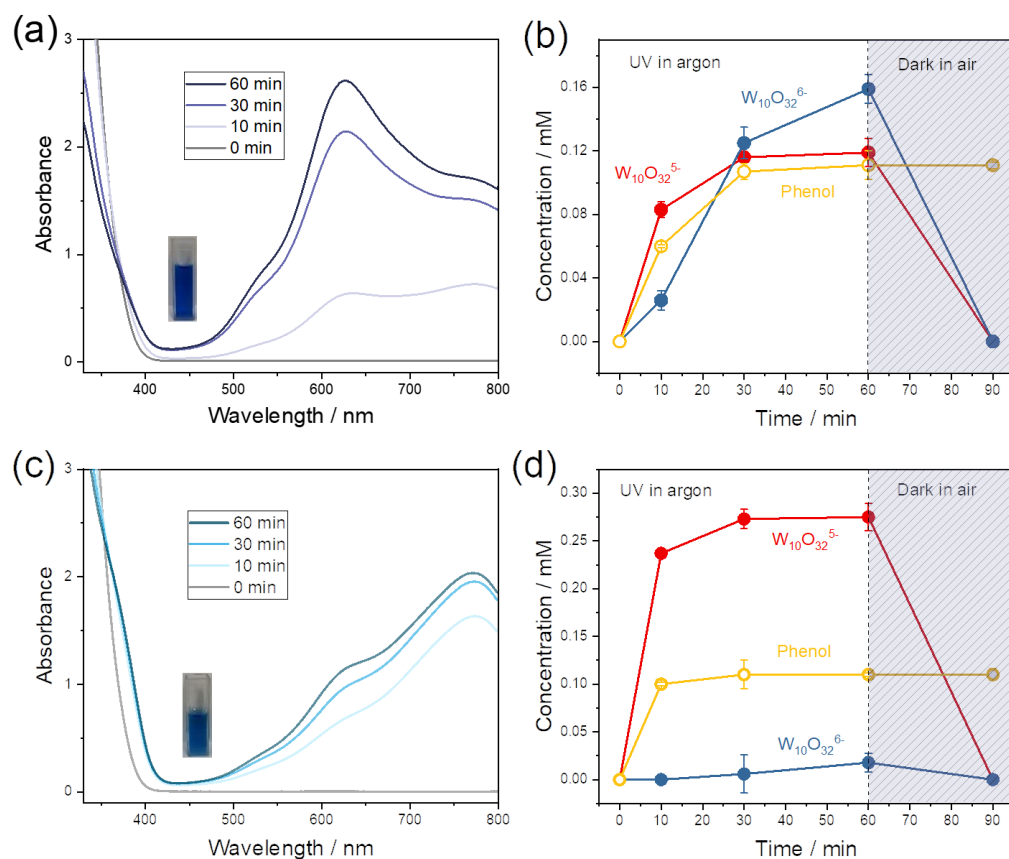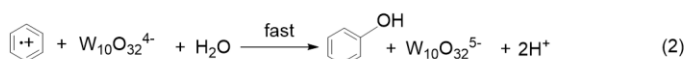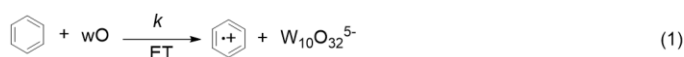
**Fig. 10** UV–VIS spectra of the reaction solution after 10, 30, 60 min of irradiation under argon in a water-acetic acid mixture (5/1, V/V) (a) and pure water (c); Time course for the phenol formation under anaerobic condition in a water-acetic acid mixture (5/1, V/V) (b) and pure water (d). Reaction condition: pH = 2; light source, 300 W xenon lamp; temperature, 10 °C; photocatalyst concentration: 0.544 mM, saturated benzene concentration, air atmosphere (1 atm).

It should be noted that there is another possible route involving hydroxyl radicals ($^{\bullet}$OH), which originated from $H_2O$ oxidation from wO, according to previous work [48]. However, this process was not important in our system because we did not observe any reduced $W_{10}O_{32}^{4-}$ species, which is direct evidence of the oxidation of $H_2O$ with wO.

Based on the above results and previous work, a plausible mechanism for the DT photooxidation of benzene to phenol is outlined in Scheme 2 [37]. Under UV irradiation, $W_{10}O_{32}^{4-}$ was raised to an excited state ($W_{10}O_{32}^{4-*}$), which rapidly relaxed to an actual excited state (wO) or original state (t < 30 ps). It has been reported that ET and HAT processes compete upon the photoactivation of C−H bonds in organic substrates. To investigate ET or HAT dominating the

mechanism, we examined the kinetic isotope effect (KIE), since the ET or HAT step is the rate-determining step based on the lifetimes of the intermediates (as shown in Scheme 2) and the steady state of $W_{10}O_{32}^{4-}$. We obtained the kinetic parameters of benzene oxidation at a certain substrate concentration, in which both the oxidation of benzene and benzene-$d_6$ obeyed the pseudo-first-order kinetic model (Fig. 11). The KIE ($k_H/k_D$) was determined to be 1, which may be ascribed to a secondary kinetic isotope effect. This KIE indicates that the ET mechanism may dominate our reaction system [49]. Two other facts also support the ET process in benzene hydroxylation in our system as follows. First, HAT mainly involves the oxidation of substrates containing weak C−H bonds, such as alcohols, while ET is present when the reaction involves oxidizable substrates, such as aromatic amines or aromatic hydrocarbons [50]. The latter situation is true for benzene, since the C−H bond in benzene is too strong to be abstracted. Second, previous work already showed no activity of benzene oxidation via the HAT process in an acetonitrile solution [34]. Hence, a benzene cation radical was believed to be produced from an ET process, which can subsequently react to give phenol through a pathway similar to the process involved in a previously reported vanadium-containing POM (Eq. 1, 2) [51].



$$\text{benzene} + wO \xrightarrow[\text{ET}]{k} \text{benzene}^{+\cdot} + W_{10}O_{32}^{5-} \qquad (1)$$

$$\text{benzene}^{+\cdot} + W_{10}O_{32}^{4-} + H_2O \xrightarrow{\text{fast}} \text{phenol} + W_{10}O_{32}^{5-} + 2H^+ \qquad (2)$$

As expected, the amount of generated $W_{10}O_{32}^{5-}$ is twice the amount of phenol generated from the stoichiometry of this pathway, showing good agreement with Fig. 6d as described above. Then, $W_{10}O_{32}^{5-}$ reoxidized with $O_2$ back to $W_{10}O_{32}^{4-}$ to complete the catalytic cycle (Eq. 3 in Scheme 1).
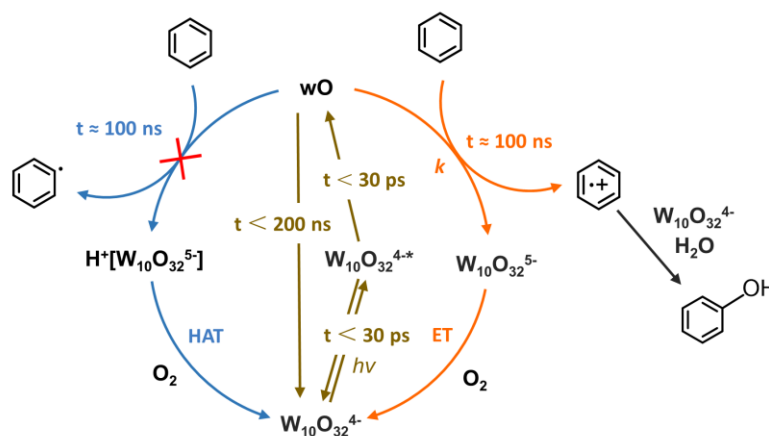


**Scheme 2.** Proposed mechanism of the photocatalytic hydroxylation of benzene to phenol.
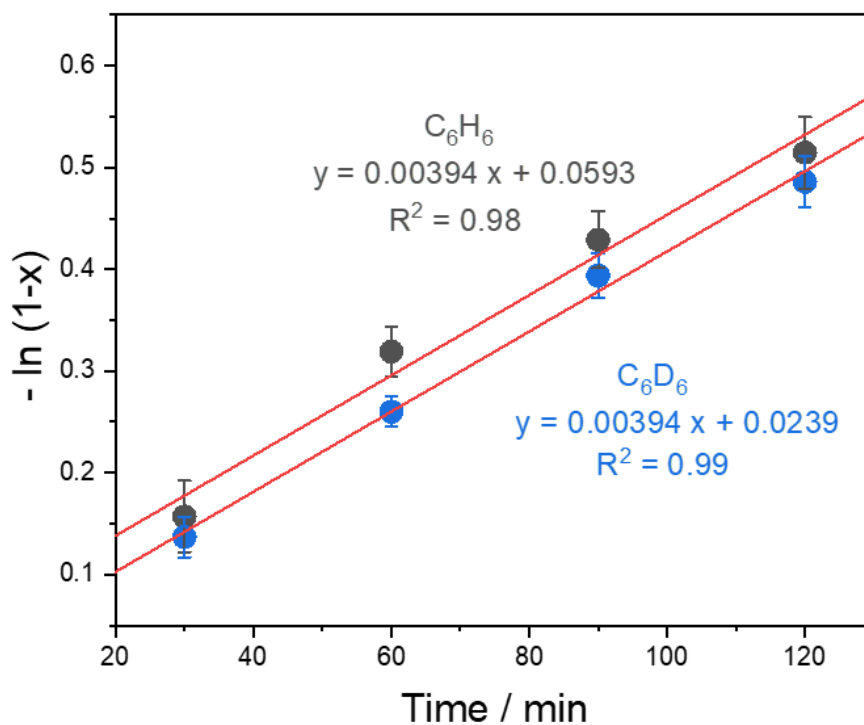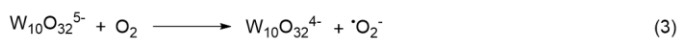
**Fig. 11.** Photocatalytic hydroxylation of benzene or benzene-$d_6$ at different time interval. Reaction condition: water/acetic acid, 5/1 (V/V); pH = 2; light source, 300 W xenon lamp; temperature, 10 °C; photocatalyst concentration, 0.136 mM, benzene concentration: 4 mM, air atmosphere (1 atm).

The detailed pathway for the reoxidation of $W_{10}O_{32}^{5-}$ is discussed as follows: first, the electron transfer from $W_{10}O_{32}^{5-}$ to $O_2$ occurs by an outer-sphere mechanism to form superoxide radicals ($^{\bullet}O_2^-$) (Eq. 3) [52], which can be rapidly transformed to a superoxide intermediate ($^{\bullet}HO_2$) (Eq. 4). Subsequently, $^{\bullet}HO_2$ can cause spontaneous disproportionation, resulting in $H_2O_2$ and $O_2$ (Eq. 5) [53]. Notably, the generation of $H_2O_2$ was confirmed in our system, which is consistent with previous work (Fig. 12). The amount of $H_2O_2$ produced during the reaction was determined spectroscopically [4]. After the photoreaction stopped, NaI (200 mM) was added to the reaction solution, and the absorption spectrum of $I_3^-$ species formed by the reaction of $I^-$ with $H_2O_2$ was measured. The concentration of $H_2O_2$ was determined from the absorbance at the absorption maximum ($\lambda$= 350 nm) of the $I_3^-$ species
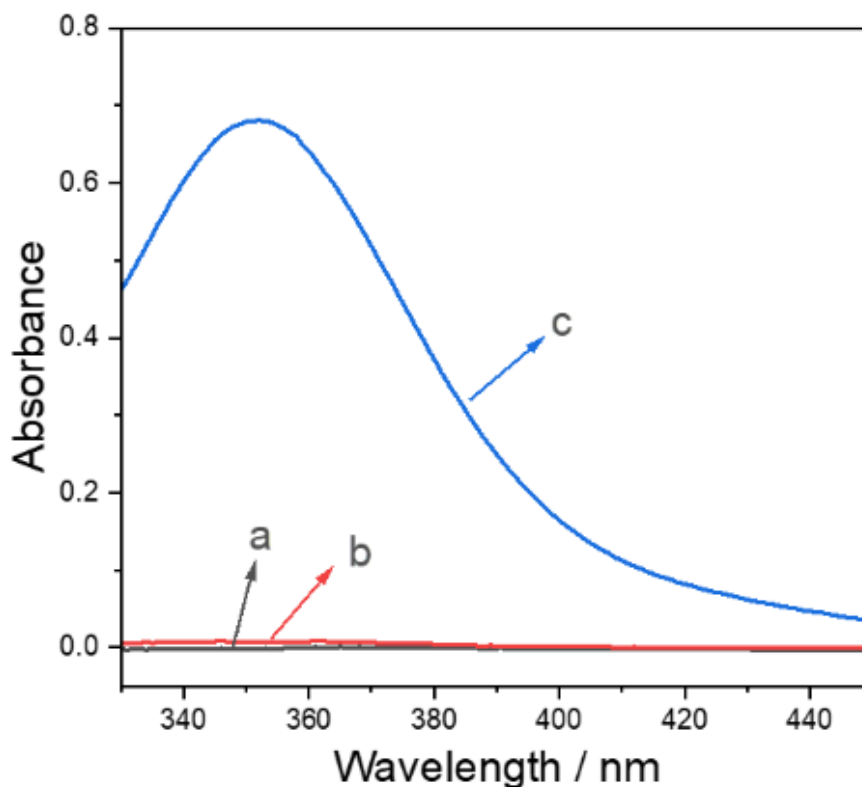
**Fig. 12.** UV-VIS spectra: aqueous solution of (a) NaI (0.2 M) before and (c) after addition of a solution of the product mixture; (b) diluted solution of the product mixture

$$W_{10}O_{32}{}^{5-} + O_2 \longrightarrow W_{10}O_{32}{}^{4-} + {}^\bullet O_2{}^- \tag{3}$$

$${}^\bullet O_2{}^- + H^+ \longrightarrow {}^\bullet HO_2 \tag{4}$$

$${}^\bullet HO_2 + {}^\bullet HO_2 \longrightarrow H_2O_2 + O_2 \tag{5}$$

Furthermore, hydroxyl radicals (${}^\bullet$OH) may be generated from $H_2O_2$, which can attack benzene to give phenol, according to this pathway (Eqs. 6 and 7) [54].

$$H_2O_2 + W_{10}O_{32}{}^{5-} + H^+ \longrightarrow {}^\bullet OH + W_{10}O_{32}{}^{4-} + H_2O \tag{6}$$
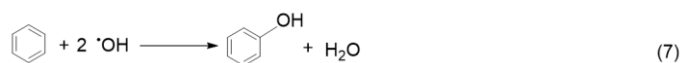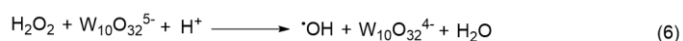


However, the $H_2O_2$-induced phenol formation process was not important in our system, which can be explained by the following reasons. According to the results shown in Fig. 10 (b and d), no phenol generation occurred, while the reduced species were reoxidized to their original state within 30 min after the light was turned off and they were exposed to air again. Hence, the direct reoxidation of $W_{10}O_{32}{}^{5-}$ with $O_2$ (Eq. 3) is dominate rather than with $H_2O_2$ (Eq. 6) in the reoxidation process. This result is consistent with previous studies, which showed that the reoxidation of POMs with $H_2O_2$ is

kinetically slower than that with $O_2$ [55-57].

*Comparison of $W_{10}O_{32}{}^{4-}$ with other photocatalysts for benzene hydroxylation*

Photocatalytic systems for benzene hydroxylation to phenol under mild conditions have been reported in recent years. Table 2 lists the previous photocatalysts for the oxidation of benzene to phenol in an $O_2$/air atmosphere. Noble metal-based heterogeneous photocatalysts, including Au-Pd/TiO$_2$ and Pt/WO$_3$, showed higher phenol yields but relatively lower selectivities than noble metal-free heterogeneous photocatalysts (Entries 1−5). For noble metal-free photocatalysts, with the exception of TiO$_2$@MCF, which showed a very low selectivity (35%), Bi$_2$WO$_6$/CdWO$_4$ and Zn$_2$Ti-LDH showed high phenol selectivities in 2−4 h. However, they generally showed a low phenol yield (14%, 7%, and 5%, respectively). In addition, organic photocatalysts showed a higher phenol yield or selectivity than heterogeneous semiconductor-based photocatalysts (Entries 6-9) in 1−24 h [58]. As an inorganic photocatalyst, $W_{10}O_{32}{}^{4-}$ showed comparable and even higher phenol yields and selectivities than most reported photocatalysts (Entries 10 and 11) in a short reaction time (1 h). Although QuCN$^+$ based system showed a similar phenol yield but higher selectivity in 1 h (Entry 6), it was performed in acetonitrile solution as a general reaction media for organic photocatalysts. Hence, $W_{10}O_{32}{}^{4-}$ as an inorganic photocatalyst in an aqueous solution showing promising application potential.

**Table 2** Comparison of the performance of the $W_{10}O_{32}{}^{4-}$ with the previous photocatalysts for aerobic oxidation of benzene.

| Entry | Photocatalysts | Atmosphere | Reaction time (h) | Phenol yield (%) | Selectivity (%) | Ref. |
|---|---|---|---|---|---|---|
| 1 | Au-Pd/TiO$_2$[a] | O$_2$ | 2.5 | 30 | - | [59] |
| 2 | Pt/WO$_3$[a] | Air | 4 | 51 | 69 | [24] |
| 3 | TiO$_2$@MCF | O$_2$ | 2 | 14 | 35 | [60] |
| 4 | Bi$_2$WO$_6$/CdWO$_4$ | O$_2$ | 3 | 7 | 99 | [25] |
| 5 | Zn$_2$Ti-LDH | Air | 4 | 5.0 | 87.2 | [26] |
| 6 | QuCN$^{+}$[b] | O$_2$ | 1 | 30 | 98 | [28] |

| 7 | [RuII(Me$_2$phen)$_3$]$^{2+}$ [b] | O$_2$ | 24 | 30 | - | [27] |
| 8 | C$_{16}$Qu-PW [b] | Air | 10 | 21 | 99 | [44] |
| 9 | QuH$_2$SO$_4$ [b] | O$_2$ | 10 | 11 | 99 | [61] |
| 10 | W$_{10}$O$_{32}$$^{4-}$ | Air | 1 | 41 | 76 | This work |
| 11 | W$_{10}$O$_{32}$$^{4-}$ | Air | 1 | 24 | 81 | |

[a] Noble metal-based photocatalysts. [b] Organic photocatalysts.

To further study the photocatalytic benzene hydroxylation behavior of W$_{10}$O$_{32}$$^{4-}$, the catalytic activity of various photocatalysts in our system was compared. As summarized in Table 3 (Entries 1–3), W$_{10}$O$_{32}$$^{4-}$ showed a much higher activity for photocatalytic benzene hydroxylation than Keggin-type POMs, such as PW$_{12}$O$_{40}$$^{3-}$ and PMo$_{12}$O$_{40}$$^{3-}$. The higher activity of W$_{10}$O$_{32}$$^{4-}$ is related to two aspects: (1) The maximum absorption of W$_{10}$O$_{32}$$^{4-}$ at 323 nm is much longer in wavelength than that of PW$_{12}$O$_{40}$$^{3-}$ (265 nm). As shown in Fig. 13, the light absorption of W$_{10}$O$_{32}$$^{4-}$ was extended to 400 nm, indicating an important overlap with the emission spectra of the xenon lamp used in our system. (2) Although the absorption of PMo$_{12}$O$_{40}$$^{3-}$ overlapped with the xenon lamp, the activity was even lower than that of PW$_{12}$O$_{40}$$^{3-}$. The reluctant reoxidation of heteropoly blue of PMo$_{12}$O$_{40}$$^{3-}$ with O$_2$ during the reaction was observed, indicating that the reaction stopped. The prevented catalytic cycle is the reason why PMo$_{12}$O$_{40}$$^{3-}$ showed a lower activity than tungsten-containing POMs in our aqueous acetic acid solution.
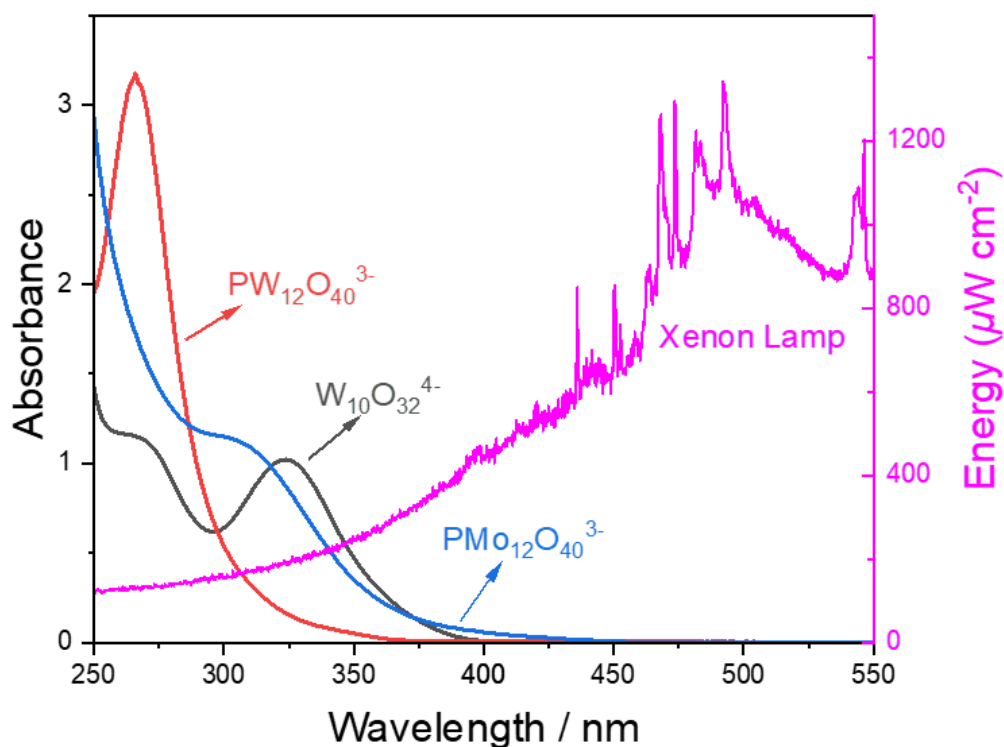
**Fig. 13.** Emission spectrum of Xenon lamp used in our system and UV–VIS spectra of $W_{10}O_{32}^{4-}$, $PW_{12}O_{40}^{3-}$, and $PMo_{12}O_{40}^{3-}$.

Notably, semiconductor-based photocatalysts, including $TiO_2$ (P25), $WO_3$, and g-$C_3N_4$, showed very low ( < 0.1) or no detectable phenol (Entries 4–6). However, $TiO_2$ showed a 17% phenol formation at a 25% benzene conversion with a 69% selectivity in pure water. Although $W_{10}O_{32}^{4-}$ showed a higher benzene conversion in pure water, the lower phenol selectivity leads to a lower phenol yield (Entries 7–8). The above result indicates that acetic acid completely prevented benzene hydroxylation over $TiO_2$, while benzene hydroxylation over $W_{10}O_{32}^{4-}$ also decreased somewhat. It has been reported that the photocatalytic hydroxylation of benzene in $TiO_2$ systems is dominated by holes and highly active radicals, especially hydroxyl radicals ($^{\bullet}OH$) (Route A, Scheme 3) [62,63]. Completely prevented benzene hydroxylation may occur due to kinetic competition by adding acetic acid for the reaction with holes and $^{\bullet}OH$. This highly active radical is not selective and scavenged by excess acetic acid, resulting in completely inhibited benzene hydroxylation of $TiO_2$ (Entries 4,8). However, in $W_{10}O_{32}^{4-}$, the wO-initiated ET process dominated the benzene hydroxylation reaction, as described above (Route B, Scheme 3). From the above results, we know that wO-initiated ET was only slightly suppressed by comparing the benzene conversion in the presence or absence of

acetic acid (Entries 1 and 7 in Table 3).
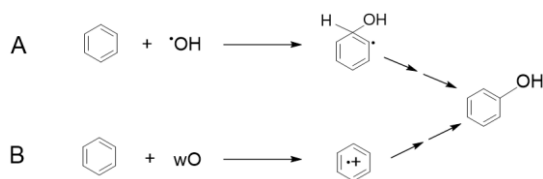


**Scheme 3.** Two routes for the photocatalytic hydroxylation of benzene to phenol.

Table 3 Photocatalytic benzene oxidation to phenol with $W_{10}O_{32}^{4-}$ in various solvents [a]



| Entry | Photocatalysts | Benzene conversion (%) | Phenol yield (%) | Selectivity (%) | Type of photocatalysts |
|---|---|---|---|---|---|
| 1 | $W_{10}O_{32}^{4-}$ | 30 | 24 | 81 | POMs |
| 2 | $PW_{12}O_{40}^{3-}$ | 5 | 4.5 | 89 | POMs |
| 3 | $PMo_{12}O_{40}^{3-}$ | 1 | 0.7 | 73 | POMs |
| 4 | $TiO_2$ | < 0.1 | < 0.1 | - | Semiconductor |
| 5 | $WO_3$ | 0 | - | - | Semiconductor |
| 6 | $g-C_3N_4$ | 0 | - | - | Semiconductor |
| 7 | $W_{10}O_{32}^{4-}$ [b] | 38 | 23 | 61 | POMs |
| 8 | $TiO_2$ [b] | 25 | 17 | 69 | Semiconductor |

[a] Reaction condition: light source, 300 W xenon lamp; temperature, 10 °C; irradiation times, 60 min; benzene concentration, 4 mM; Water/co-solvent, 5/1 (V/V); pH = 2; under ambient condition; catalyst concentration, 0.136 mM or 0.333g/L; [b] in pure water.

The hydroxylation process in the presence or absence of acetic acid was further studied using substituted benzene compounds (Table 4) [4-6]. The $W_{10}O_{32}^{4-}$ catalyst exhibited negligible hydroxylation activity for anisole in the presence or absence of acetic acid (entries 1 and 2). The amount of reduced polyanion formed in the anisole oxidation reaction in the absence of oxygen was much less than that in the benzene oxidation reaction, indicating that the electron transfer from anisole to the excited catalyst proceeds more slowly than that from benzene. $TiO_2$ was also found to show low activity for hydroxylation of anisole than benzene (entry 3). On the other hand,

74

photooxidation of nitrobenzene in water-acetic acid solution yielded the product o-nitrophenol with a conversion of 3% and selectivity of 89% (Entry 4). Similar to benzene, when nitrobenzene was used as a substrate in pure water, the conversion rate increased, but the selectivity decreased (Entry 5).

**Table 4** Photocatalytic oxidation of substituted benzene with $W_{10}O_{32}^{4-}$ in various solvents [a]

| Entry | Substrate | Conversion (%) | *ortho* selectivity (%) | *para* selectivity (%) |
|-------|-----------|----------------|-------------------------|------------------------|
| 1 | Anisole | < 0.1 | - | < 0.1 |
| 2 | Anisole [b] | < 0.1 | - | < 0.1 |
| 3 | Anisole [c] | 2 | 21 | < 0.1 |
| 4 | Nitrobenzene | 1 | 89 | < 0.1 |
| 5 | Nitrobenzene [b] | 3 | 72 | < 0.1 |

[a] Reaction condition: light source, 300 W xenon lamp; temperature, 10 °C; irradiation times, 60 min; substrate concentration, 1 mM; Water/co-solvent, 5/1 (V/V); pH = 2; under ambient condition; catalyst concentration, 0.136 mM or 0.333g/L; [b] in pure water; [c]10 mg of TiO₂ as photocatalyst.

It can be seen that the hydroxylation rates for anisole and nitrobenzene are lower than those for benzene. The lower reactivity of nitrobenzene is reasonable since a nitro group is an electron-withdrawing group, and the electron transfer from nitrobenzene to the catalyst is less progressive. On the other hand, anisole, which has an electron-donating group, also showed lower reactivity than benzene in this system, consistent with previous reports [25,67]. According to previous reports, the reason for the lower reactivity of anisole than benzene may be that the methoxy group of anisole destroys the planar structure of the molecule and increases the steric hindrance when interacting with active species such as catalyst and ˙OH [68]. It should be noted that ˙OH in the Fenton reaction showed much higher activity for phenol oxidation than benzene (Table 5). This behavior is different from $W_{10}O_{32}^{4-}$-catalyzed photooxidation, in which the rate for phenol oxidation is lower than that for benzene oxidation, indicating that OH radical is not the active species for benzene oxidation.

**Table 5** Oxidation of aromatics by Fenton reagent [a]

| Entry | Substrate | Reaction time (min) | conversion (%) |
|-------|-----------|---------------------|----------------|
| 1 | Benzene | 30 | 32 |

| 2 | Phenol | 10 | 100 |
|---|---|---|---|

Importantly, although acetic acid slightly decreased the benzene conversion, phenol oxidation was simultaneously suppressed, as described above. As a result, a higher phenol selectivity with no significant decrease in the phenol yield were obtained by adding acetic acid to our photocatalytic system, in a marked contrast with $TiO_2$.

### 3.4 Conclusion

One-pot benzene hydroxylation to phenol with $O_2$ under ambient conditions was successfully performed using $W_{12}O_{32}^{4-}$ as an inorganic photocatalyst. The phenol yield and selectivity were improved, reaching 17%-41% and 76%-82%, respectively, by adding a small amount of acetic acid as a co-solvent. On one hand, acetic acid improved the benzene solubility and suppressed the vaporization of benzene during the reaction. On the other hand, phenol oxidation was suppressed due to the presence of acetic acid, which can be competitively oxidized with wO together with the substrate. The $W_{12}O_{32}^{4-}$ activity was significantly higher than that of some other typical photocatalysts, such as $PW_{12}O_{40}^{3-}$ and $TiO_2$ (P25), in our system. An ET process differs from the hydroxyl radical pathway involved in $TiO_2$, resulting in a high phenol yield in our system. This work provided a promising method for benzene hydroxylation to phenol with $O_2$ and expanded the applications of DT-based photocatalytic organic synthesis.

### Reference

[1] S.S. Acharyya, S. Ghosh, R. Tiwari, C. Pendem, T. Sasaki, R. Bal, Synergistic Effect between ultrasmall Cu(II) oxide and $CuCr_2O_4$ spinel nanoparticles in selective hydroxylation of benzene to phenol with air as oxidant, ACS Catal., 5 (2015) 2850–2858, https://doi.org/10.1021/cs5020699.

[2] W. Wang, N. Li, H. Tang, Y. Ma, X. Yang, Vanadium oxyacetylacetonate grafted on UiO-66-NH 2 for hydroxylation of benzene to phenol with molecular oxygen, Mol. Catal., 453 (2018) 113–120, https://doi.org/10.1016/j.mcat.2018.05.003.

[3] M. Yamada, K.D. Karlin, S. Fukuzumi, One-step selective hydroxylation of benzene to phenol

with hydrogen peroxide catalysed by copper complexes incorporated into mesoporous silica-alumina, Chem. Sci., 7 (2016) 2856–2863, https://doi.org/10.1039/C5SC04312C.

[4] Y. Zhang, S.-J. Park, Stabilizing CuPd bimetallic alloy nanoparticles deposited on holey carbon nitride for selective hydroxylation of benzene to phenol, J. Catal., 379 (2019) 154–163, https://doi.org/10.1016/j.jcat.2019.09.032.

[5] B. Wang, M. Anpo, J. Lin, C. Yang, Y. Zhang, X. Wang, Direct hydroxylation of benzene to phenol on h-BCN nanosheets in the presence of $FeCl_3$ and $H_2O_2$ under visible light, Catal. Today, 324 (2019) 73–82, https://doi.org/10.1016/j.cattod.2018.07.001.

[6] J. Xu, Y. Chen, Y. Hong, H. Zheng, D. Ma, B. Xue, Y.-X. Li, Direct catalytic hydroxylation of benzene to phenol catalyzed by vanadia supported on exfoliated graphitic carbon nitride, Appl. Catal. A: Gen., 549 (2018) 31–39, https://doi.org/10.1016/j.apcata.2017.09.015.

[7] X. Ye, Y. Cui, X. Wang, Ferrocene-modified carbon nitride for direct oxidation of benzene to phenol with visible light, ChemSusChem, 7 (2014) 738-742, https://doi.org/10.1002/cssc.201301128.

[8] R.J. Schmidt, Industrial catalytic processes—phenol production, Appl. Catal. A: Gen., 280 (2005) 89–103, https://doi.org/10.1016/j.apcata.2004.08.030.

[9] A.E. ElMetwally, G. Eshaq, F.Z. Yehia, A.M. Al-Sabagh, S. Kegnæs, Iron oxychloride as an efficient catalyst for selective hydroxylation of benzene to phenol, ACS Catal., 8 (2018) 10668–10675, https://doi.org/10.1021/acscatal.8b03590.

[10] M.L. Neidig, K.F. Hirsekorn, Insight into contributions to phenol selectivity in the solution oxidation of benzene to phenol with $H_2O_2$, Catal. Commun., 12 (2011) 480–484, https://doi.org/10.1016/j.catcom.2010.10.024.

[11] S. Fukuzumi, K. Ohkubo, One-step selective hydroxylation of benzene to phenol, Asian J. Org. Chem., 4 (2015) 836–845, https://doi.org/10.1002/ajoc.201500187.

[12] A. Mancuso, O. Sacco, D. Sannino, V. Venditto, V. Vaiano, One-step catalytic or photocatalytic oxidation of benzene to phenol: possible alternative routes for phenol synthesis?, Catalysts, 10 (2020) 1424, https://doi.org/10.3390/catal10121424.

[13] S. Mishra, R. Bal, R.K. Dey, Heterogeneous recyclable copper oxide supported on activated red mud as an efficient and stable catalyst for the one pot hydroxylation of benzene to phenol,

Mol. Catal., 499 (2021) 111310, https://doi.org/10.1016/j.mcat.2020.111310.

[14] Q. Qin, Y. Liu, W. Shan, W. Hou, K. Wang, X. Ling, Y. Zhou, J. Wang, Synergistic catalysis of $Fe_2O_3$ nanoparticles on mesoporous poly(ionic liquid)-derived carbon for benzene hydroxylation with dioxygen, Ind. Eng. Chem. Res., 56 (2017) 12289–12296, https://doi.org/10.1021/acs.iecr.7b02566.

[15] X. Cai, Q. Wang, Y. Liu, J. Xie, Z. Long, Y. Zhou, J. Wang, Hybrid of polyoxometalate-based ionic salt and N-doped carbon toward reductant-free aerobic hydroxylation of benzene to phenol, ACS Sustain. Chem. Eng., 4 (2016) 4986–4996, https://doi.org/10.1021/acssuschemeng.6b01357.

[16] S. Ghosh, S.S. Acharyya, T. Kaneko, K. Higashi, Y. Yoshida, T. Sasaki, Y. Iwasawa, Confined single alkali metal ion platform in a zeolite pore for concerted benzene C–H activation to phenol catalysis, ACS Catal., 8 (2018) 11979–11986, https://doi.org/10.1021/acscatal.8b03002.

[17] Z. Long, Y. Zhang, G. Chen, J. Shang, Y. Zhou, J. Wang, L. Sun, Nitrogen-doped biomass carbons meet with polyoxometalates: synergistic catalytic reductant-free aerobic hydroxylation of benzene to phenol, ACS Sustain. Chem. Eng., 7 (2019) 4230–4238, https://doi.org/10.1021/acssuschemeng.8b05920.

[18] M. Tani, T. Sakamoto, S. Mita, S. Sakaguchi, Y. Ishii, Hydroxylation of benzene to phenol under air and carbon monoxide catalyzed by molybdovanadophosphoric acid, Angew. Chem. Int. Ed. Engl., 44 (2005) 2586–2588, https://doi.org/10.1002/anie.200462769.

[19] X. Ye, Y. Cui, X. Qiu, X. Wang, Selective oxidation of benzene to phenol by Fe-CN/TS-1 catalysts under visible light irradiation, Appl. Catal. B: Environ., 152-153 (2014) 383–389, https://doi.org/10.1016/j.apcatb.2014.01.050.

[20] P. Devaraji, N.K. Sathu, C.S. Gopinath, Ambient oxidation of benzene to phenol by photocatalysis on $Au/Ti_{0.98}V_{0.02}O_2$: Role of Holes, ACS Catal., 4 (2014) 2844–2853, https://doi.org/10.1021/cs500724z.

[21] J. He, M. Zhang, A. Primo, H. García, Z. Li, Selective photocatalytic benzene hydroxylation to phenol using surface-modified $Cu_2O$ supported on graphene, J. Mater. Chem. A, 6 (2018) 19782–19787, https://doi.org/10.1039/C8TA07095D.

[22] P. Riente, T. Noël, Application of metal oxide semiconductors in light-driven organic

transformations, Catal. Sci. Technol., 9 (2019) 5186–5232, https://doi.org/10.1039/C9CY01170F.

[23] Y. Kurikawa, M. Togo, M. Murata, Y. Matsuda, Y. Sakata, H. Kobayashi, S. Higashimoto, Mechanistic insights into visible light-induced direct hydroxylation of benzene to phenol with air and water over Pt-modified $WO_3$ photocatalyst, Catalysts, 10 (2020) 557, https://doi.org/10.3390/catal10050557.

[24] O. Tomita, B. Ohtani, R. Abe, Highly selective phenol production from benzene on a platinum-loaded tungsten oxide photocatalyst with water and molecular oxygen: selective oxidation of water by holes for generating hydroxyl radical as the predominant source of the hydroxyl group, Catal. Sci. Technol., 4 (2014) 3850–3860, https://doi.org/10.1039/C4CY00445K.

[25] P. Chen, L. Chen, Y. Zeng, F. Ding, X. Jiang, N. Liu, C.-T. Au, S.-F. Yin, Three-dimension hierarchical heterostructure of CdWO4 microrods decorated with $Bi_2WO_6$ nanoplates for high-selectivity photocatalytic benzene hydroxylation to phenol, Appl. Catal. B: Environ., 234 (2018) 311–317, https://doi.org/10.1016/j.apcatb.2018.04.028.

[26] J. Li, Y. Xu, Z. Ding, A.H. Mahadi, Y. Zhao, Y.-F. Song, Photocatalytic selective oxidation of benzene to phenol in water over layered double hydroxide: A thermodynamic and kinetic perspective, Chem. Eng. J., 388 (2020) 124248, https://doi.org/10.1016/j.cej.2020.124248.

[27] J.W. Han, J. Jung, Y.M. Lee, W. Nam, S. Fukuzumi, Photocatalytic oxidation of benzene to phenol using dioxygen as an oxygen source and water as an electron source in the presence of a cobalt catalyst, Chem Sci, 8 (2017) 7119–7125, https://doi.org/10.1039/C7SC02495A.

[28] K. Ohkubo, T. Kobayashi, S. Fukuzumi, Direct oxygenation of benzene to phenol using quinolinium ions as homogeneous photocatalysts, Angew. Chem. Int. Ed. Engl., 50 (2011) 8652–8655, https://doi.org/10.1002/ange.201102931.

[29] M.D. Tzirakis, I.N. Lykakis, M. Orfanopoulos, Decatungstate as an efficient photocatalyst in organic chemistry, Chem. Soc. Rev., 38 (2009) 2609–2621, https://doi.org/10.1039/B812100C.

[30] D. Ravelli, S. Protti, M. Fagnoni, Decatungstate anion for photocatalyzed "window ledge" reactions, Acc. Chem. Res., 49 (2016) 2232–2242, https://doi.org/10.1021/acs.accounts.6b00339.

[31] C. Tanielian, Decatungstate photocatalysis, Coordination Chemistry Reviews, 178–180 (1998)

1165–1181, https://doi.org/10.1016/S0010-8545(98)00160-X.

[32] D. Ravelli, M. Fagnoni, T. Fukuyama, T. Nishikawa, I. Ryu, Site-selective C–H functionalization by decatungstate anion photocatalysis: synergistic control by polar and steric effects expands the reaction scope, ACS Catal., 8 (2017) 701–713, https://doi.org/10.1021/acscatal.7b03354.

[33] P.J. Sarver, V. Bacauanu, D.M. Schultz, D.A. DiRocco, Y.H. Lam, E.C. Sherer, D.W.C. MacMillan, The merger of decatungstate and copper catalysis to enable aliphatic C(sp(3))-H trifluoromethylation, Nat. Chem., 12 (2020) 459–467, https://doi.org/10.1038/s41557-020-0436-1.

[34] W. Wu, Z. Fu, S. Tang, S. Zou, X. Wen, Y. Meng, S. Sun, J. Deng, Y. Liu, D. Yin, $(nBu_4N)_4W_{10}O_{32}$-catalyzed selective oxygenation of cyclohexane by molecular oxygen under visible light irradiation, Appl. Catal. B: Environ., 164 (2015) 113–119, https://doi.org/10.1016/j.apcatb.2014.08.045.

[35] P. Cheng, Y. Wang, M. Sarakha, G. Mailhot, Enhancement of the photocatalytic activity of decatungstate, $W_{10}O_{32}^{4-}$, for the oxidation of sulfasalazine/sulfapyridine in the presence of hydrogen peroxide, J. Photoch. Photobio. A, 404 (2021), https://doi.org/10.1016/j.jphotochem.2020.112890.

[36] l. Texier, J. Ouazzani, J. Delaire, C. Giannotti, Study of the mechanisms of the photodegradation of atrazine in the presence of two photocatalysts: $TiO_2$ and $Na_4W_{10}O_{32}$, Tetrahedron, 55 (1999) 3401–3412, https://doi.org/10.1016/S0040-4020(98)01150-8.

[37] I. Texier, C. Giannotti, S. Malato, C. Richter, J. Delaire, Solar photodegradation of pesticides in water by sodium decatungstate, Cataly. Today, 54 (1999) 297–307, https://doi.org/10.1016/S0920-5861(99)00191-1.

[38] S. Farhadi, Z. Momeni, Zirconia-supported sodium decatungstate ($Na_4W_{10}O_{32}/ZrO_2$): An efficient, green and recyclable photocatalyst for selective oxidation of activated alcohols to carbonyl compounds with $O_2$, J. Mol. Catal. A: Chem., 277 (2007) 47–52, https://doi.org/10.1016/j.molcata.2007.07.024.

[39] X. Shi, S. Liu, C. Duanmu, M. Shang, M. Qiu, C. Shen, Y. Yang, Y. Su, Visible-light photooxidation of benzene to phenol in continuous-flow microreactors, Chem. Eng. J., 420

(2021) 129976, https://doi.org/10.1016/j.cej.2021.129976.

[40] D.C. Duncan, T.L. Netzel, C.L. Hill, Early-time dynamics and reactivity of polyoxometalate excited states. identification of a short-lived LMCT excited state and a reactive long-lived charge-transfer intermediate following picosecond flash excitation of $[W_{10}O_{32}]^*$ in acetonitrile, Inorg. Chem. , 34 (1995) 4640–4646, https://doi.org/10.1021/ic00122a021.

[41] D.C. Duncan, C.L. Hill, Synthesis and characterization of the mixed-valence diamagnetic two-electron-reduced isopolytungstate $[W_{10}O_{32}]^{6-}$. Evidence for an asymmetric d-electron distribution over the tungsten sites, Inorg. Chem., 35 (1996) 5828–5835, https://doi.org/10.1021/ic960226w.

[42] C. Lu, P. Zhang, S. Jiang, X. Wu, S. Song, M. Zhu, Z. Lou, Z. Li, F. Liu, Y. Liu, Y. Wang, Z. Le, Photocatalytic reduction elimination of $UO^{22+}$ pollutant under visible light with metal-free sulfur doped g-$C_3N_4$ photocatalyst, Appl. Catal. B: Environ., 200 (2017) 378–385, https://doi.org/10.1016/j.apcatb.2016.07.036.

[43] S.C. Termes, M.T. Pope, Reduction of the decatungstate anion in nonaqueous solution and its confirmation as "polytungstate-Y", Inorg. Chem., 17 (1978) 500–501, https://doi.org/10.1021/ic50180a064.

[44] L. Zhang, Q. Hou, Y. Zhou, J. Wang, Phosphotungstic anion-paired quinoline salt for heterogeneous photocatalytic hydroxylation of benzene to phenol with air, Mol. Catal., 473 (2019) 110397, https://doi.org/10.1016/j.mcat.2019.110397.

[45] J. Dai, Y. Guo, L. Xu, G. Zhuang, Y. Zheng, D. Sun, J. Huang, Q. Li, Bovine serum albumin templated porous $CeO_2$ to support Au catalyst for benzene oxidation, Mol. Catal., 486 (2020) 110849, https://doi.org/10.1016/j.mcat.2020.110849.

[46] S. Rafqah, P.W.-W. Chung, C. Forano, M. Sarakha, Photocatalytic degradation of metsulfuron methyl in aqueous solution by decatungstate anions, J. Photoch. Photobio. A, 199 (2008) 297–302, https://doi.org/10.1016/j.jphotochem.2008.06.012.

[47] K. Nomiya, Y. Sugie, K. Amimoto, M. Miwa, Charge-transfer absorption spectra of some tungsten(VI) and molybdenum(VI) polyoxoanions, Polyhedron, 6 (1987) 519–524, https://doi.org/10.1016/S0277-5387(00)81018-9.

[48] A. Molinari, R. Argazzi, A. Maldotti, Photocatalysis with $Na_4W_{10}O_{32}$ in water system:

Formation and reactivity of OH radicals, J. Mol. Catal. A: Chem., 372 (2013) 23–28, https://doi.org/10.1016/j.molcata.2013.01.037.

[49] J.K. Kochi, R.T. Tang, T. Bernath, Mechanisms of aromatic substitution. Role of cation-radicals in the oxidative substitution of arenes by cobalt(III), J. Am. Chem. Soc., 95 (1972) 7114–7123, https://doi.org/10.1021/ja00802a036.

[50] S. Montanaro, D. Ravelli, D. Merli, M. Fagnoni, A. Albini, Decatungstate as photoredox catalyst: benzylation of electron-poor olefins, Org. lett., 14 (2012) 4218–4221, https://doi.org/10.1021/ol301900p.

[51] B.B. Sarma, R. Carmieli, A. Collauto, I. Efremenko, J.M.L. Martin, R. Neumann, Electron transfer oxidation of benzene and aerobic oxidation to phenol, ACS Catal., 6 (2016) 6403–6407, https://doi.org/10.1021/acscatal.6b02083.

[52] A. Allaoui, M.A. Malouki, P. Wong-Wah-Chung, Homogeneous photodegradation study of 2-mercaptobenzothiazole photocatalysed by sodium decatungstate salts: Kinetics and mechanistic pathways, J. Photoch. and Photobio. A, 212 (2010) 153–160, https://doi.org/10.1016/j.jphotochem.2010.04.010.

[53] H. Hori, Y. Takano, K. Koike, K. Takeuchi, H. Einaga, Decomposition of environmentally persistent trifluoroacetic acid to fluoride ions by a homogeneous photocatalyst in water, Environ. Sci. Technol. , 37 (2003) 418–422, https://doi.org/10.1021/es025783y.

[54] W. Wang, H. Tang, X. Jiang, F.E. Huang, Y. Ma, Quinone-amine polymers as metal-free and reductant-free catalysts for hydroxylation of benzene to phenol with molecular oxygen, Chem. Commun., 55 (2019) 7772–7775, https://doi.org/10.1039/C9CC03623G.

[55] O. Snir, Y. Wang, M.E. Tuckerman, Y.V. Geletii, I.A. Weinstock, Concerted proton-electron transfer to dioxygen in water, J. Am. Chem. Soc. 132 (2010) 11678–11691. ttps://doi.org/10.1021/ja104392k.

[56] M. Kim, I.A. Weinstock, Y.V. Geletii, C.L. Hill, Oxidation of reduced Keggin heteropolytungstates by dioxygen in water catalyzed by Cu(II), ACS Catal. 5 (2015) 7048–7054. https://doi.org/10.1021/acscatal.5b01771.

[57] Y.V. Geletii, C.L. Hill, R.H. Atalla, I.A. Weinstock, Reduction of $O_2$ to superoxide anion ($O_2$ $^{\cdot-}$) in water by heteropolytungstate cluster-anions, J. Am. Chem. Soc. 128 (2006) 7033–17042,

https://doi.org/10.1021/ja064244g.

[58] L. Chen, J. Tang, L.-N. Song, P. Chen, J. He, C.-T. Au, S.-F. Yin, Heterogeneous photocatalysis for selective oxidation of alcohols and hydrocarbons, Appl. Catal. B: Environ., 242 (2019) 379–388, https://doi.org/10.1016/j.apcatb.2018.10.025.

[59] R. Su, L. Kesavan, M.M. Jensen, R. Tiruvalam, Q. He, N. Dimitratos, S. Wendt, M. Glasius, C.J. Kiely, G.J. Hutchings, F. Besenbacher, Selective photocatalytic oxidation of benzene for the synthesis of phenol using engineered Au-Pd alloy nanoparticles supported on titanium dioxide, Chem. Commun., 50 (2014) 12612–12614, https://doi.org/10.1039/C4CC04024D.

[60] G. Zhang, J. Yi, J. Shim, J. Lee, W. Choi, Photocatalytic hydroxylation of benzene to phenol over titanium oxide entrapped into hydrophobically modified siliceous foam, Appl. Catal. B: Environ., 102 (2011) 132–139, https://doi.org/10.1016/j.apcatb.2010.11.034.

[61] Z. Long, L. Sun, M. Zhang, Y. Zhang, C. Zong, Z. Xue, T. Wang, G. Chen, Metal-free photocatalytic aerobic hydroxylation of benzene catalyzed by the commercially available quinoline sulfate, Catal. Commun., 121 (2019) 1-4, https://doi.org/10.1016/j.catcom.2018.11.018.

[62] H. Park, W. Choi, Photocatalytic conversion of benzene to phenol using modified $TiO_2$ and polyoxometalates, Catal. Today, 101 (2005) 291–297, https://doi.org/10.1016/j.cattod.2005.03.014.

[63] O. Tomita, R. Abe, B. Ohtani, Direct synthesis of phenol from benzene over platinum-loaded tungsten(VI) oxide photocatalysts with water and molecular oxygen, Chem. Lett., 40 (2011) 1405–1407, https://doi.org/10.1246/cl.2011.1405.

[64] A.Yamaguchi, T. Watanabe, K. Saito, S. Kuwano, Y. Murakami, N. Mimura, O. Sato, Direct conversion of lignocellulosic biomass into aromatic monomers over supported metal catalysts in supercritical water, Mol. Catal., 477 (2019) 110557, https://doi.org/10.1016/j.mcat.2019.110557.

[65] X. Gao, S. Zhu, Y. Li, Selective hydrogenolysis of lignin and model compounds to monophenols over $AuPd/CeO_2$, Mol. Catal., 462 (2019) 69–76, https://doi.org/10.1016/j.mcat.2018.10.022.

[66] Y. Liu, W. Gao, H. Zhou, X. Yi, Y. Bao, Highly reactive bulk lattice oxygen exposed by simple

water treatment of LiCoO$_2$ for catalytic oxidation of airborne benzene, Mol. Catal., 492 (2020) 111003, https://doi.org/10.1016/j.mcat.2020.111003.

[67] J.K. Joseph, S. Singhal, S.L. Jain, R. Sivakumaran, B. Kumar, B.Sain, Studies on vanadium catalyzed direct hydroxylation of aromatic hydrocarbons using hydrogen peroxide as oxidant, Catal. Today, 141 (2009) 211–214, https://doi.org/10.1016/j.cattod.2008.05.037.

[68] J.H. Yang, G. Sun, Y. Gao, H. Zhao, P. Tang, J. Tan, A.H. Lu, D. Ma, Direct catalytic oxidation of benzene to phenol over metal-free graphene-based catalyst, Energ. Environ. Sci., 6 (2013) 793–798, https://doi.org/10.1039/C3EE23623D.

# Chapter 4:

Investigating the potential of supported $H_3PW_{12}O_{40}$ as heterogenous photocatalyst for benzene oxidation to phenol

# Chapter 4: Investigating the potential of supported $H_3PW_{12}O_{40}$ as heterogenous photocatalyst for benzene oxidation to phenol

## 4.1 Introduction

Polyoxometalates are anionic nanoclusters of early transition metal oxides with various structures [1]. They are usually used for homogeneous catalytic reactions due to their high solubility in polar solvents. Among polyoxometalates, Keggin-type phosphotungstic acids ($H_3PW_{12}O_{40}$; denoted HPW) have been frequently studied due to their high Brønsted acidity and reversible redox properties. They can also be used as photocatalysts, as they absorb near-ultraviolet light and can be excited into highly reactive chemical species (HPW*) [2]. The HPW* species acts as a better oxidant than HPW in the ground state for the oxidation of organic substrates, resulting in the formation of products and heteropoly blues (reduced state of HPW). The generated heteropolyblue is then readily reoxidized by $O_2$ to complete the catalytic cycle [3]. Based on this reaction mechanism, we reported photocatalytic benzene oxidation to phenol with HPW in a homogenous reaction system, which showed high phenol yield and selectivity.

In addition to homogeneous catalytic reactions, heteropoly acids immobilized on $TiO_2$, carbon, $Al_2O_3$, $ZrO_2$, zeolites, and metal-organic frames (MOFs) can be used for heterogeneous catalytic reactions [4–8]. Bertolini et al. synthesized HPW-$TiO_2$ composites for selective oxidation of toluene to benzaldehyde under photoirradiation [4]. Qu et al. prepared mesoporous HPW-$ZrO_2$ composites for photocatalytic degradation of aqueous 4-nitrophenol (4-NP) and dye methylene blue (MB) [8]. HPW has been encapsulated in MOFs as an efficient and recyclable photocatalyst for the degradation of harmful sulfamethazine in water [9]. Thus, the effectiveness of HPW as a photocatalyst has been demonstrated in heterogeneous catalysts.

Mesoporous silica is a promising support material due to its high surface area, high stability, and ordered mesoporous structure [10, 11]. A common method to immobilize HPW is to impregnate the support with a solution containing HPWs and then evaporate the solvent [12–14]. By using this

method, HPWs can be immobilized on almost all supports, including mesoporous silica [15]. Recent reports have outlined a direct sol-gel synthesis route for incorporating HPW into mesoporous silica by encapsulating HPW during the synthesis of silica materials [16–21]. In the directly synthesized sample, a chemical interaction is formed between the Keggin units and silica species, resulting in a homogeneous dispersion of HPW and improved stability [22]. This chemical interaction is evidenced by Fourier-transform infrared (FTIR) spectroscopy [17]. In addition, the high dispersion of HPW was also confirmed by X-ray diffraction (XRD): there was no peak observed for the samples prepared by the direct sol-gel method, while all HPW peaks were observed in the XRD pattern for the samples prepared by an impregnation method [16, 22].

Supported heteropoly acids have been reported as photocatalysts for organic synthesis and degradation of pollutants in aqueous solutions [3, 7, 23–29]. In these heterogeneous systems, leaching of polyanion species generally occurs due to their high solubility in water [30]. This leaching is believed to be responsible for a decrease in photocatalytic activity after successive reaction cycles [30]. However, no attention has been given to the contribution of the leached polyanions to homogenous catalytic reactions, which should not be neglected since polyanions have already been proven to be efficient homogeneous photocatalysts. Hence, a detailed study of the leaching behavior and activity of leached polyanions is crucial for a comprehensive understanding of the photocatalytic oxidation processes on supported heteropoly acid catalysts.

In this work, HPW was supported on mesoporous silica SBA-15 by a direct sol-gel method and a wet impregnate method. The structural and textural properties of the photocatalysts were fully characterized, and their applicability for photocatalytic benzene oxidation with $O_2$ in a heterogenous system has been investigated. To gain insight into the reaction mechanism, we investigated the leaching behavior of the supported HPW catalysts and the activity of leached species as homogenous photocatalysts. Leaching kinetic studies were carried out to investigate the interaction between HPW and SBA-15. In addition, the applicability of the supported HPW catalysts to solid-gas phase catalytic reactions was investigated.

## 4.2 Experimental

*Materials*

Pluronic P123 and tetraethyl orthosilicate (TEOS, 98%) were purchased from Sigma–Aldrich

(Japan). Hydrochloric acid (HCl), $H_3PW_{12}O_{40}$ (HPW), benzene, and other reagents were purchased from Wako (Japan). HPW was purified by ether extraction and recrystallization from water before use.

*Preparation of photocatalysts*

Supported HPW catalysts were prepared by a direct synthesis method and impregnation method. In the direct sol-gel method, the samples were prepared using a slight modification of a previously reported method (Scheme 1) [17]. First, 2.5 g of Pluronic P123 was dissolved in 40 g of deionized water and 25 g of 6 M HCl under stirring at 40 °C for 30 min before P123 was completely dissolved. Next, a 10 mL calculated amount of HPW aqueous solution was added dropwise under vigorous stirring. After 24 h, 5.4 g of TEOS was added dropwise into the mixture under rapid stirring. A white precipitate was observed to be formed, and the mixture was subsequently stirred for another 24 h (40 °C) to allow sufficient interaction between silica and HPW. Then, the obtained white suspension was transferred into a Pyrex bottle and subjected to an aging process for 24 h at 80 °C under static conditions. Finally, the white suspension was removed from the bottle, washed with deionized water, and filtered to obtain a white solid. The solid was dried at 60 °C for 12 h and then heated at 500 °C for 4 h in air. The template (P123) was not completely removed by heat treatment at 300 °C and 400 °C, and the sample was observed to turn a brown color, as shown in Fig. 1.
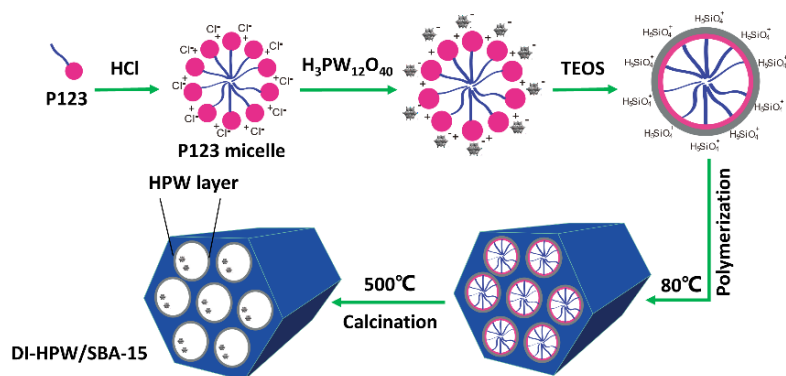


**Scheme 1** Illustration of the preparation of DI-HPW/SBA-15 composite
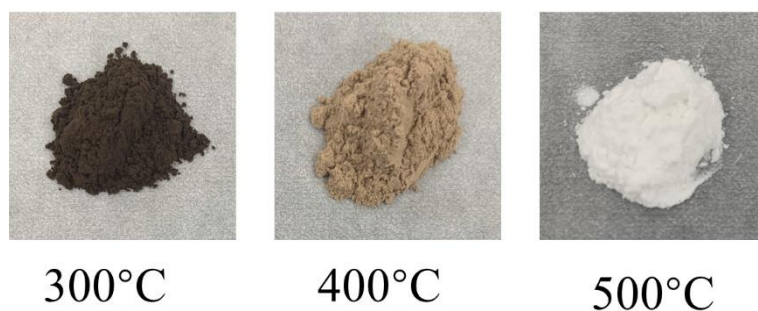
**Fig. 1.** Photograph of DI-HPW$_3$/SBA-15 calcinated at different temperature

The catalysts prepared by adding calculated amounts (10 wt.%, 20 wt.%, 30 wt.%, and 40 wt.%) of HPW are denoted as DI-HPW$_1$/SBA-15, DI-HPW$_2$/SBA-15, DI-HPW$_3$/SBA-15, and DI-HPW$_4$/SBA-15. SBA-15 was prepared by using the same method without the addition of HPW to the silica precursor solution. The HPW/SBA-15 catalysts prepared by the impregnation method with calculated amounts (10 wt.%, 20 wt.%, 30 wt.%, and 40 wt.%) of HPW are denoted as IM-HPW$_1$/SBA-15, IM-HPW$_2$/SBA-15, IM-HPW$_3$/SBA-15, and IM-HPW$_4$/SBA-15, respectively.

*Catalyst characterization*

The Fourier-transform infrared (FT-IR) experiment was carried out using a spectrometer. A diffuse reflectance UV3100 system equipped with a diffuse reflectance accessory (Shimadzu, Japan) was used to obtain UV-VIS spectra. The X-ray diffraction (XRD) patterns were scanned at 40 kV and 40 mA (the step rate was 2°/min) by using a RINT 2200 diffractometer (RIGAKU, Japan) with Cu-K$\alpha$ radiation (1.54 Å). Porosimetry measurements were conducted via N$_2$ physisorption using a Quantachrome Nova 4200e porosimeter: samples were degassed at 200 °C for 2 h before analysis by nitrogen adsorption at −196 °C. The surface area and pore size distribution were estimated as the main textural parameters based on the Brunauer–Emmett–Teller (BET) and Barrett–Joyner–Halenda (BJH) methods. The STEM observations were carried out using a JEM-ARM200F system (JEOL, Japan). The $^{31}$P MAS-NMR was recorded using a JNM-ECA400 (JEOL, Japan).

*Photocatalytic performance study*

Photocatalytic oxidation of benzene to phenol was conducted in a 100 mL photochemical reactor equipped with a water jacket to maintain the temperature at 10 °C. The top of the reactor

contained an illumination window fabricated from high-strength quartz glass. In a typical run, a mixture of 25 mL water and 5 mL acetonitrile containing 7 mM benzene was added to the reactor before being exposed to air. Then, 0.1 g of photocatalyst was added with continuous stirring for 15 min until adsorption equilibrium was reached. A 300 W xenon lamp was used as the irradiation source for the photocatalytic reactions. After each irradiation time interval, sample aliquots were withdrawn from the reactor with a syringe and filtered to be immediately analyzed with high-performance liquid chromatography (HPLC). The mobile phase was composed of 65% phosphoric solution (0.2%) and 35% acetonitrile with a flow rate of 1 cm$^3$/min.

The benzene conversion, phenol yield, and selectivity were calculated using the following formulas:

$$Benzene\ conversion = (1 - \frac{remained\ benzene\ concentration}{initial\ benzene\ concentration}) \times 100\%$$

$$Phenol\ yield = \frac{produced\ phenol\ concentration}{initial\ benzene\ concentration} \times 100\%$$

$$Phenol\ selectivity = \frac{Phenol\ yield}{Benzene\ conversion} \times 100\%$$

*Leaching kinetic experiment*

The interaction of HPW and silica support was tested with a leaching kinetic experiment. Typically, a 0.1 g sample was added into a 200 mL strong acid aqueous solution (pH = 1) with vigorous stirring at room temperature. The strong acid solution and large water amount was utilized to facilitate the HPW leaching. Sample aliquots (1 mL) were withdrawn from the suspension with a syringe after each irradiation time interval. The solution was obtained by filtering out the catalyst and immediately analyzed with UV-VIS spectroscopy to determine the amount of leached HPW.

## 4.3 Results and discussion

*Catalyst structure*

Fig. 2 shows the XRD patterns for SBA-15, DI-HPW/SBA-15, and IM-HPW/SBA-15. The DI-HPW/SBA-15 sample calcined at 500 °C shows only a single broad diffraction peak at approximately 23.2–23.7°, which is the same as that for SBA-15. The samples synthesized at relatively lower temperatures (300 and 400 °C) did not show any HPW peaks, as was the case for the sample synthesized at 500 °C (Fig. 3) [16]. On the other hand, the XRD pattern for the IM-

HPW/SBA-15 composites show characteristic peaks for crystalline HPW, and the peak intensities increase with increasing amount of HPW added, indicating the presence of aggregated HPW (Fig. 2b). The elemental mapping for DI-HPW$_4$/SBA-15 by STEM and EDS is shown in Fig. 4. W, O, Si, and P are relatively uniformly distributed, indicating that HPW is highly dispersed on SBA-15.
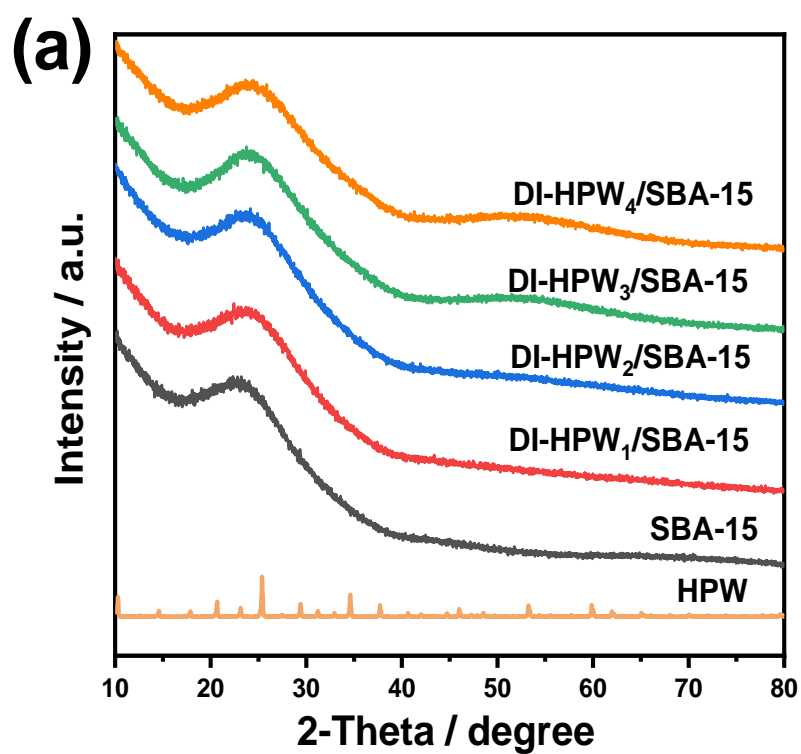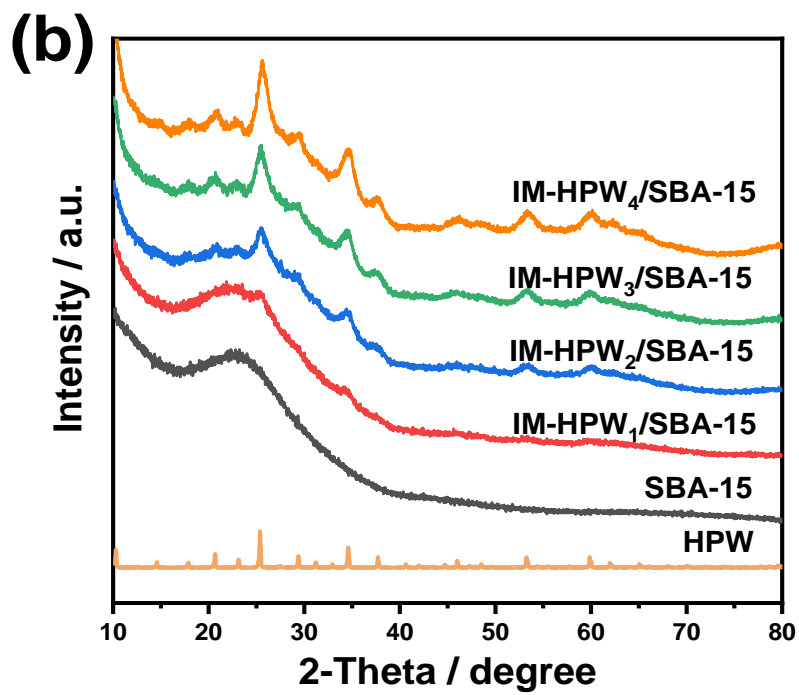
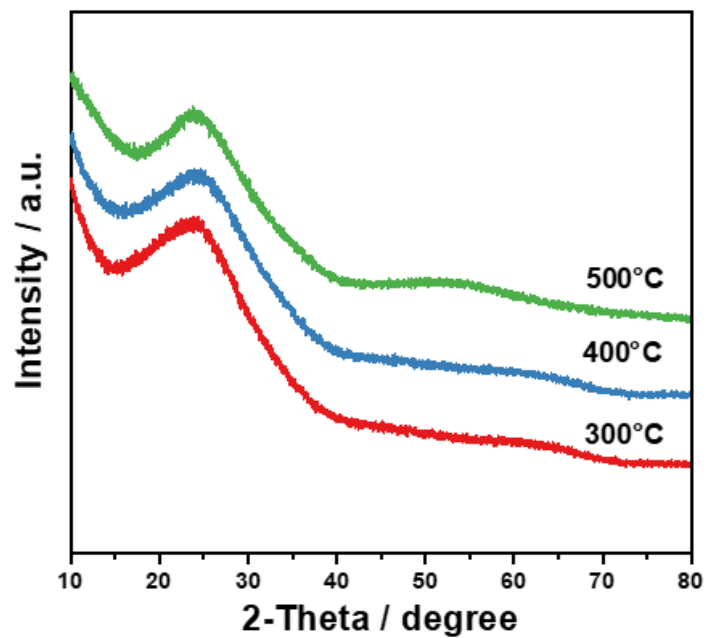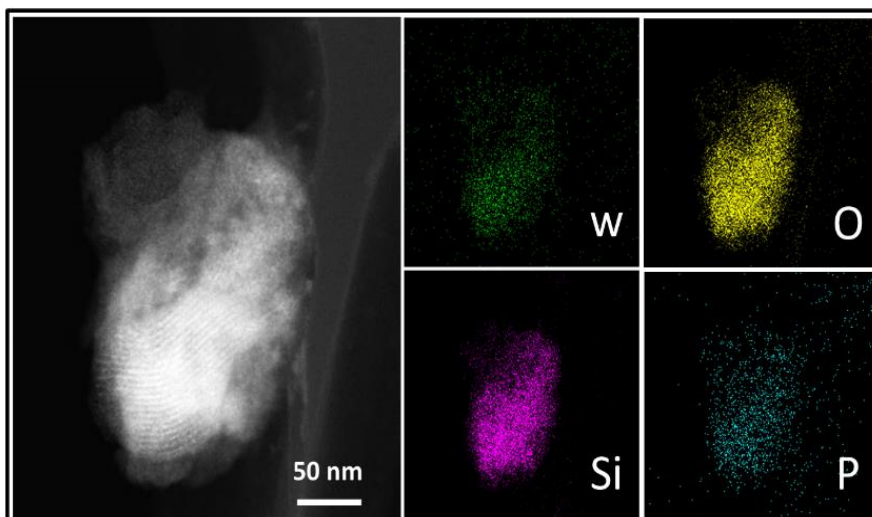**Fig. 2.** (a, b) XRD patterns of HPW/SBA-15 composites;



**Fig. 3.** XRD of IM-HPW/SBA-15 composites

**Fig. 4**. STEM and EDS elemental mapping of W, O, Si, and P on DI-HPW$_4$/SBA-15

Fig. 5 shows N$_2$ adsorption-desorption isotherms for SBA-15- and SBA-15-supported HPW catalysts. All samples exhibit typical IV-type isotherms and H1-type hysteresis loops at high relative pressures. In the DI-HPW$_1$/SBA-15, DI-HPW$_2$/SBA-15, and DI-HPW$_3$/SBA-15 composites, the isotherms have similar shapes, and hysteresis loops are observed in the same relative pressure range (0.5–0.7), but this relative pressure range is higher than that of SBA-15. This finding suggests that the pore structure of the SBA-15 support is changed by the deposition of HPW. This structural change is also supported by the pore distribution curves obtained by the BJH method. As shown in Fig. 5b, the pore size distributions for the SBA-15 and DI-HPW/SBA-15 composites are narrow, but their average sizes are different. The pore size for DI-HPW/SBA-15 is slightly larger than that for SBA-15. For the IM-HPW/SBA composite, the isotherms for each sample are similar to those for SBA-15, but the amount of adsorbed N$_2$ decreases with increasing HPW loading (Fig. 5c). The pore size range is also unchanged, and the pore volume decreases monotonically as the HPW loading is increased (Fig. 5d). The textural properties of SBA-15 and all SBA-15-supported HPW are summarized in Table 1. All the DI-HPW/SBA-15 composites show a high total surface area, i.e., in the range of 364–707 m$^2$/g, which decreases with increasing HPW loading (Table 1). Similarly, the surface area of IM-HPW/SBA-15 decreases from 505 m$^2$/g to 232 m$^2$/g with increasing HPW addition.
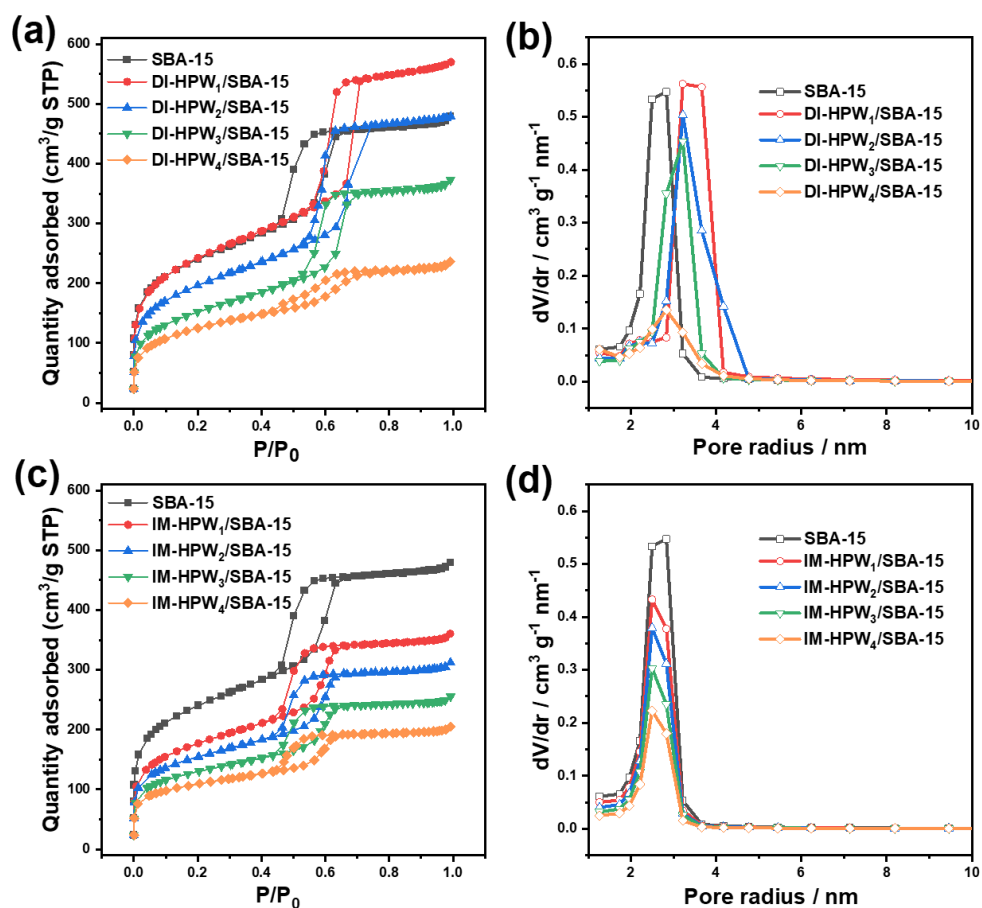
**Fig. 5.** (a and c) Nitrogen adsorption-desorption isotherms and (b and d) Pore size radius distributions of the SBA-15 (SBA) and the HPW/SBA-15 composites.

**Table 1.** Textural properties of the SBA-15 and HPW/SBA-15 composites.

| Catalyst | $S_{BET}$ (m$^2$/g) | Pore diameter (nm) | Pore volume (cm$^3$/g) |
|---|---|---|---|
| SBA-15 | 675 | 4.4 | 0.74 |
| DI-HPW$_1$/SBA-15 | 707 | 5.0 | 0.88 |
| DI-HPW$_2$/SBA-15 | 584 | 5.0 | 0.74 |
| DI-HPW$_3$/SBA-15 | 461 | 5.0 | 0.58 |
| DI-HPW$_4$/SBA-15 | 364 | 4.0 | 0.36 |
| IM-HPW$_1$/SBA-15 | 505 | 4.4 | 0.56 |
| IM-HPW$_2$/SBA-15 | 437 | 4.4 | 0.48 |
| IM-HPW$_3$/SBA-15 | 373 | 4.2 | 0.39 |

94

| IM-HPW$_4$/SBA-15 | 232 | 4.1 | 0.32 |

FTIR was utilized to investigate the structure of the DI-HPW/SBA-15 and IM-HPW/SBA-15 samples (Fig. 6 and Fig. 7). A mechanical mixture of HPW and SBA-15 was also tested as a reference. As shown in Fig. 6a, pure HPW shows IR bands at approximately 1079 cm$^{-1}$ (stretching frequency of P–O in the central PO$_4$ tetrahedron of HPW molecules), 987 cm$^{-1}$ (terminal bands for W=O$_d$ in the exterior WO$_6$ octahedron), and 890 cm$^{-1}$ and 806 cm$^{-1}$ (bands for the W–O$_b$–W and W–O$_c$–W bridges, respectively), corresponding to asymmetric vibrations associated with Keggin ions [31, 32]. The bands for P–O and W–O$_c$–W overlap due to the stretching of Si–O–Si in SBA–15 [33]. The W=O$_d$ band for all DI-HPW/SBA-15 composites shifts from 987 cm$^{-1}$ to 966 cm$^{-1}$ compared with the spectra obtained for bulk HPW, which is consistent with previous studies [17, 22]. This shift is due to the effect of chemical interactions between HPW molecules and the silica frameworks described above, which interfere with the symmetry of the Keggin unit. For comparison, there is no shift in the IM-HPW/SBA-15 composites, as is the case for the mixture of HPW and SBA-15, indicating a physical absorption of HPW on the surface of SBA-15. In addition, no bands for W–O$_b$–W were found in the DI-HPW/SBA-15 composites (Fig. 6b), which is consistent with previous works [17, 22]. This can be due to the masking effect of other high-intensity bands, although the collapse of the Keggin structure cannot be completely excluded [17].
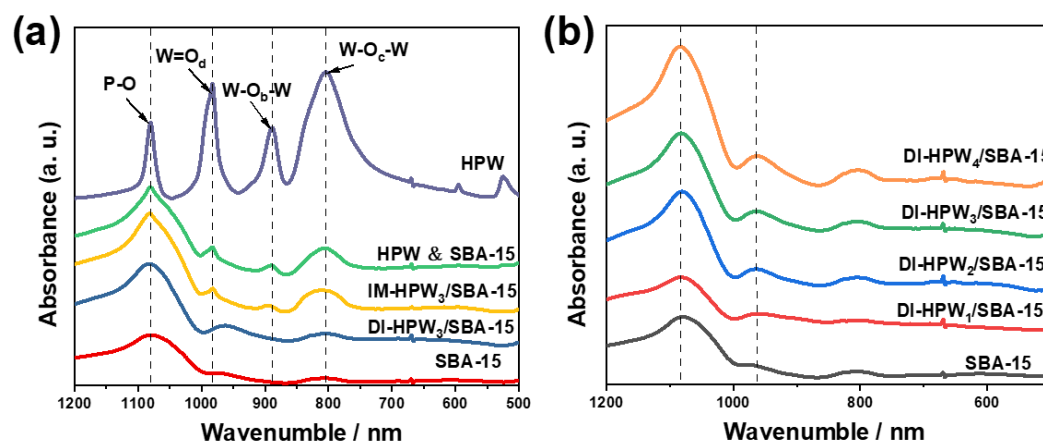


**Fig. 6** FT-IR spectra of (a) different samples and (b) DI-HPW/SBA-15 composites with different HPW loading amounts.
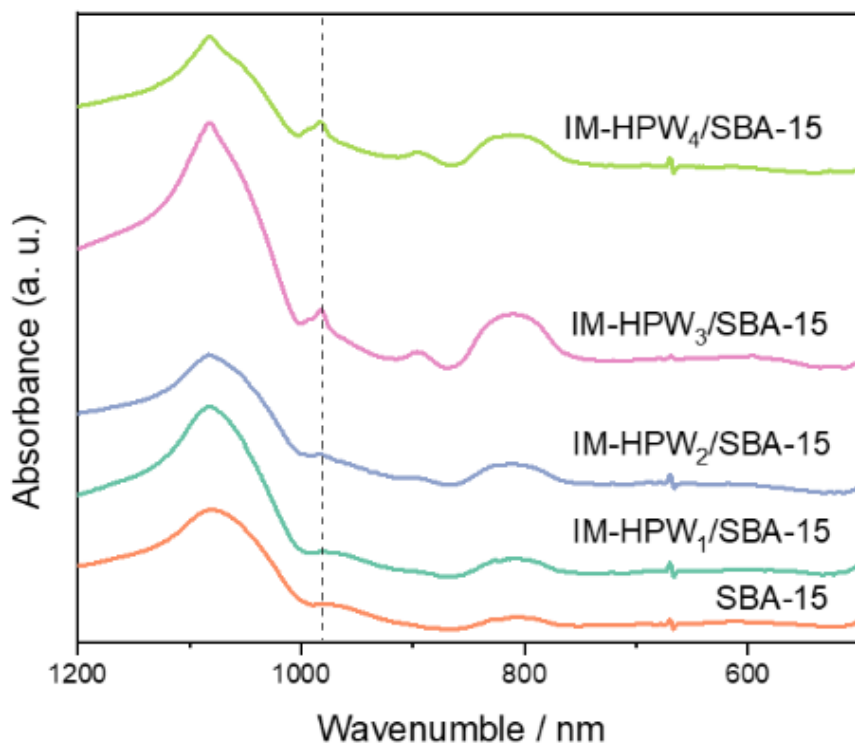
**Fig. 7.** FT-IR of IM-HPW/SBA-15 composites

The structure of DI-HPW/SBA-15 was investigated using ^{31}P MAS-NMR spectroscopy. As shown in Fig. 8, three peaks due to different structural states of HPW were observed. The peaks at -15.0 ppm and -14.1 ppm are assigned to $PW_{12}O_{40}^{3-}$ anions interacting with the support. The strong peaks at -15.0 ppm and -14.1 ppm indicate that Keggin structures are maintained in DI-HPW/SBA-15. The peak at $-12.5$ ppm can be assigned to the lacunary polyanion ($PW_{11}O_{39}^{7-}$) and the fragmented forms of the heteropoly anion ($-12.5$ ppm) [34, 35]. However, this peak is relatively lower in intensity than the main peaks, indicating the occurrence of partial decomposition of Keggin anions to lacunary anions.
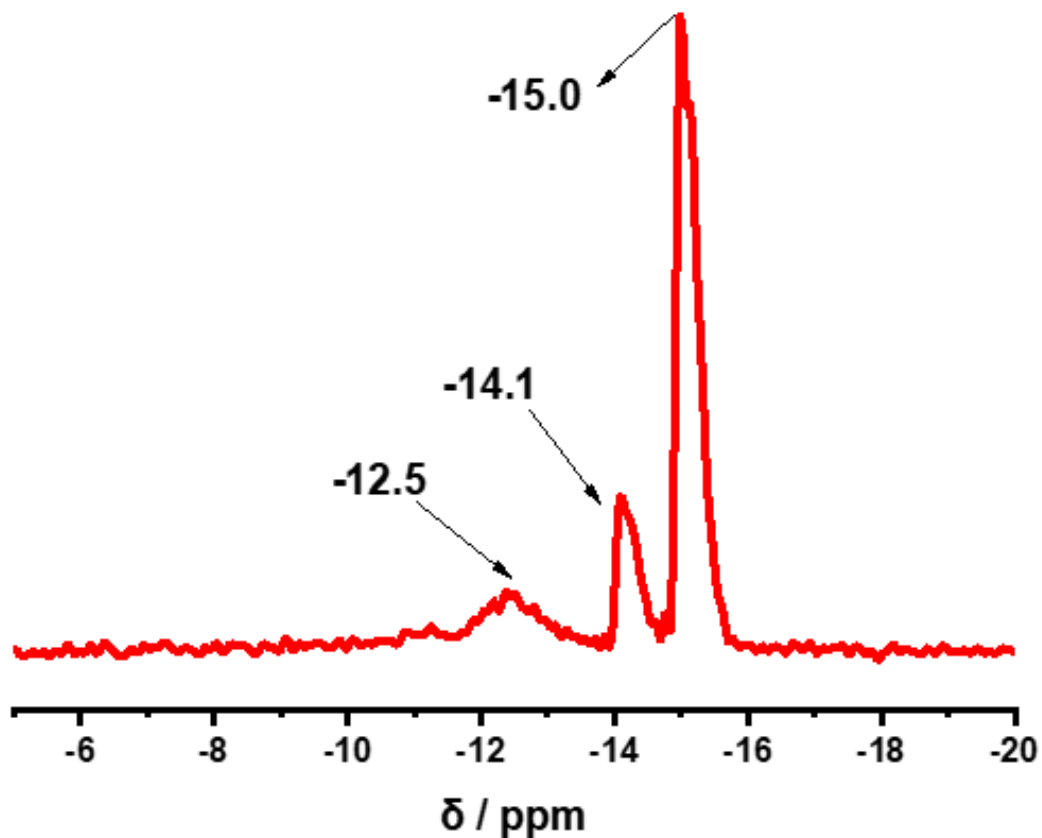
**Fig. 8** ^{31}P MAS-NMR spectra of DI-HPW/SBA-15

UV-VIS diffuse reflectance spectroscopy was used to investigate the light absorption properties of SBA-15 and HPW/SBA-15 composites. SBA-15 absorbs very little light in the UV and visible regions. When HPW is immobilized on SBA-15, the absorption of DI-HPW/SBA-15 in the UV region gradually increases with increased loading of HPW (Fig. 9a). The same trend was observed for IM-HPW/SBA-15, but the absorption bands for IM-HPW/SBA-15 are different from those for DI-HPW/SBA-15 in the wavelength region from 350 nm to 450 nm (Fig. 9b and c). This difference may be due to the partial decomposition of HPW in DI-HPW/SBA-15, as mentioned above.
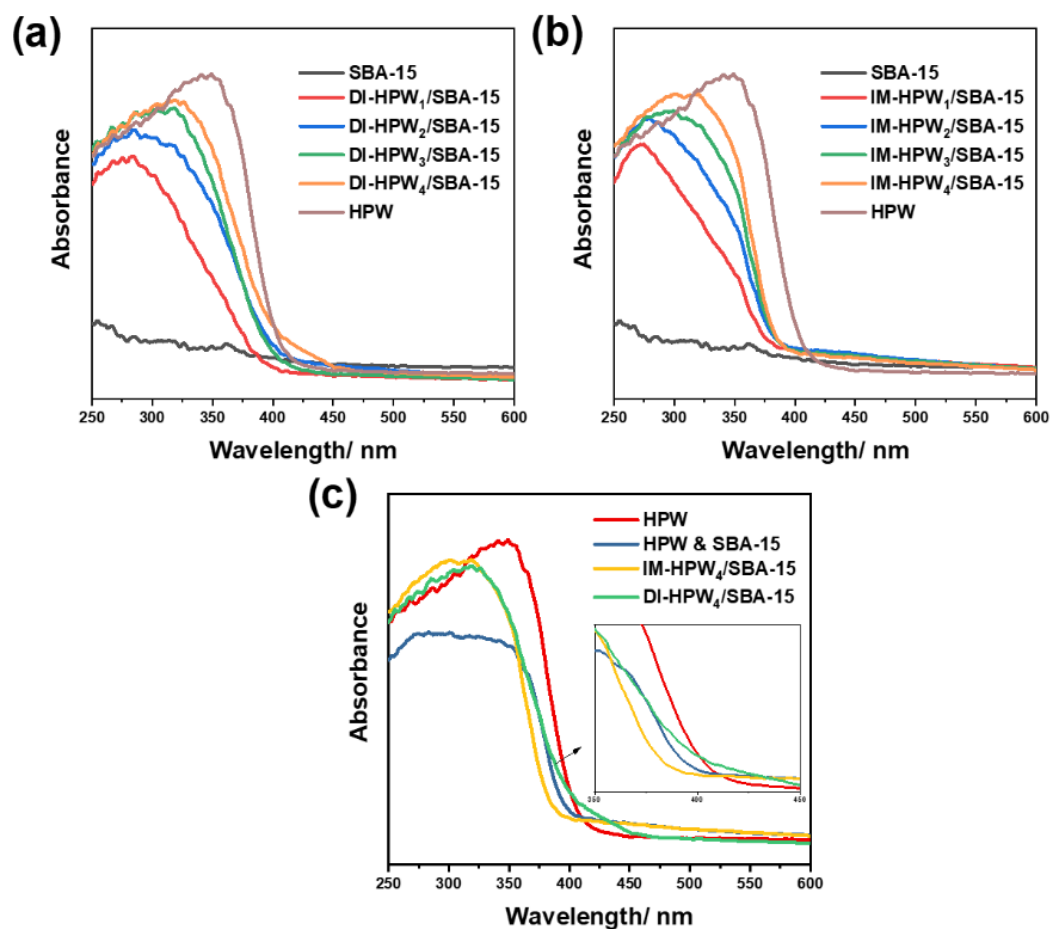
**Fig. 9.** UV–VIS diffuse reflectance spectra of SBA-15, HPW, and HPW/SBA-15 composites

*Photocatalytic assessments of HPW in the HPW/SBA-15 composites*

Photocatalytic benzene oxidation over the as-prepared HPW/SBA-15 composites was conducted under an air atmosphere and low temperature (10 °C) in an aqueous solution with a small amount of acetonitrile as a cosolvent. We first investigated the dependence of benzene oxidation and phenol formation on different pure HPW as homogenous photocatalysts, as shown in Fig. 10. No benzene conversion was observed in the dark under our reaction conditions. The benzene conversion and phenol yield increased with the increase of HPW in a low mass amount. However, a saturation of phenol formation was observed when HPW mass was higher than 16 mg. The phenol selectivity only showed slight decrease in a high HPW mass amount. In the DI-HPW$_4$/SBA-15 (Fig. 11), the benzene conversion was 26.3% with a phenol yield at 16.3%. A similar benzene conversion (26.4%) and phenol yield (16.7%) was obtained using the IM-HPW$_4$/SBA-15. Furthermore, the unsupported HPW in high mass amount also showed a similar benzene conversion and selectivity

with both DI-HPW₄/SBA-15 and IM-HPW₄/SBA-15. Furthermore, DI-HPW₄/SBA-15 shows a higher benzene conversion than $TiO_2$ (P25), $WO_3$ and $C_3N_4$ (Table 2). Thus, DI-HPW₄/SBA-15 can efficiently oxidize benzene by light irradiation in an aqueous solution.
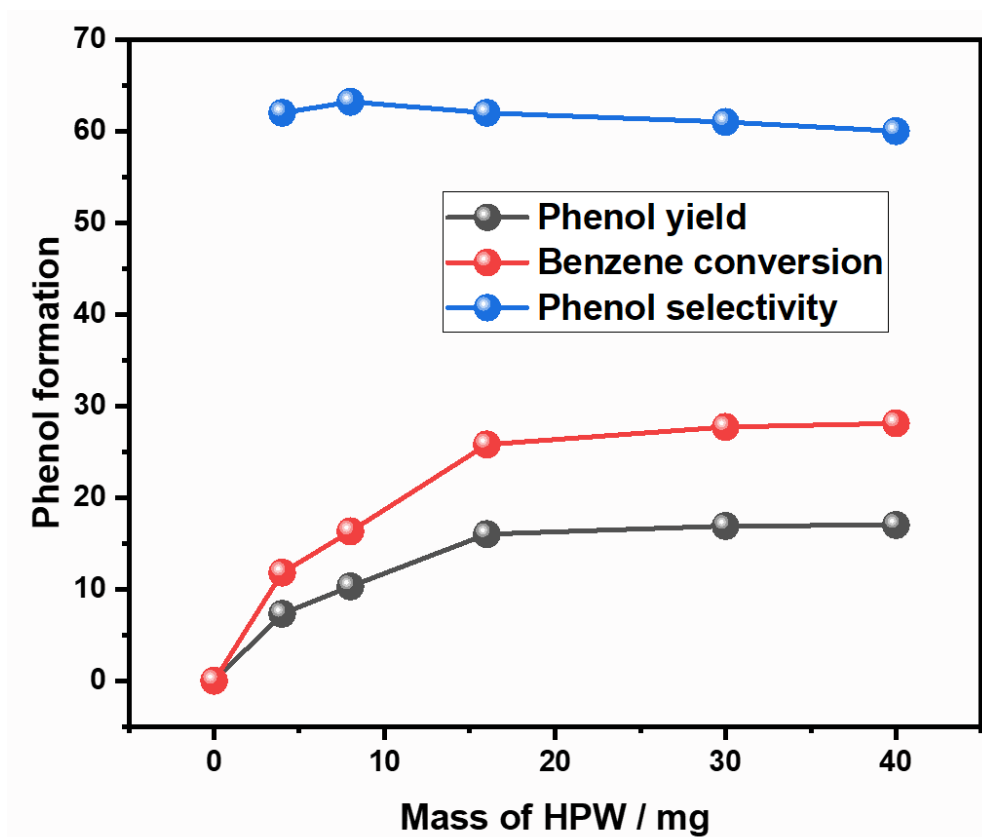


**Fig. 10.** Time dependence of benzene conversion over unsupported HPW. Reaction condition: light source, 300 W xenon lamp; temperature, 10 °C; initial benzene concentration, 7 mM; reaction time, 120 min; under ambient condition.
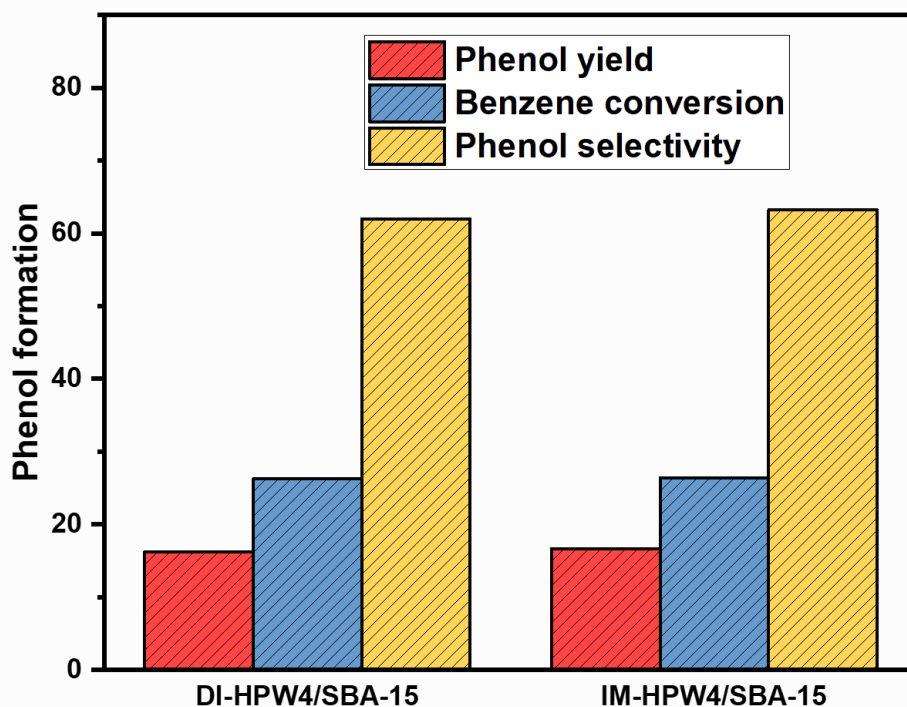
**Fig. 11.** Phenol formation over DI-HPW₄/SBA-15 and IM-HPW₄/SBA-15. Reaction condition: light source, 300 W xenon lamp; temperature, 10 °C; initial benzene concentration, 7 mM; catalyst amount, 100 mg; reaction time, 120 min; under ambient condition.

**Table 2** Comparison of different photocatalysts for benzene oxidation

| Photocatalysts | Benzene conversion (%) |
|---|---|
| $TiO_2$ (P25) | 25.5 |
| $WO_3$ | < 1.0 |
| $C_3N_4$ | < 1.0 |

Reaction condition: light source, 300 W xenon lamp; temperature, 10 °C; initial benzene concentration, 7 mM; photocatalyst amount, 50 mg; reaction time, 120 min; under ambient condition.

It has been reported that the leaching of HPW from various supported HPW catalysts generally occurs, resulting in a loss of catalytic activity after successive reaction cycles [36–38]. This decrease in activity has been explained by a decrease in the amount of supported HPW as a heterogeneous catalyst. However, the contribution of the leached species to homogeneous photocatalytic reactions has rarely been mentioned. Unveiling the role of leached species is important to the in-depth study

of the properties of supported HPW catalysts.

The DI-HPW$_4$/SBA-15 and IM-HPW$_4$/SBA-15 catalysts were recovered by filtration, and their recyclability was investigated. As shown in Fig. 12a, the phenol yield decreases from 16.3% to 12.7% in the second run. A further decrease is observed in the third run, but the benzene conversion remains at 8.1%. As shown in Fig. 12b, the amount of HPW leached from DI-HPW/SBA-15 in the first and second runs is 160 mg/g and 121 mg/g of catalyst, respectively. On the other hand, IM-HPW$_4$/SBA-15 in the second run shows a benzene conversion of 0.1%, which is much lower than that in the first run. Almost all HPW was leached from IM-HPW$_4$/SBA-15 in the first run. These results show that although DI-HPW$_4$/SBA-15 is significantly more stable than IM-HPW$_4$/SBA-15 in successive reaction cycles, the leaching of HPW from the HPW$_4$/SBA-15 complex is not negligible. The HPW$_4$/SBA-15 composites prepared by the direct method show less HPW leaching than those prepared by the impregnation method, which may be due to the strong HPW-support interaction. The leaching of HPW was also supported by the increased surface area of DI-HPW/SBA-15 after reaction, as shown in Fig. 13.
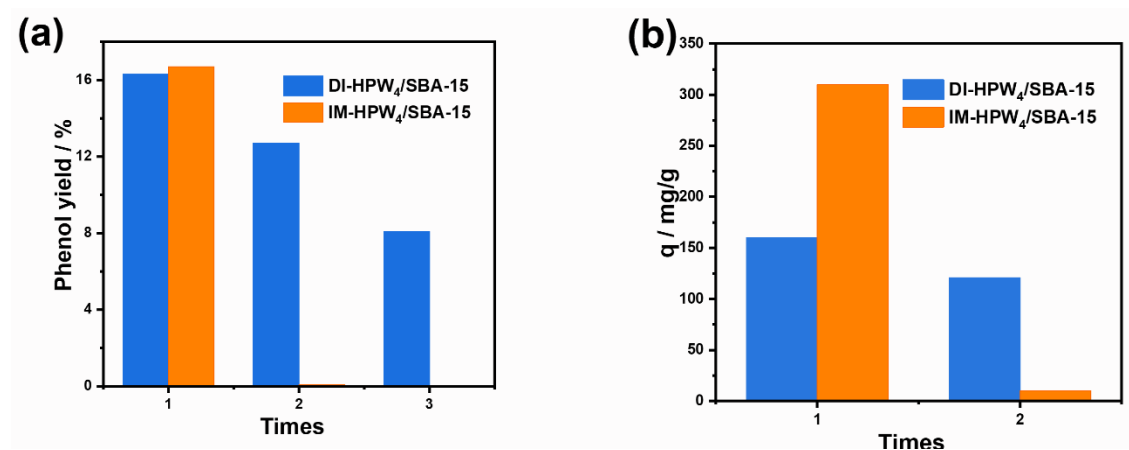


**Fig. 12.** (a) Recyclability of DI-HPW$_4$/SBA-15 and IM-HPW$_4$/SBA-15 (b) Leaching amount of HPW from per gram of HPW/SBA-15 composite in each cycle.
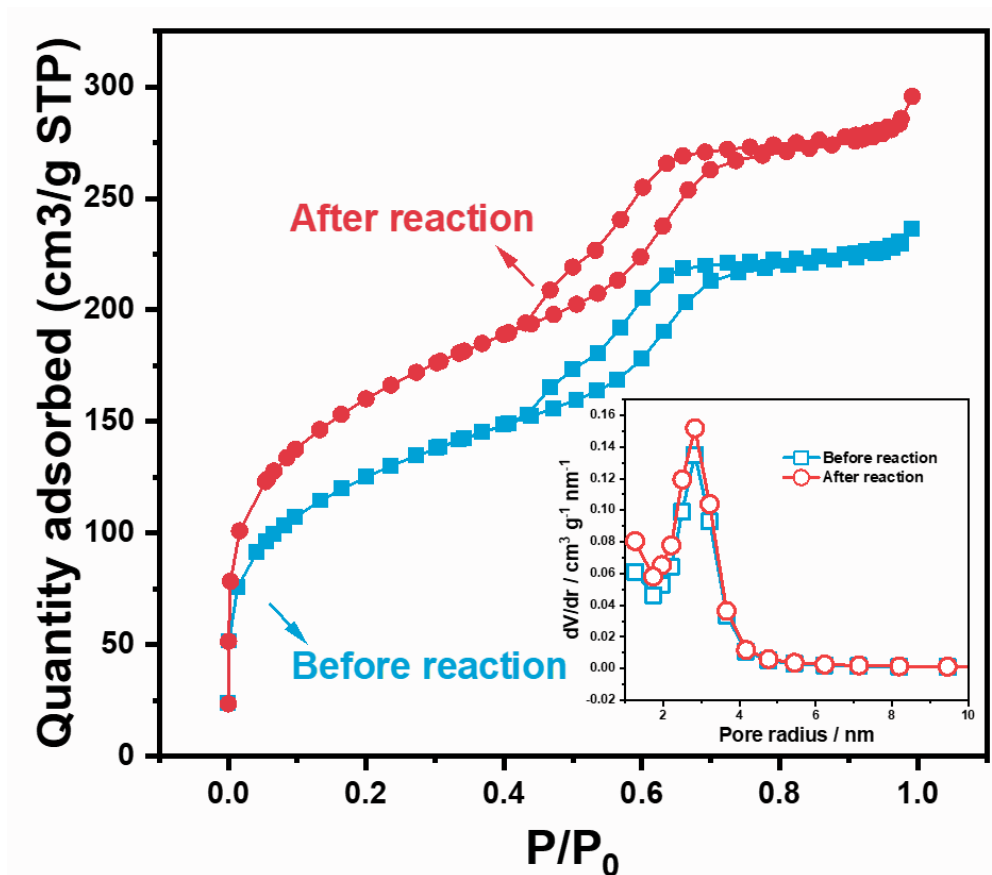
**Fig. 13.** Nitrogen adsorption-desorption isotherms and Pore size radius distributions of the DI-HPW/SBA-15 composites before and after reaction.

As described above, DI-HPW$_4$/SBA-15 shows similar activity compared with IM-HPW$_4$/SBA-15 and HPW. By It seems likely that the HPW leached from the DI-HPW/SBA-15 composites are the main active species. The lower leached amount of HPW leads the lower activity of DI-HPW$_4$/SBA-15. The following control experiments were carried out to further check whether the reaction proceeds mainly in a heterogeneous or homogenous system. After immersion of DI-HPW$_4$/SBA-15 in reaction solution for 1 h, the solid was filtered, and the filtrate was used for benzene photooxidation. As shown in Fig. 14, the activity for benzene conversion is almost comparable with that of DI-HPW$_4$/SBA-15, indicating that the homogenous reaction catalyzed by the leaching species is dominated in the photocatalytic oxidation of benzene to phenol.
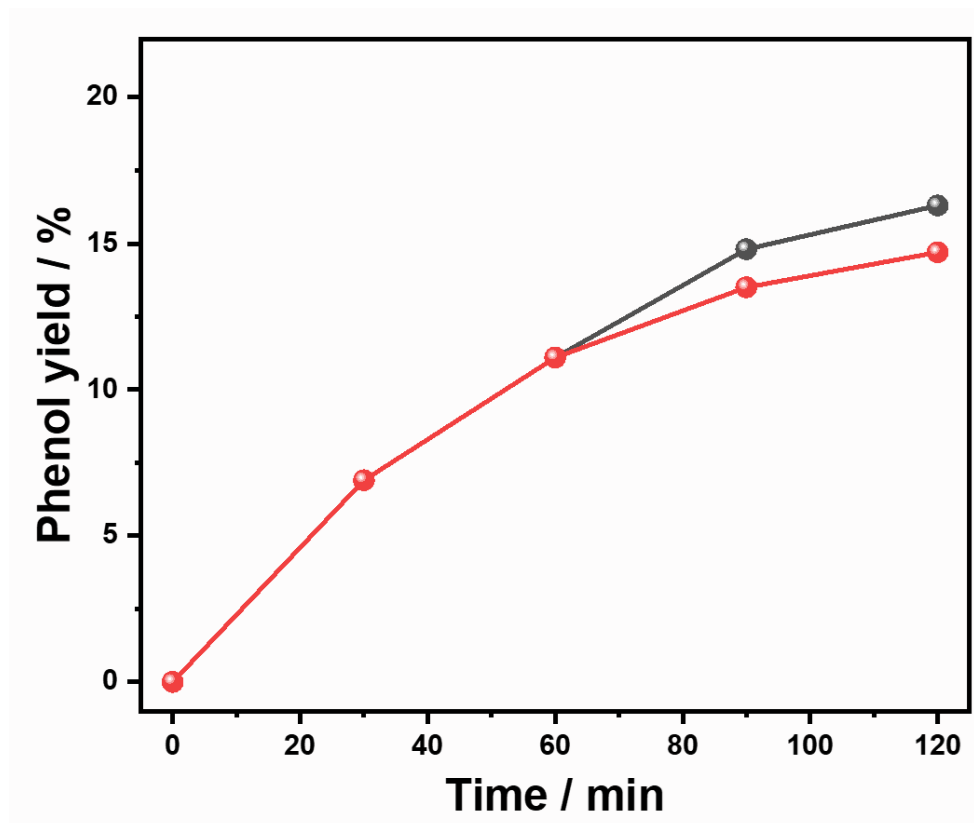
**Fig. 14.** Time dependence of benzene conversion over DI-HPW$_4$/SBA-15 (black line), DI-HPW$_4$/SBA-15 removed after 60 min (red line). Reaction condition: light source, 300 W xenon lamp; temperature, 10 °C; initial benzene concentration, 7 mM; catalyst amount, 100 mg; under ambient condition.

*Leaching kinetics*

A dissolution kinetics study was carried out to further investigate the interaction between HPW and SBA-15 in DI-HPW$_4$/SBA-15. For this purpose, 0.1 g of the photocatalyst was stirred in 250 mL of a strongly acidic aqueous solution, and the leached amount of HPW ($q_t$, mg/g) was investigated by UV-VIS spectroscopy (Fig. 15). Here, $q_t$ represents the leached amount of HPW (mg) per gram of HPW/SBA-15 composite after a certain time. As shown in Fig. 14a, the $q_t$ value for IM-HPW$_4$/SBA-15 increases rapidly to 290 mg/g within 130 min and then increases slowly to 320 mg/g at 320 min. On the other hand, the $q_t$ value from DI-HPW/SBA-15 reaches 67 mg/g within 130 min and then increases continuously to 93 mg/g without a rate change (Fig. 15b). This observation clearly shows that the elution rate of HPW from DI-HPW/SBA-15 is much slower than that of IM-HPW/SBA-15.

The intraparticle diffusion model (proposed by Weber and Morris) is used herein [39–41]. Since this model is widely utilized in the study of adsorption behavior, we employ it to understand the leaching (desorption) behavior of HPW from the composite. The rate parameter $k_i$ for intraparticle diffusion can be defined by the following equation:

$$q_t = k_i t^{0.5} + C$$

where C is a constant related to the thickness of the boundary layer: the larger the value of C, the greater the boundary layer effect. According to this model, the relationship between $t^{0.5}$ and $q_t$ is shown in Figs. 15c and d. A Morris plot of $q_t$ versus $t^{0.5}$ gives a straight line in DI-HPW/SBA-15, indicating that the leaching process is controlled only by intraparticle diffusion [42]. However, the data exhibit two steps that influence the leaching process for IM-HPW/SBA-15. The first step involves boundary layer diffusion or external surface desorption, while the second step involves a gradual desorption stage attributed to intraparticle diffusion [43]. This different leaching behavior also supports the strong interaction between the HPW and SBA-15 in DI-HPW/SBA-15.
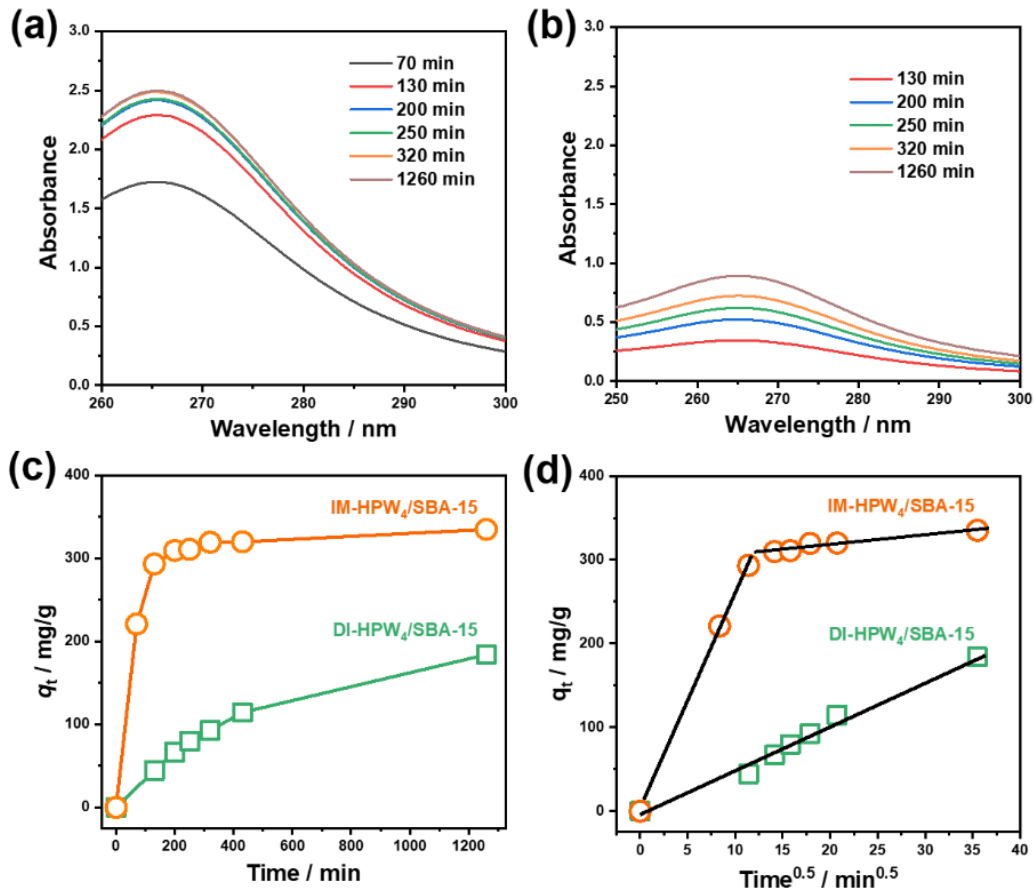


**Fig. 15.** (a, b) UV-VIS spectra and (c) time courses of leached HPW from DI-HPW$_4$/SBA-15 and

IM-HPW$_4$/SBA-15. (d) Intraparticle diffusion model with HPW$_4$/SBA-15 and IM-HPW$_4$/SBA-15.

*Photocatalytic properties of HPW/SBA-15*

As described above, partially decomposed species are generated on SBA-15, while the homogenous reaction over the leached species is dominant in an aqueous solution. The leaching also leads the directly study of heterogenous reaction more difficult since the accompany of homogenous reaction in the liquid phase reaction is inevitable. To further study the catalytic properties of supported HPW as heterogenous photocatalysts, we carried out gas-solid heterogeneous photooxidation of formic acid with DI-HPW/SBA-15 in the presence or absence of water vapor (Fig.16). We selected formic acid herein because it is a small molecular substrate that can be easily oxidized. However, a negligible conversion of formic acid (<0.1) was observed, while TiO$_2$ (P25) was found to exhibit a high conversion for formic acid (92.9%; Table 3). Furthermore, the DI-HPW/SBA-15 showed a color change from white to blue within 10 min even in a pure O$_2$ atmosphere, which did not return to white after the irradiation was stopped within 30 min. This blue color is due to the generation of heteropoly blue (the reduced species of HPW, HPW$_{red}$).
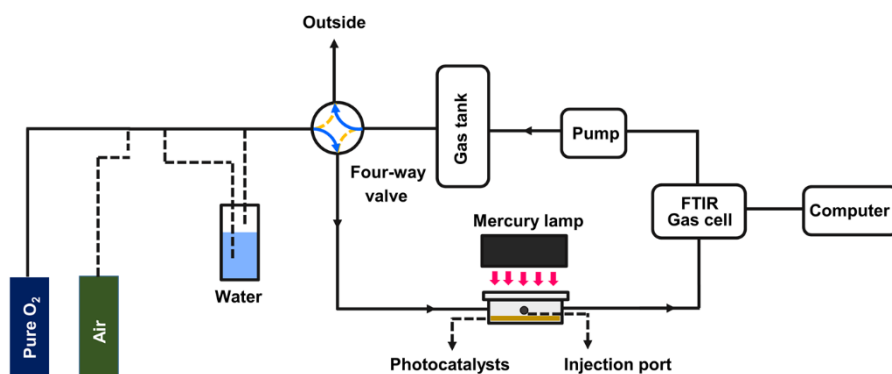


**Fig. 16.** Experimental setup of photocatalytic oxidation of formic acid in a gas-solid region. The imaginary line represents an alternative route.

**Table 3** Photocatalytic oxidation of formic acid in gas-solid region [a]

| Photocatalysts | Atmosphere | Water vapor | Conversion of formic acid / % |
|---|---|---|---|
| DI-HPW$_2$/SBA-15 | Air | No | <0.1 |
| DI-HPW$_2$/SBA-15 | O$_2$ | No | <0.1 |
| DI-HPW$_3$/SBA-15 | O$_2$ | No | <0.1 |
| DI-HPW$_3$/SBA-15 | O$_2$ | Yes | <0.1 |
| TiO$_2$(P25) | Air | No | 92.9% |

The photocatalytic oxidation of formic acid in a gas-solid region was carried out by a closed circulating system (Fig. 16). The DI-HPW/SBA-15 (0.05 g) was uniformly dispersed on a mesh as support (with a diameter of 5.5 cm). A 100 mL photochemical reactor equipped with an illumination window on the top was utilized in our system. Before reaction, the reaction system was purged with simulated air or pure $O_2$. Then, formic acid (2 μmL) was injected into this circulated system (500 mL/min) with an injection syringe. The formic acid was vaporized into the gas phase due to the low concentration. A 500 W mercury lamp was used as the irradiation source after 15min to reach an adsorption equilibrium. The concentrations of formic acid and $CO_2$ were recorded using an FTIR spectrometer (PerkinElmer, spectrum 100, FT-IR spectrometer, USA) equipped with a gas cell (optical length = 2.4 m).

The result in Table 3 showed the negligible formic acid conversion (<0.1) after irradiation in all controlled conditions, while $TiO_2$ (P25) shown a significantly higher formic acid conversion (92.9%) as comparison. On the contrary, the $TiO_2$ shown a lower benzene conversion (14.5%) than that of DI-HPW/SBA-15 in aqueous solution, indicating the high activity of the leached species as homogenous photocatalysts (Table 3). Hence, HPW shows high activity in the homogenous solution, but almost no activity in the heterogenous reaction.
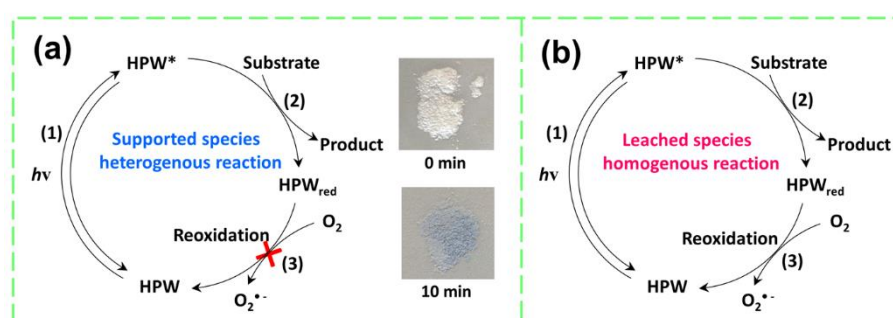


**Scheme 2 Comparation of photocatalytic reaction over supported HPW as (a) heterogeneous reaction and (b) leached HPW as a homogenous reaction.**

The general photocatalytic reaction over HPW (or supported HPW) involves the following

steps (Scheme 2): (1) Photoexcitation of the ground-state species (HPW) to the ligand-to-metal charge-transfer excited-state complex, HPW*; (2) HPW* reacts with the substrate with an electron transfer process and generates products and $HPW_{red}$; (3) The $HPW_{red}$ is reoxidized by an oxidant ($O_2$) to the original state (HPW). The first and second steps proceed with the supported HPW, as evidenced by the observation of $HPW_{red}$ in the gas-solid reaction. However, $HPW_{red}$ is maintained even under a pure $O_2$ atmosphere, indicating that the reoxidation of the process (the third step) for HPW/SBA-15 does not proceed. This incomplete catalytic cycle may be the reason for the low photocatalytic activity of HPW/SBA-15. Similar situation may occur in the liquid-solid reaction, leading to the low reactivity of heterogenous reaction. Another possibility is that the homogenous reaction is kinetic faster than heterogenous reaction, resulting in the homogenous reaction dominated in the reaction process. The high activity is observed in the homogenous photocatalytic reaction with leached species since HPW is readily reoxidized with $O_2$ (Scheme 2b). The fast reoxidation process is evidenced by the high activity described above and the fact that no $HPW_{red}$ species were observed during the homogenous reaction.

### 4.4 Conclusion

SBA-15-supported HPW was synthesized by a direct method and an impregnation method and characterized in detail. The as-prepared DI-HPW/SBA-15 shows high HPW dispersion, while the pore structure of SBA-15 is maintained after HPW loading. Chemical interaction of HPW with the silica support was observed by FT-IR, $^{31}P$ MAS-NMR, and a leaching kinetic experiment, which promotes the enhanced stability of DI-HPW/SBA-15. However, partial decomposition of HPW to some lacunary species in DI-HPW/SBA-15 is supported by $^{31}P$ MAS-NMR and UV-Vis spectral observations for the leaching solution. DI-HPW/SBA-15 shows higher surface area but significantly lower activity than IM-HPW/SBA-15 and HPW in photocatalytic benzene oxidation in an aqueous solution. To gain insight into the reaction process, we found that the homogenous reaction dominates the photocatalytic processes, while the heterogeneous reaction is prevented and negligible. This work points out that the photocatalytic reaction process over HPW is preferred under homogenous reactions rather than heterogeneous reactions, which provides helpful insight into the photocatalytic reaction processes over supported POMs.

## References

[1] Y.F. Song, R. Tsunashima, Recent advances on polyoxometalate-based molecular and composite materials, Chem. Soc. Rev., 41 (2012) 7384–7402, https://doi.org/10.1039/C2CS35143A.

[2] H. Hori, Y. Takano, K. Koike, S. Kutsuna, H. Einaga, T. Ibusuki, Photochemical decomposition of pentafluoropropionic acid to fluoride ions with a water-soluble heteropolyacid photocatalyst, Appl. Catal. B: Environ., 46 (2003) 333–340, https://doi.org/10.1016/S0926-3373(03)00225-X.

[3] H.T. Do, L.A. Phan Thi, N.H. Dao Nguyen, C.W. Huang, Q.V. Le, V.H. Nguyen, Tailoring photocatalysts and elucidating mechanisms of photocatalytic degradation of perfluorocarboxylic acids (PFCAs) in water: a comparative overview, J. Chem. Technol. Biot., (2020), https://doi.org/10.1002/jctb.6333.

[4] G.R. Bertolini, L.R. Pizzio, A. Kubacka, M.J. Muñoz-Batista, M. Fernández-García, Composite $H_3PW_{12}O_{40}$–$TiO_2$ catalysts for toluene selective photo-oxidation, Appl. Catal. B: Environ., 225 (2018) 100–109, https://doi.org/10.1016/j.apcatb.2017.11.055.

[5] X. Cai, Q. Wang, Y. Liu, J. Xie, Z. Long, Y. Zhou, J. Wang, Hybrid of polyoxometalate-based ionic salt and N-doped carbon toward reductant-free aerobic hydroxylation of benzene to phenol, ACS Sustain. Chem. Eng., 4 (2016) 4986–4996, https://doi.org/10.1021/acssuschemeng.6b01357.

[6] J. Cheng, Z. Zhang, X. Zhang, J. Liu, J. Zhou, K. Cen, Hydrodeoxygenation and hydrocracking of microalgae biodiesel to produce jet biofuel over $H_3PW_{12}O_{40}$-Ni/hierarchical mesoporous zeolite Y catalyst, Fuel, 245 (2019) 384–391, https://doi.org/10.1016/j.fuel.2019.02.062.

[7] S.Y. Lai, K.H. Ng, C.K. Cheng, H. Nur, M. Nurhadi, M. Arumugam, Photocatalytic remediation of organic waste over Keggin-based polyoxometalate materials: A review, Chemosphere, 263 (2021) 128244, https://doi.org/10.1016/j.chemosphere.2020.128244.

[8] X. Qu, Y. Guo, C. Hu, Preparation and heterogeneous photocatalytic activity of mesoporous $H_3PW_{12}O_{40}$/$ZrO_2$ composites, J. Mol. Catal. A: Chem., 262 (2007) 128–135, https://doi.org/10.1016/j.molcata.2006.08.026.

[9] G. Li, K. Zhang, C. Li, R. Gao, Y. Cheng, L. Hou, Y. Wang, Solvent-free method to encapsulate polyoxometalate into metal-organic frameworks as efficient and recyclable photocatalyst for

harmful sulfamethazine degrading in water, Appl. Catal. B: Environ., 245 (2019) 753–759, https://doi.org/10.1016/j.apcatb.2019.01.012.

[10] Y. Guo, K. Li, X. Yu, J.H. Clark, Mesoporous $H_3PW_{12}O_{40}$-silica composite: Efficient and reusable solid acid catalyst for the synthesis of diphenolic acid from levulinic acid, Appl. Catal. B: Environ., 81 (2008) 182–191, https://doi.org/10.1016/j.apcatb.2007.12.020.

[11] M. Zhang, W. Zhu, H. Li, M. Li, S. Yin, Y. Li, Y. Wei, H. Li, Facile fabrication of molybdenum-containing ordered mesoporous silica induced deep desulfurization in fuel, Colloid Surface A, 504 (2016) 174–181, https://doi.org/10.1016/j.colsurfa.2016.05.077.

[12] L. Frattini, M.A. Isaacs, C.M.A. Parlett, K. Wilson, G. Kyriakou, A.F. Lee, Support enhanced α-pinene isomerization over HPW/SBA-15, Appl. Catal. B: Environ., 200 (2017) 10–18, https://doi.org/10.1016/j.apcatb.2016.06.064.

[13] O.A. Kholdeeva, N.V. Maksimchuk, G.M. Maksimov, Polyoxometalate-based heterogeneous catalysts for liquid phase selective oxidations: Comparison of different strategies, Catal. Today, 157 (2010) 107–113, https://doi.org/10.1016/j.cattod.2009.12.016.

[14] Tayebee, Lee, Frattini, Rostami, $H_3PW_{12}O_{40}$/SBA-15 for the Solventless synthesis of 3-substituted indoles, Catalysts, 9 (2019) 409, https://doi.org/10.3390/catal9050409.

[15] E.I. García-López, G. Marcì, I. Krivtsov, J. Casado Espina, L.F. Liotta, A. Serrano, Local structure of supported Keggin and Wells–Dawson heteropolyacids and its influence on the catalytic activity, The Journal of Physical Chemistry C, 123 (2019) 19513–19527, https://doi.org/10.1021/acs.jpcc.9b03659.

[16] B.C. Gagea, Y. Lorgouilloux, Y. Altintas, P.A. Jacobs, J.A. Martens, Bifunctional conversion of n-decane over HPW heteropoly acid incorporated into SBA-15 during synthesis, J. Catal., 265 (2009) 99–108, https://doi.org/10.1016/j.jcat.2009.04.017.

[17] P.-Y. Hoo, A.Z. Abdullah, Direct synthesis of mesoporous 12-tungstophosphoric acid SBA-15 catalyst for selective esterification of glycerol and lauric acid to monolaurate, Chem. Eng. J., 250 (2014) 274–287, https://doi.org/10.1016/j.cej.2014.04.016.

[18] C. Pezzotta, G. Fleury, M. Soetens, S. Van der Perre, J.F.M. Denayer, O. Riant, E.M. Gaigneaux, Improving the selectivity to 4-tert-butylresorcinol by adjusting the surface chemistry of heteropolyacid-based alkylation catalysts, J. Catal., 359 (2018) 198–211,

https://doi.org/10.1016/j.jcat.2018.01.010.

[19] L. Yang, J. Li, X. Yuan, J. Shen, Y. Qi, One step non-hydrodesulfurization of fuel oil: Catalyzed oxidation adsorption desulfurization over HPWA-SBA-15, J. Mol. Catal. A: Chem., 262 (2007) 114–118, https://doi.org/10.1016/j.molcata.2006.08.058.

[20] L. Yang, Y. Qi, X. Yuan, J. Shen, J. Kim, Direct synthesis, characterization and catalytic application of SBA-15 containing heteropolyacid $H_3PW_{12}O_{40}$, J. Mol. Catal. A: Chem., 229 (2005) 199–205, https://doi.org/10.1016/j.molcata.2004.11.024.

[21] J. Toufaily, M. Soulard, J.L. Guth, J. Patarin, L. Delmote, T. Hamieh, M. Kodeih, D. Naoufal, H. Hamad, Synthesis and characterization of new catalysts formed by direct incorporation of heteropolyacids into organized mesoporous silica, Colloid Surface A, 316 (2008) 285–291, https://doi.org/10.1016/j.colsurfa.2007.09.015.

[22] X. Sheng, J. Kong, Y. Zhou, Y. Zhang, Z. Zhang, S. Zhou, Direct synthesis, characterization and catalytic application of SBA-15 mesoporous silica with heteropolyacid incorporated into their framework, Micropor. Mesopor. Mat., 187 (2014) 7–13, https://doi.org/10.1016/j.micromeso.2013.12.007.

[23] G. Marcì, E.I. García-López, L. Palmisano, Heteropolyacid-based materials as heterogeneous photocatalysts, Eur. J. Inorg. Chem., 2014 (2014) 21–35, https://doi.org/10.1002/ejic.201300883.

[24] Y. Hou, J. Ma, T. Wang, Q. Fu, Phosphotungstic acid supported on magnetic core–shell nanoparticles with high photocatalytic activity, Mat. Sci. Semicon. Processing, 39 (2015) 229–234, https://doi.org/10.1016/j.mssp.2015.05.015.

[25] S. Farhadi, M. Afshari, M. Maleki, Z. Babazadeh, Photocatalytic oxidation of primary and secondary benzylic alcohols to carbonyl compounds catalyzed by $H_3PW_{12}O_{40}/SiO_2$ under an $O_2$ atmosphere, Tetrahedron Lett., 46 (2005) 8483–8486, https://doi.org/10.1016/j.tetlet.2005.10.019.

[26] S. Farhadi, M. Zaidi, Polyoxometalate–zirconia ($POM/ZrO_2$) nanocomposite prepared by sol–gel process: A green and recyclable photocatalyst for efficient and selective aerobic oxidation of alcohols into aldehydes and ketones, Appl. Catal. A: Gen., 354 (2009) 119–126, https://doi.org/10.1016/j.apcata.2008.11.024.

[27] Y. Guo, C. Hu, Heterogeneous photocatalysis by solid polyoxometalates, J. Mol. Catal. A: Chem., 262 (2007) 136–148, https://doi.org/10.1016/j.molcata.2006.08.039.

[28] B. Yue, Y. Zhou, J. Xu, Z. Wu, X. Zhang, Y. Zou, S. Jin, Photocatalytic degradation of aqueous 4-chlorophenol by silica-immobilized polyoxometalates, Environ. Sci. Technol.,36 (2002) 1325–1329, https://doi.org/10.1021/es011038u.

[29] A. Molinari, A. Maldotti, A. Bratovcic, G. Magnacca, Photocatalytic properties of sodium decatungstate supported on sol–gel silica in the oxidation of glycerol, Catal. Today, 206 (2013) 46–52, https://doi.org/10.1016/j.cattod.2011.11.033.

[30] J. Lan, Y. Wang, B. Huang, Z. Xiao, P. Wu, Application of polyoxometalates in photocatalytic degradation of organic pollutants, Nanoscale Adv., 3 (2021) 4646–4658, https://doi.org/10.1039/D1NA00408E.

[31] Y. Chen, Y. Cao, G.-P. Zheng, B.-B. Dong, X.-C. Zheng, Comparative study on the structural and catalytic properties of mesoporous hexagonal silica anchored with $H_3PW_{12}O_{40}$: Green synthesis of benzoic acid from benzaldehyde, Adv. Powder Technol., 25 (2014) 1351–1356, https://doi.org/10.1016/j.apt.2014.03.020.

[32] N. Narkhede, V. Brahmkhatri, A. Patel, Efficient synthesis of biodiesel from waste cooking oil using solid acid catalyst comprising 12-tungstosilicic acid and SBA-15, Fuel, 135 (2014) 253–261, https://doi.org/10.1016/j.fuel.2014.06.062.

[33] V. Brahmkhatri, A. Patel, 12-Tungstophosphoric acid anchored to SBA-15: An efficient, environmentally benign reusable catalysts for biodiesel production by esterification of free fatty acids, Appl. Catal. A: Gen., 403 (2011) 161–172, https://doi.org/10.1016/j.apcata.2011.06.027.

[34] T.H. Kang, J.H. Choi, Y. Bang, J. Yoo, J.H. Song, W. Joe, J.S. Choi, I.K. Song, Dehydration of glycerin to acrolein over $H_3PW_{12}O_{40}$ heteropolyacid catalyst supported on silica-alumina, J. Mol. Catal. A: Chem., 396 (2015) 282–289, https://doi.org/10.1016/j.molcata.2014.10.015.

[35] P. Madhusudhanrao, A. Wolfson, S. Kababya, S. Vega, M. Landau, Immobilization of molecular $H_3PW_{12}O_{40}$ heteropolyacid catalyst in alumina-grafted silica-gel and mesostructured SBA-15 silica matrices, J. Catal., 232 (2005) 210–225, https://doi.org/10.1016/j.jcat.2005.03.006.

[36] C.F. Oliveira, L.M. Dezaneti, F.A.C. Garcia, J.L. de Macedo, J.A. Dias, S.C.L. Dias, K.S.P. Alvim, Esterification of oleic acid with ethanol by 12-tungstophosphoric acid supported on zirconia☆, Appl. Catal. A: Gen., 372 (2010) 153–161, https://doi.org/10.1016/j.apcata.2009.10.027.

[37] A.I. Tropecêlo, M.H. Casimiro, I.M. Fonseca, A.M. Ramos, J. Vital, J.E. Castanheiro, Esterification of free fatty acids to biodiesel over heteropolyacids immobilized on mesoporous silica, Appl. Catal. A: Gen., 390 (2010) 183–189, https://doi.org/10.1016/j.apcata.2010.10.007.

[38] J. Alcañiz-Monge, B.E. Bakkali, G. Trautwein, S. Reinoso, Zirconia-supported tungstophosphoric heteropolyacid as heterogeneous acid catalyst for biodiesel production, Appl. Catal. B: Environ., 224 (2018) 194–203, https://doi.org/10.1016/j.apcatb.2017.10.066.

[39] F.-C. Wu, R.-L. Tseng, R.-S. Juang, Initial behavior of intraparticle diffusion model used in the description of adsorption kinetics, Chem. Eng. J., 153 (2009) 1–8, https://doi.org/10.1016/j.cej.2009.04.042.

[40] B. An, Cu(II) and As(V) Adsorption kinetic characteristic of the multifunctional amino groups in chitosan, Processes, 8 (2020) 1194, https://doi.org/10.3390/pr8091194.

[41] S.K. Singh, T.G. Townsend, D. Mazyck, T.H. Boyer, Equilibrium and intra-particle diffusion of stabilized landfill leachate onto micro- and meso-porous activated carbon, Water Res., 46 (2012) 491–499, https://doi.org/10.1016/j.watres.2011.11.007.

[42] A. Pholosi, E.B. Naidoo, A.E. Ofomaja, Intraparticle diffusion of Cr(VI) through biomass and magnetite coated biomass: A comparative kinetic and diffusion study, S. Afr. J. Chem. Eng., 32 (2020) 39–55, https://doi.org/10.1016/j.sajce.2020.01.005.

[43] Z. Cheng, X. Liu, M. Han, W. Ma, Adsorption kinetic character of copper ions onto a modified chitosan transparent thin membrane from aqueous solution, J. Hazard. Mater., 182 (2010) 408–415, https://doi.org/10.1016/j.jhazmat.2010.06.048.

# Chapter 5:

Semiconductor-based photocatalysts for benzene oxidation to phenol: a comparative study

# Chapter 5: Semiconductor-based photocatalysts for benzene oxidation to phenol: a comparative study

## 5.1 Introduction

Photocatalysis has been reported to be a green alternative to benzene oxidation to phenol, since it can use $O_2$ as oxidant under ambient temperature and pressure [1]. Light-induced holes will be generated on the semiconductor-based photocatalysts for benzene oxidation to phenol. In addition, several high active radicals especially hydroxyl radical will be generated from the holes and electrons under aerobic condition. However, high activity and non-selectivity of these radicals generally leading to unselective oxidation to produce phenolic byproducts and $CO_2$. As a result, very few papers have been published for photocatalytic oxidation of benzene to phenol with $O_2$, which generally showed low phenol yield or selectivity. For example, Li et al., synthesized a layered double hydroxide ($Zn_2Ti$-LDH) for photocatalytic benzene oxidation to phenol (4.6% of phenol yield and 81.1% of selectivity) [2]. Chen et al., used a $Bi_2WO_6/CdWO_4$ as photocatalyst and $O_2$ as oxidant, they achieved 7.3% of phenol yield and 99% of phenol selectivity in the hydroxylation of benzene to phenol [3].

To achieve high phenol yield, we reported that polyoxometalates (POMs) including phosphotungstic acid ($H_3PW_{12}O_{40}$) and sodium decatungstate ($Na_4W_{10}O_{32}$) can be efficient inorganic homogenous photocatalysts for benzene oxidation to phenol under certain conditions. However, recovery of these inorganic photocatalysts after reaction is difficult. In addition, supported $H_3PW_{12}O_{40}$ has been proved to be shown low activity as heterogenous photocatalysts, while the leached species as homogenous photocatalysts dominated in the photocatalytic reaction. Hence, it is important to develop new kinds of heterogenous photocatalysts for efficient benzene oxidation to phenol. Recently, Tomita et al., reported that platinum-loaded tungstic oxide ($Pt/WO_3$) photocatalytically produced phenol from benzene with selectivity in aqueous solution under aerobic condition [4]. The selectivity (41.7-79.3%) was much higher than titanium oxide ($TiO_2$) photocatalyst (both the unmodified and Pt-loaded) which generated $CO_2$ as a main product (10.9-36.9% of phenol selectivity).

114

In this chapter, we carried out comprehensive research to compare the activity of some typical semiconductor-based photocatalysts with different band structure (Fig. 1) including $TiO_2$, $C_3N_4$, $WO_3$, $ZnWO_4$, $Bi_2WO_6$ for efficient selective oxidation of benzene to phenol. The structural and textural properties of the photocatalysts were characterized. This work is important to explore which photocatalysts is the most suitable for selective oxidation of benzene to phenol.
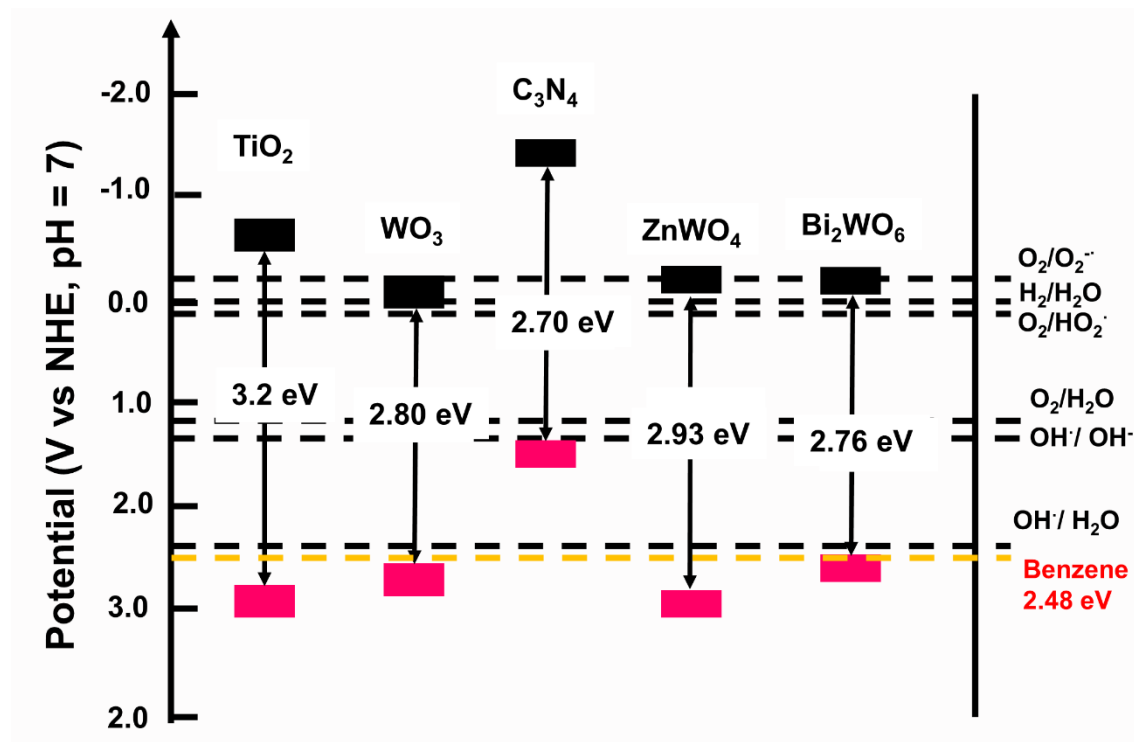


**Fig. 1.** Band edge alignments of photocatalysts

## 5.2 Experimental

*Materials*

Pluronic P123, tetraethylorthosilicate (TEOS), $Na_2WO_4$ $2H_2O$, $H_2WO_4$ and citric acid were purchased from Sigma–Aldrich (Japan). Hydrochloric acid (HCl), $H_3PW_{12}O_{40}$ (HPW), benzene, and other reagents were purchased from Wako (Japan).

*Preparation of $Bi_2WO_6$ sheet*

$Bi_2WO_6$ sheet was synthesized by a hydrothermal method as reported in previous work with small modification [3]. Typically, 1.24 g of $Na_2WO_4 \cdot 2H_2O$ dissolved in 40 mL water called solution A. 3.64 g of $Bi(NO_3)_3 \cdot 5H_2O$ was added into 30 mL of 0.4 M $HNO_3$ aqueous solution, which sonicated for 30 min before the solution completely transparent called solution B. Then, the solution

A was added dropwise to the solution B. After sonication for 30 min, the suspension was transferred into a 100 mL Teflon-lined autoclave and heated at 160 °C for 20 h. After the solution cooled to room temperature, the solid was collected by centrifugation, washed thoroughly with water and ethanol, and dried at 60 °C. Subsequently, the sample was calcinated in air at 350 °C for 3 h.

*Preparation of ZnWO₄*

ZnWO$_4$ sample was prepared by a hydrothermal method as reported by previous paper [5]. First, 5 mmol of Zn(NO$_3$)$_2$·6H$_2$O was dissolved into 45 mL of deionized water with continuous magnetic stirring. Then 15 mmol of Na$_2$WO$_4$·2H$_2$O was added into the solution. The mixture was stirred for another 30 min, then moved into a 100 mL of Teflon-lined stainless reactor and reacted at 200 °C for 24 h. The collected ZnWO$_4$ was washed with absolute ethanol and deionized water three times respectively and dried at 60 °C.

*Preparation of C₃N₄*

The C$_3$N$_4$ was synthesized by using urea as a precursor calcinated under 500 °C for 4 h with a rate of 5 °C/min.

*Preparation of Pt-loaded photocatalysts*

Pt-loaded photocatalysts were prepared by a photoreduction method [4]. Typically, H$_2$PtCl$_6$·4H$_2$O aqueous solution was injected into the methanol solution with photocatalyst suspension under anerobic condition. After stirring for 10 min, the suspension was irradiated with 300 W xenon lamp. The

As-prepared sample in the reactor was collected and washed with water and ethanol several times, and dried at 60 °C for characterization and use.

*Catalyst characterization*

A diffuse reflectance UV3100 system equipped with a diffuse reflectance accessory (Shimadzu, Japan) was used to obtain UV-Vis spectra. The X-ray diffraction (XRD) patterns were scanned at 40 kV and 40 mA (the step rate was 2°/min) by using a RINT 2200 diffractometer (RIGAKU, Japan)

with Cu-Kα radiation (1.54 Å).

*Photocatalytic performance study*

Photocatalytic oxidation of benzene to phenol was conducted in a 100 mL photochemical reactor equipped with a water jacket to maintain the temperature at 10 °C. The top of the reactor contained an illumination window fabricated from high-strength quartz glass. In a typical run, a mixture of 30 mL water containing 2 mM benzene was added to the reactor before being exposed to air. Then, 75 mg of photocatalyst was added with continuous stirring for 15 min until adsorption equilibrium was reached. A 300 W xenon lamp was used as the irradiation source for the photocatalytic reactions. After each irradiation time interval, sample aliquots were withdrawn from the reactor with a syringe and filtered to be immediately analyzed with high-performance liquid chromatography (HPLC). The mobile phase was composed of 65% phosphoric solution (0.2%) and 35% acetonitrile with a flow rate of 1 cm$^3$/min.

The benzene conversion, phenol yield, and selectivity were calculated using the following formulas:

$$Benzene\ conversion = (1 - \frac{remained\ benzene\ concentration}{initial\ benzene\ concentration}) \times 100\%$$

$$Phenol\ yield = \frac{produced\ phenol\ concentration}{initial\ benzene\ concentration} \times 100\%$$

$$Phenol\ selectivity = \frac{Phenol\ yield}{Benzene\ conversion} \times 100\%$$

## 5.3 Results and discussion

*XRD pattern*

All photocatalysts have been characterized with XRD pattern to confirm their phase structure, as shown in Fig. 2. The TiO$_2$ (P25) showed both peaks of rutile phase and anatase phase of TiO$_2$ [6]. The commercial WO$_3$ showed strong peaks at 23.1°, 23.6°, and 24.4°, which are ascribed to the characteristic (002), (020), and (200) crystal planes of monoclinic WO$_3$ (JCPDS No. 43-1035), respectively [7]. The peaks at 27.4° in the XRD patterns of C$_3$N$_4$ is due to the stacking of the conjugated aromatic system [8]. All the diffraction peaks can be indexed to the ZnWO$_4$ with the standard card (JCPDS card no. 73-0554) [9]. The XRD pattern of Bi$_2$WO$_6$ corresponding to the Russellite ortho-rhombic phase (JCPDS 39-0256) [10].
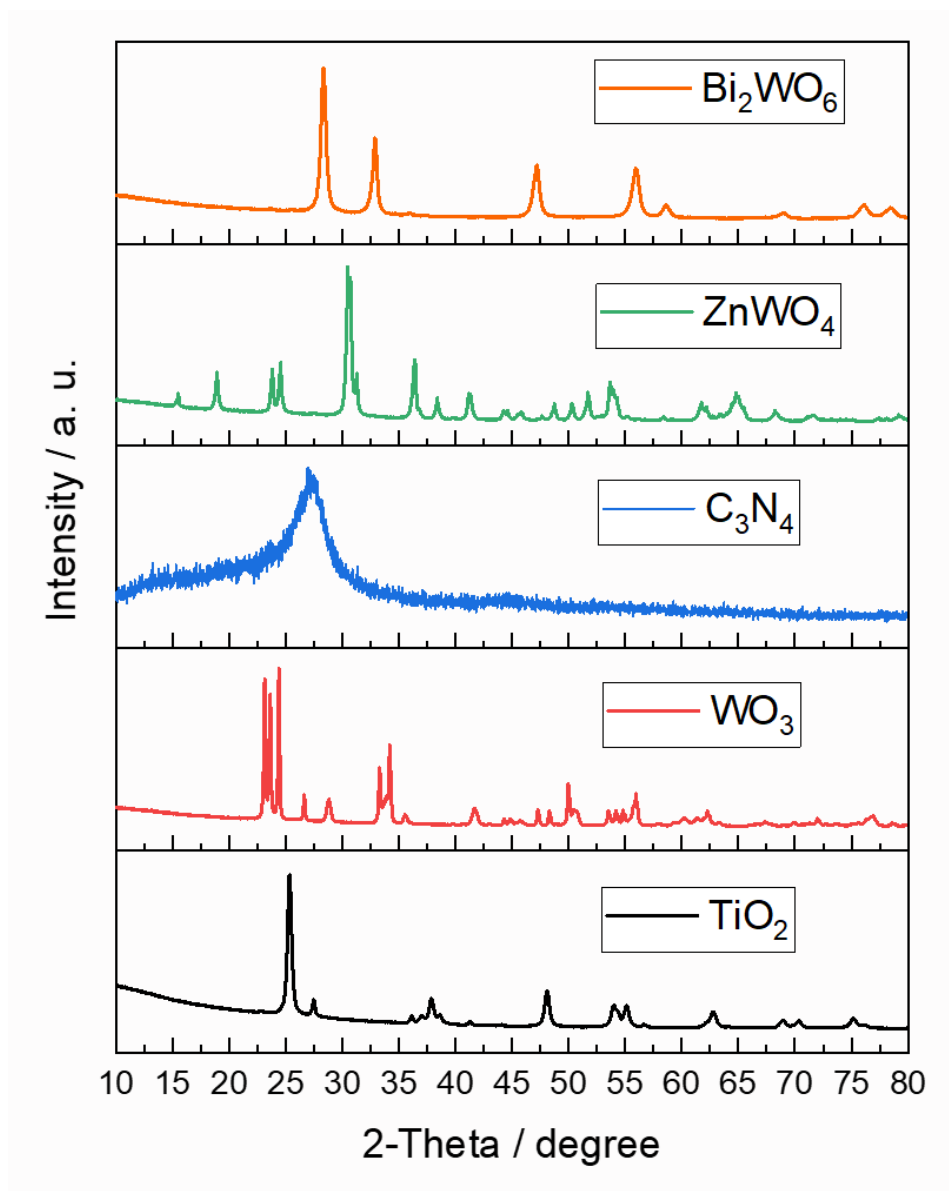
**Fig. 2.** XRD pattern of different photocatalysts

*Photocatalytic benzene oxidation to phenol*

We first confirmed that no phenol formed without light irradiation and photocatalysts. Hence, phenol generated in our reaction system is due to the photocatalytic reaction. As the most studied, $TiO_2$ showed much higher phenol yield (15.1 %) than the other photocatalysts. However, the phenol selectivity (35%) is low (Table 1, entry 1 and 2). It has been reported that benzene oxidation with $TiO_2$ ascribed to both holes and hydroxyl radical ($OH^\cdot$) [11]. Typically, directly oxidation of benzene to $CO_2$ can be easily occurred by hole after absorption of benzene on the surface, which dramatically

decrease the phenol selectivity. This process has been supported by a control experiment, in which TiO$_2$ oxidation benzene under argon atmosphere. In this case, phenol was generated with low yield (2% at 2h) and almost no phenolic byproducts due to the overoxidation of phenol. In this case, holes are the main active species even the OH$^\cdot$ can also be generated due to the oxidation of water. However, the phenol selectivity was lower than 30%, likely due to the directly oxidation of benzene to phenol with hole. In the case of aerobic condition, large amount of OH$^\cdot$ can attack benzene to generate phenol, resulting a high phenol yield and selectivity. However, excess OH$^\cdot$ also lead to the overoxidation of phenol, resulting the generation of large amounts of phenolic byproducts. The low selectivity (37%) of ZnWO$_4$ as photocatalyst may be ascribed to the similar situation.

C$_3$N$_4$ is a widely studied none-metal photocatalysts for various application, including H$_2$ production, pollutant degradation and selective oxidation. Recently, C$_3$N$_4$ has been reported for benzene hydroxylation using H$_2$O$_2$ as oxidant. However, there is no activity for benzene conversion and phenol formation in our system. A possible reason is that only O$_2^\cdot$ but no OH$^\cdot$ generated during the reaction. In addition, the value band (VB) of C$_3$N$_4$ is higher than that of benzene oxidation potential as shown in Fig. 1. Hence, no phenol generated when using C$_3$N$_4$ as photocatalyst for benzene oxidation (Entry 3).

**Table 1** Photocatalytic benzene oxidation to phenol with different photocatalysts [a]

| Entry | Photocatalysts | Source | Reaction time (h) | Phenol yield (%) | Selectivity (%) |
|---|---|---|---|---|---|
| 1 | TiO$_2$ | Commercial | 2 | 15 | 35 |
| 2 | TiO$_2$ [b] | Commercial | 2 | 2 | 29 |
| 3 | WO$_3$ | Commercial | 4 | 1 | 56 |
| 4 | WO$_3$ [b] | Commercial | 4 | - | - |
| 5 | C$_3$N$_4$ | Polymerization | 4 | <0.1 | - |
| 6 | ZnWO$_4$ | Hydrothermal | 2 | 5 | 37 |
| 7 | Bi$_2$WO$_6$ | Hydrothermal | 4 | 3 | 55 |

[a] Reaction condition: light source, 300 W xenon lamp; temperature, 10 °C; catalyst amount, 75 mg; benzene concentration, 2 mM; solution, pure water; under ambient condition; [b] without

oxygen.

Recently, $WO_3$ and $Bi_2WO_6$ as visible light photocatalysts have been widely studied including for photocatalytic benzene oxidation to phenol. They showed higher phenol selectivity in our reaction system. According to previous work, the higher phenol selectivity is due to the lower absorption of benzene on the surface [4]. As a result, a suppressed directly oxidation to $CO_2$ by holes has been achieved, which is different with that of $TiO_2$. In another word, an indirect oxidation route by $OH^.$ oxidation is dominant in these systems. However, the benzene conversion and phenol yield were much lower than that of $TiO_2$ due do the fast recombination of photo-induced holes and electrons. A co-catalyst such as Pt is reported efficient for accumulation of electrons for $O_2$ reduction, which as a main route for production of oxygen containing species such as $H_2O_2$ and $OH^.$. As a result, $Pt$-$WO_3$ showed even higher phenol yield (24%) and selectivity (61%) than that of $Pt$-$TiO_2$ (Table 2).

**Table 2** Photocatalytic benzene oxidation to phenol with different Pt loaded photocatalysts

| Entry | Photocatalysts | Reaction time (h) | Phenol yield (%) | Selectivity (%) |
|-------|----------------|-------------------|------------------|-----------------|
| 1 | $Pt$-$TiO_2$ | 1 | 15 | 35 |
| 2 | $Pt$-$WO_3$ | 1 | 32 | 78 |
| 3 | $Pt$-$C_3N_4$ | 4 | $<0.1$ | - |
| 4 | $Pt$-$Bi_2WO_6$ | 4 | 3 | 41 |

Reaction condition: light source, 300 W xenon lamp; temperature, 10 °C; catalyst amount, 75 mg; benzene concentration, 2 mM; solution, pure water; under ambient condition.

**5.4 Conclusion**

Several typical semiconductor-based photocatalysts have been studied for benzene oxidation to phenol. The relationship between the band structure, active species and phenol formation was proposed and discussed in detailed. The VB position of photocatalyst need to lower than benzene oxidation potential. Hence, $C_3N_4$ showed no phenol formation which is contrast with other four kinds of photocatalysts including $TiO_2$, $WO_3$, $ZnWO_4$, $Bi_2WO_6$. On the other hand, directly oxidation of benzene to phenol more likely occurred with holes, resulting lower phenol selectivity of $TiO_2$ and $ZnWO_4$ than $WO_3$ and $Bi_2WO_6$. The OH radical can be accumulated by suitable co-

catalyst such as Pt, enhancing phenol formation over WO$_3$. In the future, other efficient photocatalyst or nonnoble cocatalyst is desirable for novel photocatalyst for selective benzene oxidation to phenol.

**Reference**

[1] L. Chen, J. Tang, L.-N. Song, P. Chen, J. He, C.-T. Au, S.-F. Yin, Heterogeneous photocatalysis for selective oxidation of alcohols and hydrocarbons, Applied Catalysis B: Environmental, 242 (2019) 379-388.

[2] J. Li, Y. Xu, Z. Ding, A.H. Mahadi, Y. Zhao, Y.-F. Song, Photocatalytic selective oxidation of benzene to phenol in water over layered double hydroxide: A thermodynamic and kinetic perspective, Chemical Engineering Journal, 388 (2020).

[3] P. Chen, L. Chen, Y. Zeng, F. Ding, X. Jiang, N. Liu, C.-T. Au, S.-F. Yin, Three-dimension hierarchical heterostructure of CdWO4 microrods decorated with Bi2WO6 nanoplates for high-selectivity photocatalytic benzene hydroxylation to phenol, Applied Catalysis B: Environmental, 234 (2018) 311-317.

[4] O. Tomita, B. Ohtani, R. Abe, Highly selective phenol production from benzene on a platinum-loaded tungsten oxide photocatalyst with water and molecular oxygen: selective oxidation of water by holes for generating hydroxyl radical as the predominant source of the hydroxyl group, Catal. Sci. Technol., 4 (2014) 3850-3860.

[5] D. Ma, L. Yang, Z. Sheng, Y. Chen, Photocatalytic degradation mechanism of benzene over ZnWO4: Revealing the synergistic effects of Na-doping and oxygen vacancies, Chemical Engineering Journal, 405 (2021).

[6] J. Wang, J. Yu, X. Zhu, X.Z. Kong, Preparation of hollow TiO2 nanoparticles through TiO2 deposition on polystyrene latex particles and characterizations of their structure and photocatalytic activity, NANO EXPRESS, 7 (2012) 646.

[7] J. Ke, H. Zhou, J. Liu, X. Duan, H. Zhang, S. Liu, S. Wang, Crystal transformation of 2D tungstic acid H2WO4 to WO3 for enhanced photocatalytic water oxidation, J Colloid Interface Sci, 514 (2018) 576-583.

[8] X. Bai, L. Wang, Y. Wang, W. Yao, Y. Zhu, Enhanced oxidation ability of g-C3N4 photocatalyst via C60 modification, Applied Catalysis B: Environmental, 152-153 (2014) 262-270.

[9] B. Guan, L. Hu, G. Zhang, D. Guo, T. Fu, J. Li, H. Duan, C. Li, Q. Li, Facile synthesis of ZnWO4nanowall arrays on Ni foam for high performance supercapacitors, RSC Adv., 4 (2014) 4212-4217.

[10] X. Fan, X. Yue, J. Luo, C. Wang, Facile synthesis of carbon-Bi2WO6 with enhanced visible-light photocatalytic activities, Journal of Nanoparticle Research, 18 (2016).

[11] T.D. Bui, A. Kimura, S. Higashida, S. Ikeda, M. Matsumura, Two routes for mineralizing benzene by TiO2-photocatalyzed reaction, Applied Catalysis B: Environmental, 107 (2011) 119-127.

# Chapter 6:

General conclusion and outlook

# Chapter 6: General conclusion and outlook

This thesis focuses on the photocatalytic benzene oxidation to phenol, which is one of the most important but challenging chemical reaction. The polyoxometalate including $H_3PW_{12}O_{40}$ and $Na_4W_{10}O_{32}$ showed high activity for benzene oxidation to phenol under typical reaction condition. The application of supported $H_3PW_{12}O_{40}$ for heterogenous photocatalytic benzene oxidation to phenol was also investigated. The photocatalytic benzene oxidation to phenol by semiconductor-based photocatalysts was discussed as well.

In Chapter 2, the $H_3PW_{12}O_{40}$ can utilized as a photocatalysts for efficient oxidation of benzene to phenol in an aqueous acetonitrile solution. Due to the unique catalytic reaction mechanism, the oxidation process has been significantly adjusted by the reaction conditions, especially by adding acetonitrile as co-solvent. By adding 50% acetonitrile into the solvent, the phenol overoxidation significantly suppressed due to the inhibited precompexation between catalysts and phenol molecular. On the other hand, benzene showed different reaction mechanism which still can be oxidized in this reaction condition. Hence, benzene can be oxidized but phenol can not be oxidized in our reaction system, resulting a unnormal but high phenol yield and selectivity.

In Chapter 3, we change the organic cation of decatungstate to inorganic cation (Na+), achieved high phenol yield and selectivity in an aqueous solution. Acetic acid as co-solvent involved in the oxidation process, which increased the phenol formation. This behavior is significantly different with that of $TiO_2$, which showed no activity by adding acetic acid as co-solvent. The totally different reaction mechanism with $TiO_2$ leading to the high phenol formation (phenol yield, 24%; phenol selectivity, 81%) in this reaction system.

In chapter 4, we tried to support $H_3PW_{12}O_{40}$ into mesoporous silica by a direct method and impregnate method. The textural and structure have been fully characterized and proved that the higher stability of the sample prepared by the direct method. However, the leaching of active species into the aqueous solution is inevitable even the direct method can improve the stability of the supported sample. We found that the leaching species for homogenous photocatalytic reaction is dominant in the reaction. The heterogenous reaction by the supported $H_3PW_{12}O_{40}$ showed low reaction rate for benzene oxidation in aqueous solution. We also showed the significant low reaction

in the gas-phase formic acid oxidation, by using TiO$_2$ as a reference photocatalysts. The low reaction rate may be due to the suppressed reoxidation of photocatalysts in the redox cycle.

In chapter 5, we investigated several typical type of semiconductor photocatalysts for selective oxidation of benzene to phenol. The band structure and active species were considered for the different reaction mechanism. Low phenol selectivity toward phenol due to the unselective of the holes and radicals generated from semiconductor-based photocatalysts such as TiO$_2$ and ZnWO$_4$. Pt loaded WO$_3$ showed much higher phenol yield compared with commercial WO$_3$ because the promoted OH radical generation. All this founding is crucial to develop novel photocatalysts for benzene oxidation to phenol in the future.

In a word, oxidation of absorbed benzene molecular on the surface of semiconductor photocatalysts will directly promote oxidation to CO$_2$ by holes. The indirectly oxidation of benzene with OH radical is more promising for efficient oxidation of benzene to phenol. Hence, WO$_3$ and some other suitable photocatalysts is highly desired to be developed and modified for efficient benzene oxidation to phenol in the future.

# Acknowledgement